Aus der Klinik für Neurologie, Abteilung für Experimentelle Neurologie
der Medizinischen Fakultät Charité – Universitätsmedizin Berlin

DISSERTATION

Effects of $CD4^+$ T cells on tissue remodeling and autoreactive responses after experimental stroke

zur Erlangung des akademischen Grades
Doctor of Philosophy (PhD)

vorgelegt der Medizinischen Fakultät
Charité – Universitätsmedizin Berlin

von

Tian Zhang
aus Urumqi, China

Datum der Promotion: 14.09.2018

TABLE OF CONTENTS

1. ABSTRACT

1.1 Summary

Lymphocytes, mainly $CD4^+$ T cells, have been identified as one of the key mediators of tissue damage and autoreactivity after stroke. However, potential therapies targeting delayed infiltration of $CD4^+$ T cells are largely unexplored. Here, I investigated the effects of delayed infiltration of $CD4^+$ T cells on tissue remodeling, functional recovery and autoreactive responses by B cells post stroke.

Ischemic stroke was induced by 60 minute middle cerebral artery occlusion (MCAo) in wild type (WT) C57Bl/6 and 2D2 mice in which $CD4^+$ T cells had been genetically modified so that their autoreactive T cell receptors recognize myelin oligodendrocyte glycoprotein. Delayed infiltration of $CD4^+$ T cells was blocked by monoclonal antibodies starting on day 3 after stroke. Tissue remodeling was evaluated by quantitative real-time polymerase chain reaction and histology. Leukocyte infiltration and B-cell autoreactivity were quantified by histology and flow cytometry. Functional recovery was monitored by gait analysis and neurological scoring.

$CD4^+$ T cells infiltrated earlier and accumulated significantly more in the ischemic hemisphere on day 14 in 2D2 mice compared with WT mice. Additionally, the infarct size on day 1 post stroke in 2D2 mice was also significantly larger than in WT mice.

The anti-mouse CD4 antibody completely depleted $CD4^+$ cells in the blood, spleen and ischemic brain. Even though infarct size was not significantly reduced, CD4 depletion significantly impaired the entry of B cells as well as the proliferation of activated macrophages and periendothelial cells in 2D2 mice on day 14 post stroke. However, the absence of $CD4^+$ T cells and subsequent blockage of B-cell infiltration had limited influence on tissue fibrosis and motor recovery. The inhibition of B-cell infiltration by CD4 depletion was not significant in WT mice on day 14 post stroke.

In both 2D2 and WT mice with control treatment, infiltrating B cells formed follicle-like aggregates in the ischemic hemispheres. In WT mice, B cells could form follicle-like aggregates up to 7 weeks post stroke. Interestingly, the delayed impairment of memory was more severe at 7 weeks than at 2 weeks post stroke.

In conclusion, migration of B cells towards the ischemic brain depended on the infiltration of autoreactive $CD4^+$ T cells. Follicle-like B cell aggregates temporally correlated with cognitive decline post stroke. Therefore, approaches to prevent delayed infiltration of adaptive immune cells might serve as a potential treatment for stroke patients. Further investigation into improving the understanding and development of novel therapies is warranted.

1.1 Zusammenfassung

Lymphozyten, hauptsächlich CD4+ T-Zellen, wurden als einer der Schlüsselfaktoren für Gewebeschäden und Autoreaktivität nach Schlaganfall identifiziert. Potentielle Therapien, die die verzögerte Infiltration von CD4+ T-Zellen verhindern, sind jedoch weitgehend unerforscht. In meiner Doktorarbeit untersuchte ich die Auswirkungen der verzögerten Infiltration von CD4+ T-Zellen auf die Gewebeumstrukturierung, die funktionelle Erholung und die Autoreaktivität von B-Zellen nach Schlaganfall.

Ein ischämischer Schlaganfall wurde durch 60 minütige Okklusion der mittleren zerebralen Arterie (middle cerebral artery occlusion, MCAo) in Wildtyp (WT) C57Bl/6- und 2D2 Mäusen induziert. 2D2 Mäuse besitzen genetisch modifizierte CD4+ T-Zellen so, dass ihre T-Zell-Rezeptoren das Myelin Oligodendrozyten Glykoprotein erkennen und die somit hohes autoreaktives Potenzial aufweisen. Die verzögerte Infiltration von CD4+ T-Zellen wurde in den Mäusen durch Verabreichung monoklonaler Antikörper blockiert, beginnend am Tag 3 nach dem Schlaganfall. Die Gewebeumstrukturierung wurde mittels quantitativer real-time Polymerase-Kettenreaktion und Histologie untersucht. Leukozyteninfiltration und B-Zell-Autoreaktivität nach Schlaganfall wurden durch Histologie und Durchflusszytometrie quantifiziert. Zur Untersuchung der funktionellen Erholung wurden Ganganalyse und neurologische Scores eingesetzt.

In 2D2 Mäusen infiltrierten CD4+ T-Zellen früher und an Tag 14 in größerer Zahl in die ischämische Hemisphäre verglichen mit WT-Mäusen. Zusätzlich war die Infarktgröße am Tag 1 nach Schlaganfall in 2D2-Mäusen signifikant größer als die in WT-Mäusen.

Der anti-Maus CD4 Antikörper führte zur vollständigen Depletion von CD4+ Zellen in Blut, Milz und im ischämischen Gehirn. Obwohl die Infarktgröße durch die Behandlung nicht signifikant reduziert wurde, beeinträchtigte die CD4-Depletion signifikant den Eintritt von B-Zellen, die Proliferation von aktivierten Makrophagen sowie periendothelialen Zellen in 2D2-Mäusen am Tag 14 nach dem Schlaganfall. Die Abwesenheit von CD4+ T-Zellen und die resultierende Blockierung von B-Zellen hatten jedoch einen begrenzten Einfluss auf die Gewebsfibrose und die motorische Erholung. Die Hemmung der B-Zell-Infiltration durch CD4-Depletion war am Tag 14 nach Schlaganfall in WT-Mäusen nicht signifikant.

Sowohl in 2D2 Kontrollen als auch in WT Mäusen mit Kontrollbehandlung bildeten B-Zellen follikelartige Aggregate in ischämischen Hemisphären. In WT-Mäusen konnten B-Zellen bis zu 7 Wochen nach Schlaganfall follikelartige Aggregate aufrechterhalten. Die längerfristige Beeinträchtigung des Gedächtnisses nach 7 Wochen war dabei schwerer als 2 Wochen nach dem Schlaganfall.

Zusammenfassend konnte ich in dieser Arbeit zeigen, dass die Migration von B-Zellen ins ischämische Gehirn von der Infiltration autoreaktiver CD4+ T-Zellen abhängt. Follikelartige B-Zell-Aggregate korrelieren zeitlich mit kognitiver Beeinträchtigung nach Schlaganfall. Daher könnten Ansätze zur Verhinderung einer verzögerten Infiltration von adaptiven Immunzellen als potentielle Behandlung von Schlaganfallpatienten dienen. Weitere Untersuchungen zur Verbesserung unseres Verständnisses und der Entwicklung neuer Therapien stehen in den nächsten Jahren an.

2. INTRODUCTION

2.1 Stroke

Stroke is the fifth leading cause of adult death and a leading cause of long-term disability in the United States (Association 2016). Moreover, the United States has 6.4 million stroke survivors (prevalence of 3%), and there are approximately 600,000 new strokes and 200,000 recurrent strokes per year (Benjamin, Griggs et al. 2016). Of all strokes, about 87% of are ischemic infarctions, 10% primary hemorrhages, and 3% subarachnoid hemorrhages (SAHs) (Benjamin, Griggs et al. 2016). Advanced imaging techniques further enable the distinction between "strokes" (involving abrupt onset of sudden weakness and difficulty with vision, speaking, thinking or coordination) and "silent brain infarction" (a temporary blockage of blood flow to the brain, lacking clinically overt stroke-like symptoms) (Fisher 1965, Vermeer, Longstreth et al. 2007, Benjamin, Griggs et al. 2016). However, the so-called "silent strokes" are not merely silent; they are associated with subtle deficits and future risk for stroke and dementia (van Rooij, Schaapsmeerders et al. 2014, Smith, Saposnik et al. 2017).

Acute ischemic stroke (AIS) is characterized by the sudden loss of blood circulation to an area of the brain, typically in a vascular territory, resulting in a corresponding loss of neurologic function (Catanese, Tarsia et al. 2017). Either thrombotic or embolic occlusion of a cerebral artery can be the cause of AIS (Benjamin, Griggs et al. 2016). Large-artery infarctions often involve thrombotic in situ occlusions on atherosclerotic lesions in the carotid, vertebrobasilar, and cerebral arteries, typically proximal to major branches. However, large-artery infarctions (14-30%) may also be cardioembolic (Arboix and Alio 2010).

The brain is perfused by paired carotid and vertebral arteries. The common carotid arteries bifurcate into the internal and external carotid arteries. The middle cerebral artery (MCA) is the largest branch of the internal carotid artery and is the single largest artery most commonly affected by ischemic stroke (Benjamin, Griggs et al. 2016). The territory supplied by MCA involves the outer convex brain surface, nearly all the basal ganglia, and the posterior and anterior internal capsules. Therefore, infarcts that occur within the vast distribution of MCA lead to diverse neurologic sequelae (Benjamin, Griggs et al. 2016).

Recanalization strategies, including intravenous recombinant tissue-type plasminogen activator (rt-PA) and endovascular procedure (Catanese, Tarsia et al. 2017), are mainly considered for stroke

patients when attempting to establish revascularization so that the ischemic penumbra, where reduction of blood flow leads to only mild excitotoxicity and inflammation with delayed cell death, can be rescued before irreversible injury occurs (Mergenthaler, Dirnagl et al. 2004). To date, rt-PA is the only drug approved by the US Food and Drug Administration (FDA) to treat ischemic stroke. It needs to be administered within 4.5 hours after stroke onset and only after computed tomography scanning has ruled out hemorrhagic stroke or (early) signs of tissue damage. Moreover, endovascular approaches to remove the blood clot, namely mechanical thrombectomy, have recently been proven to be effective in patients with occlusion in the internal cerebral artery and proximal MCA if administered within 6 hours of acute stroke symptoms (Catanese, Tarsia et al. 2017).

2.2 Animal models of ischemic stroke

Stroke is the leading cause of adult disability in industrialized countries. In addition to acute neurological deficits that can be directly attributed to the affected brain areas, additional cognitive decline (Makin, Turpin et al. 2013) and long-term psychiatric consequences, such as post-stroke depression (Robinson and Jorge 2016), may emerge without a correspondingly injured brain region in patients with chronic stroke (Sommer 2017). Therefore, stroke research has increasingly focused on the sub-acute and chronic phases after stroke because more patients might be eligible for therapeutic interventions in a prolonged time window. These delayed mechanisms include critical pathophysiological pathways such as post-stroke inflammation, activation of adaptive immunity, vascular remodeling, neuronal plasticity and regeneration (Becker 2010, Iadecola and Anrather 2011). Experimental stroke models with clinical relevance, low mortality and high reproducibility are required to analyze these mechanisms and to subsequently evaluate novel drug targets. To meet this need, preclinical stroke researchers perform experimental stroke, preferably on rodents, especially mice, for which a broad spectrum of transgenic models are available (Fluri, Schuhmann et al. 2015).

Proximal occlusion of the MCA via the intraluminal suture technique (so called filament or suture model) is probably the most frequently used animal stroke model (Carmichael 2005). The filament MCA occlusion (MCAo) model offers the advantage of inducing reproducible transient or permanent ischemia of the MCA territory in a relatively non-invasive manner, while the coagulation model needs a craniotomy right above the MCA branch for applying focal electrocoagulation and cannot induce transient occlusion (Fluri, Schuhmann et al. 2015). Moreover, filament occlusion of

the MCA with reperfusion after 60 min results in reproduction of pan-necrotic lesions in the cortex and striatum (Engel, Kolodziej et al. 2011). In contrast, models of distal (to the branching of the lenticulo-striate arteries) MCAo typically spare the striatum and primarily injure only the neocortex (Llovera, Roth et al. 2014).

Human strokes are mostly small in size ranging from 28–80 mm^3 and translating to 4.5–14% of the ipsilateral hemisphere (Carmichael 2005). Only malignant infarction can damage over 30% of one hemisphere. There is a clear risk that many studies of MCAo in mice do not model the usual cases of small and focal human stroke, but instead model malignant infarction (Carmichael 2005) with extensive cytotoxic edema, diminished collateral flow and only a relatively small rim of penumbra (Heiss 2016). When the infarct size extends into larger volumes of the hemisphere, the damage involves regions supplied by the MCA as well as deep regions such as the hippocampus, hypothalamus and/or thalamus (El Amki, Clavier et al. 2015). This limitation makes it harder to model human stroke, which damages only specific neuronal circuits (such as in the motor cortex), and the recovery following a functional reorganization in the brain. Nevertheless, the MCAo model with larger infarction has the advantage of providing measurable pathophysiology to study vascular remodeling and adaptive immune responses in the ischemic brain during subacute and even chronic phases.

2.3 Immunology of stroke

2.3.1 Cerebral ischemia induced immunodepression and susceptibility to infections

Although early mortality results from direct complication after large strokes, infections, and pneumonia in particular, are the leading cause of death in the post-acute phase of stroke. Infections after central nervous system (CNS) injury, such as stroke, traumatic brain injury (TBI) and spinal cord injury (SCI), may be attributed to exposure to invasive medical procedures and prolonged hospitalization, dysphagia, aspiration, etc. (Meisel, Schwab et al. 2005). The high incidence of infections in stroke patients is likely to be caused by an impaired immune function and subsequent susceptibility to infection (Dirnagl, Klehmet et al. 2007). As early as 1974, an immunosuppressive state was conceptualized in stroke (Howard and Simmons 1974). In a mouse model of focal cerebral ischemia with bacterial infection developing spontaneously within 24 hours after the onset of stroke, rapid suppression of peripheral cellular immune responses involving mainly lymphocyte apoptosis

and defective interferon (IFN)-ɣ production by T and natural killer (NK) cells preceded the bacterial infection (Prass, Meisel et al. 2003). Blocking the sympathetic nervous system but not the hypothalamic-pituitary-adrenal (HPA) axis prevented the occurrence of infection after stroke. Another study using a similar MCAo model demonstrated that stroke induced short activation of hepatic invariant NKT (iNKT) cells and changed their phenotype towards producing immunosuppressive type 2 helper T cell (Th2) cytokine, interleukin (IL)-10 (Wong, Jenne et al. 2011). Furthermore, in both studies administration of β-adrenoceptor blocker propranolol retained inflammatory type 1 helper T cell (Th1) phenotype of lymphocytes and dramatically reduced infection after stroke.

The nervous and immune systems actively communicate with each other. The central and peripheral autonomic nervous systems have sensors for the status of the immune system (Felten, Felten et al. 1987). After processing input from the CNS, in particular the frontal premotor cortex (fpmCTX), the hypothalamus, the pituitary and the brain stem, homeostatic signals can be sent to various organs via three major pathways of neuroimmunomodulation: the HPA axis, the sympathetic-adrenal-medullary (SAM) axis and the para sympathetic nervous system (vagus nerve) (Meisel, Schwab et al. 2005). Production of glucocorticoid hormones and catecholamines in the blood upon activation of the HPA and the SAM axes results in suppressive immunomodulation of both immune cell activation and inflammatory cytokine production. This anti-inflammatory response was considered adaptive and protective to limit an overwhelming systemic inflammatory response which could result in shock and multiple organ failure (Meisel, Schwab et al. 2005). It was later determined that CNS injury induces a disturbance in the normally well-balanced interplay between the immune system and the CNS. This is the mechanism by which CNS injury leads to secondary immunodeficiency (CNS injury-induced immunodepression, CIDS) (Figure 1) and infection (Meisel, Schwab et al. 2005).

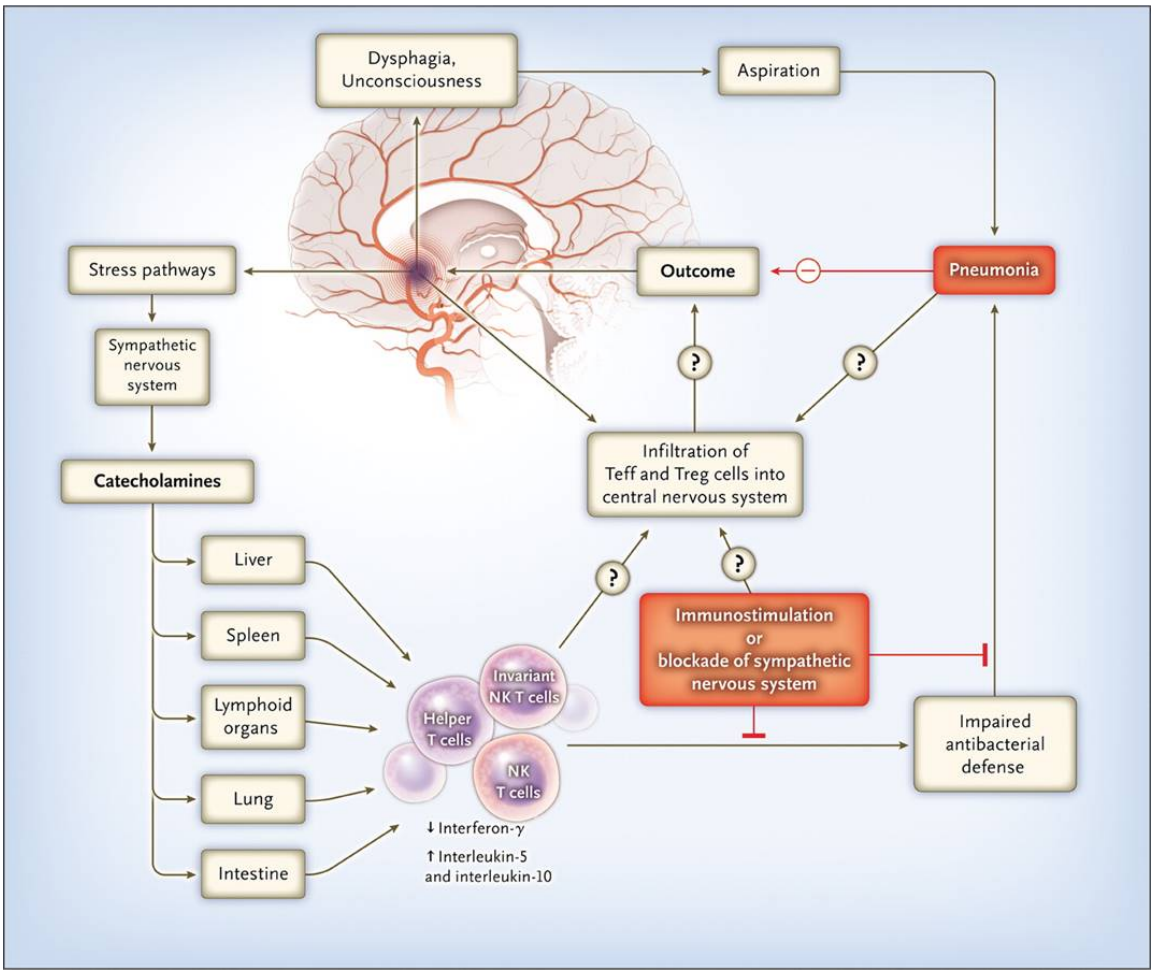

Figure 1. Schematic representation of stroke injury-induced immunodepression (SIDS).
Stroke-induced immunosuppression is characterized by impaired function of invariant natural killer T cells as well as other immune cells, including helper T cells and antigen-presenting cells through over-activation of stress pathways, especially those of the sympathetic nervous system. The resulting breakdown of antimicrobial defenses and neurologic deficits (such as dysphagia and unconsciousness) following stroke, frequently lead to pneumonia that in turn may worsen outcome. Adapted from Meisel and Meisel (2011).

To maximally fight infection secondary to stroke-induced immunodepression and related mortality, stroke patients are routinely prescribed antibiotics if there is evidence of ongoing infection in the clinical setting. Considering that infection usually develops within a fixed time window of 2-7 days after stroke onset (Meisel 2015), preventative antibiotic treatment might also be appropriate. At least in experimental stroke it has been proven that a preventative approach similarly reduces post-stroke

mortality and enables better neurologic outcome compared to the standard approach (Hetze, Engel et al. 2013). However in the Preventative Antibiotics Stroke Study (PASS), preventive ceftriaxone does not improve functional outcome at 3 months in adults with acute stroke (Westendorp, Vermeij et al. 2015). Surprisingly, post-hoc subgroup analysis in PASS suggests that preventive antibiotic therapy improves neurological outcome only in patients simultaneously treated with intravenous thrombolysis. A subsequent clinical trial (STROKE-INF) assessed the effectiveness of antibiotic prophylaxis in reducing pneumonia in patients with dysphagia after acute stroke and recommended no antibiotic prophylaxis since only urinary tract infections (UTIs), and not post-stroke pneumonia, were less frequent in the antibiotics group (Kalra, Irshad et al. 2015). In addition, no benefit of antibiotic prophylaxis was reproduced in a subgroup of patients with intravenous thrombolysis. Therefore further trials are still needed to investigate the potential mechanism.

It is also worth mentioning that infection or systemic inflammation can exacerbate functional outcome of acute stroke by boosting cellular immune responses towards a more destructive T helper 1 (Th1) response against CNS antigens rather than a protective T regulatory (Treg) response (Becker, Kalil et al. 2011). To exclude the confounding effect of infection, it is beneficial to employ preventative antibiotic treatment in experimental stroke with a focus on investigating the effects of immunological modulation on post-stroke recovery.

2.3.2 Drainage of CNS antigens and extravasation of leukocytes into brain parenchyma

CNS is classically considered an “immune privileged” site owing to the presence of the blood-brain barrier (BBB) restricting entry of immune cells into the CNS and the lack of a classical lymphatic drainage system within the CNS parenchyma. Usually, systemic inflammation or infections cannot induce bystander damage beyond the blood-brain barrier, while the constant immune surveillance of the CNS only takes place within the meningeal compartment (Kipnis, Gadani et al. 2012, Ransohoff and Engelhardt 2012). This phenomenon and stroke-induced immunodepression jointly serve as an endogenous mechanism to prevent autoimmune responses directed against brain antigens after CNS injury. However, two major extracellular fluids, cerebrospinal fluid (CSF) in the ventricles and subarachnoid spaces and interstitial fluid (ISF) in the extracellular spaces of the brain and spinal cord parenchyma, can carry CNS antigens which are released after CNS injury or antigen-presenting cells (APCs) to cervical or lumbar lymph nodes (Louveau, Smirnov et al. 2015). Neuronal antigens are present in cervical lymph nodes (CLN) of multiple sclerosis (MS) patients (van Zwam, Huizinga

et al. 2009). Moreover, brain proteins have been detected in the CSF and blood as well as carried on APCs in draining LN of stroke patients (Planas, Gomez-Choco et al. 2012), and their concentration is related to the extent of brain damage (Jauch, Lindsell et al. 2006). In mice at 24 hours after there is significantly increasing drainage of CNS antigen, mainly proteolipid protein (PLP) and neurofilament light (NF-L) positive cells, in both superficial and deep CLNs compared with 72 hours after MCAo (van Zwam, Huizinga et al. 2009). This process, which takes place both in the draining LNs and the spleen, facilitates recognition of CNS antigens (usually not available to the immune system in a healthy state) by peripheral lymphocytes and initiates the development of detrimental autoreactivity against CNS antigens (Ren, Akiyoshi et al. 2012, Ortega, Noorbhai et al. 2015, Zierath, Kunze et al. 2015) or potentially protective tolerance (Steinman and Nussenzweig 2002, Becker 2009, Gee, Zierath et al. 2009).

In addition to drainage and presentation of CNS antigens to the periphery, ischemia/reperfusion injury is also associated with immune cell recruitment, which contributes to both damage of the vessels and the surrounding tissue. Neurons can respond rapidly to focal ischemia, which is attributed to functional coupling with CNS vessels. The anatomical structure is the so-called neurovascular unit (NVU) which is composed of a monolayer of specialized endothelial cells (ECs) interconnected by complex tight junctions (TJs), the underlying endothelial basement membrane (BM) and a second BM, known as the parenchymal BM as it marks the border to the CNS parenchyma (Enzmann, Mysiorek et al. 2013) (Figure 2). Together with the ensheathing layer of astrocyte endfeet, the parenchymal BM defines the glia limitans (Engelhardt and Wolburg 2004), interconnecting to the surrounding neurons. Only capillaries have just one composite BM fused by endothelial and parenchymal BMs, while in all brain parenchymal vessels the endothelial and parenchymal BMs are structurally and biochemically distinct entities. Perivascular space, namely "Virchow-Robin space" or the "perivascular cuff", is formed between these two BMs. Extravasation and aggregation of leukocytes within the perivascular space is typically seen in the inflamed brain under immunofluorescent microscopy (Figure 2). Activated leukocytes expressing adhesion molecules, selectins, and integrins roll, activate and attach to the brain endothelium via ligation with their corresponding receptors and finally transmigrate through the endothelial layer of BBB (Engelhardt 2006, Wilson, Weninger et al. 2010). Only recently have CNS inflammation studies (Wu, Ivars et al. 2009, Yousif, Di Russo et al. 2013) highlighted the contribution of the following acellular BM layers to lymphocyte extravasation and hence barrier functions at the level of post-

capillary venules. Furthermore, disease symptoms are only induced upon leukocyte penetration of the final parenchymal BM as well as glial limitans and entry into CNS parenchyma (Agrawal, Anderson et al. 2006).

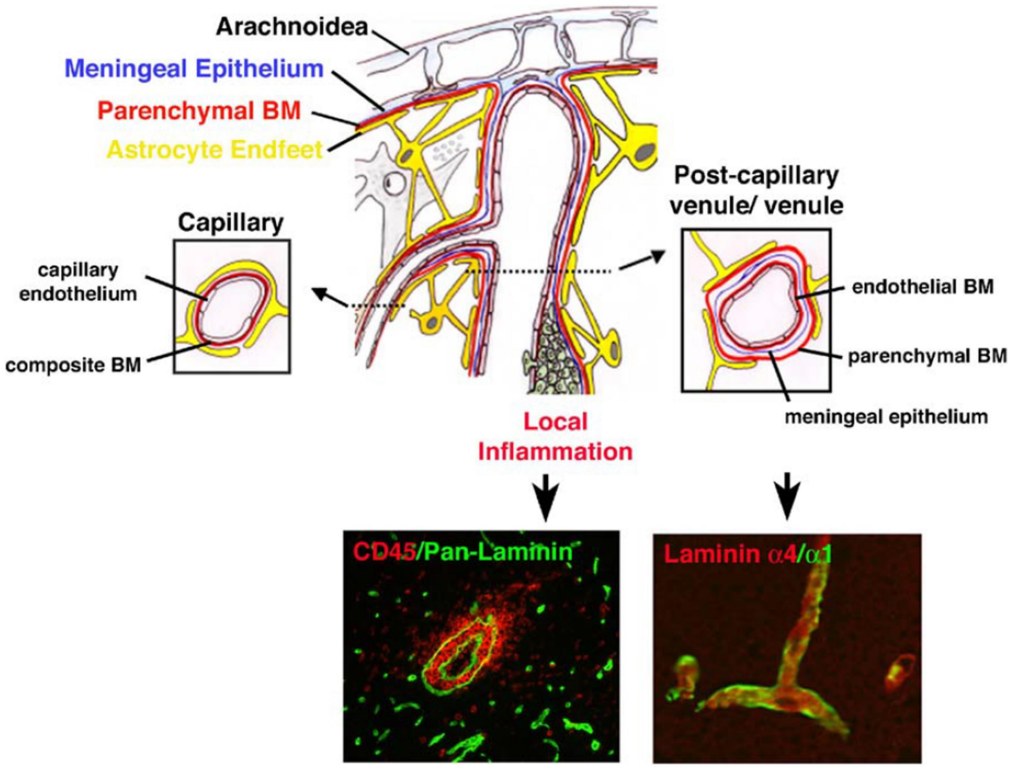

Figure 2. Cellular and acellular architecture of CNS blood vessels.

Schematic representation and immunofluorescence examples of cell and basement membrane (BM) layers supporting CNS blood vessels. Larger blood vessels consist of an inner endothelial cell layer with BM (containing laminins α4 and α5), bordered by the meningeal epithelium and its BM (containing laminin α1), and an outer astroglial BM (containing laminin α2) and astrocyte endfeet. Meningeal and astroglial BMs are collectively termed the parenchymal BM as they delineate the border to the brain parenchyma. Endothelial and parenchymal BMs usually merge as one layer. Only the accumulation of inflammatory immune cells ("perivascular cuff") in the perivascular space makes endothelial and parenchymal BMs distinguishable. Adapted from Engelhardt and Sorokin (2009).

2.3.3 Inflammation-induced tissue remodeling after ischemic stroke

Apart from basement membranes that are composed of complex assemblies of four major glycoprotein families, laminins, collagen type IV isoforms, nidogens, and heparan sulfate proteoglycans, brain lacks another form of extracellular matrix (ECM): interstitial matrix of the stroma in most tissues. In brain, the fibrogenic stromal cells are restricted only to blood vessels and meninges, hence, there is normally little or no fibrous protein, such as collagen types I and III or fibronectin (Engelhardt and Sorokin 2009). However, disruption of the BBB and inflammation can cause scar formation or tissue fibrosis (a ubiquitous healing mechanism to compensate tissue defects) in CNS parenchyma. The fibrotic scar is characterized by the deposition of fibrous ECMs in the neural parenchyma such as collagens, laminins and fibronectin. These molecules are deposited by invading stromal cells (myofibroblasts), which are normally absent. The stromal cells may originate from meningeal precursors (eg, pial cells of the leptomeningeal lining), perivascular fibroblasts or pericytes ("type A pericytes") (Fernandez-Klett and Priller 2014). No contribution of bone marrow-derived cells is reported (Fernandez-Klett, Potas et al. 2013).

Pericytes (PCs), the most abundant vascular mural cells, are embedded within BMs and positioned at the interface between endothelial cells, neurons and astrocytes. They contribute to the modulation of blood flow (Fernandez-Klett and Priller 2015) and determine the formation and integrity of the BBB (Armulik, Genove et al. 2010). After experimental traumatic brain injury, at ultrastructural level some PCs acutely migrate into the parenchyma adjacent to blood vessels while others degenerate (Dore-Duffy, Owen et al. 2000). In spinal cord injury models, a novel subpopulation of vascular mural cells share with PCs the perivascular location and a common set of markers, including platelet-derived growth factor receptor beta (PDGFRβ). These cells proliferate extensively into fibroblast-like cells that generate fibrous ECMs and outnumber astrocytes after spinal cord injury (Goritz, Dias et al. 2011). Most relevantly, it was reported that capillary PCs are rapidly lost after cerebral ischemia in both experimental and human stroke, while perivascular PDGFRβ^{+} stromal cells induce scar formation in mouse ischemic brain (Fernandez-Klett, Potas et al. 2013). Moreover, nerve growth factor (NGF), brain-derived neurotrophic factor (BDNF) and vascular endothelial growth factor a (VEGFa) might also be involved in tissue remodeling since both neurogenesis and angiogenesis can contribute to neural plasticity and recovery after ischemic stroke (Font, Arboix et al. 2010).

Astrocytes react to CNS injury by building a dense wall of filamentous processes, namely "glia scar", to seal the lesion (Cregg, DePaul et al. 2014). They undergo only modest proliferation in response to injury, and this proliferation is confined to a thin layer at the lesion margin without invasion into the ischemic core (Faulkner, Herrmann et al. 2004, Jiang, Zhao et al. 2016). For years it has been thought that the glia scar was the main impediment to regenerating axons attempting to reach their distal targets residing in the lesion. However, with a complex of interacting cell types in the lesion, the glia scar can have both detrimental and beneficial properties (Cregg, DePaul et al. 2014, Raposo and Schwartz 2014).

Fibrosis is part of inflammation. Breakdown of the BBB and leakage of inflammatory cytokines and profibrotic factors into the CNS parenchyma are considered key events in scar formation. Indeed, cytokines such as IL-1β, IL-6 and tumor necrosis factor (TNF)-α that aggravate fibrosis in peripheral tissues (Duffield, Lupher et al. 2013) are also expressed by activated microglia or infiltrating inflammatory cells in the injured CNS. The appearance of alternatively activated macrophages can also secrete anti-inflammatory and profibrotic factors such as tissue growth factor (TGF)-β1 and PDGF that has been associated with the accumulation of (myo)fibroblasts and the deposition of fibrillar ECMs (Murray and Wynn 2011). ECMs, such as chondroitin sulfate proteoglycans (CSPGs) with covalently bound glycosaminoglycans (GAGs), can enhance cell migration through their ability to bind L-selectins and P-selectins as well as inflammatory chemokines (Raposo and Schwartz 2014). However, no studies have carefully examined whether T lymphocytes are actively involved in scar formation and could possibly play a modulatory role in tissue remodeling after stroke.

2.3.4. Innate immune responses after ischemic stroke

Ischemic stroke causes sterile inflammation with chronic potential caused by the diminished immunosuppression during the delayed phase of injury. Both innate immunity and adaptive immunity can sense "danger signals" from dying and dead cells in the penumbra and the infarct Besides extracellular nucleotides and neurotransmitters, a wide variety of molecular signals are also released from the intracellular compartment or are generated by the action of lytic enzymes escaped from dead cells on matrix proteins (Iadecola and Anrather 2011). The so-called danger-associated molecular pattern molecules (DAMPs) activate pattern recognition receptors including Toll-like receptors (TLRs) and scavenger receptors, which are widely expressed on microglia, perivascular

macrophages and brain endothelial cells (Marsh, Williams-Karnesky et al. 2009). Thus it takes only hours to active innate immunity after stroke onset.

Microglia arise from the embryonic yolk sac and function as innate immune cells of the CNS. Following activation, microglia contribute to post-stroke inflammation by producing TNF, IL-1β, reactive oxygen species (ROS) and other proinflammatory mediators. **Blood monocytes** are direct precursors of tissue macrophages. After cerebral ischemia, inflammatory monocytes are rapidly recruited to the site of injury where they differentiate into macrophages and dendritic cells (DCs) (Felger, Abe et al. 2010). Functional **macrophages** can be classified into two groups: M1 macrophages that produce proinflammatory cytokines (IL-1β, IL-12, IL-23 and TNF), chemokines, ROS and NO, promoting a Th1 immune response, and M2 macrophages that produce anti-inflammatory cytokines (IL-10 and TGF-β1), IL-1ra and arginase (Mantovani, Biswas et al. 2013). Microglia and infiltrating macrophages constitute the predominant phagocytes that remove dead cells and tissue debris after stroke (Schilling, Besselmann et al. 2005, Denes, Vidyasagar et al. 2007). **DCs** are specialized APCs and therefore act as the interface between innate and adaptive immunity. Cells with DC markers appear in the brain parenchyma after focal ischemia and originate from resident and blood-borne cells (Felger, Abe et al. 2010). **Neutrophils** are also rapidly recruited to the site of tissue infection or inflammation. They have been frequently associated with tissue damage after cerebral ischemia for their expression of matrix metalloproteinases (MMPs) which are involved in degradation of BMs, leading to disruption of the BBB and hemorrhagic transformation (Hamann, Okada et al. 1995), and abundant proteases that are considered the main causes of neuronal cell death. However, it is under debate whether neutrophil can infiltrate into the ischemic brain or simply accumulate within NVU (Enzmann, Mysiorek et al. 2013, Perez-de-Puig, Miro-Mur et al. 2015).

2.3.5 Adaptive immune responses after ischemic stroke

In the acute phase of ischemia, innate immune cells as well as a subset of effector lymphocytes, such as IL-17 producing **γδ**T cells recognizing nonpeptide antigens, can contribute to early damage (Shichita, Sugiyama et al. 2009). Nevertheless, to initiate cellular immunity during the delayed phase of ischemia, T cells require major histocompatibility complex (MHC)-restricted antigen presentation by APCs and recognition of antigens via highly variant TCRs. Therefore, the activation of adaptive immunity usually is delayed by an interval of 7–10 days, from antigen presentation to

clonal expansion of autoreactive T cells and immune attack on the target organ. $CD4^+$ T cells (MHC class II-restricted) become helper T cells which coordinate and modulate immune responses, while $CD8^+$ T cells (MHC class I restricted) have the actual cytotoxic function following ischemic stroke (Li, Wang et al. 2013). It is the cytokine environment that determines the differentiation and polarization of naïve $CD4^+$ T cells in ischemic brain (Figure 3). Development of Th1 effector cells is promoted by IL-12 produced by activated macrophages. Th1 cells secrete IFN-ɣ and TNF which further stimulate innate and T cell-induced immune responses leading to cytotoxicity. However, T cells can also be protective. TGF-β produced by neurons, glia, microglia and macrophages promotes the development of Treg cells secreting the protective cytokine IL-10 and inhibiting Th1 and Th2 responses. On the other hand, induction of mucosal tolerance with CNS antigens can lead to the establishment of anti-inflammatory Th2 cells producing IL-10 (Frenkel, Huang et al. 2005) and Treg cells producing IL-10 and TGF-β (Gee, Zierath et al. 2009). Therefore, it is more relevant to modulate T cells and evaluate their interconnection with other immune cells and delayed effects on tissue remodeling as well as neurological recovery after stroke.

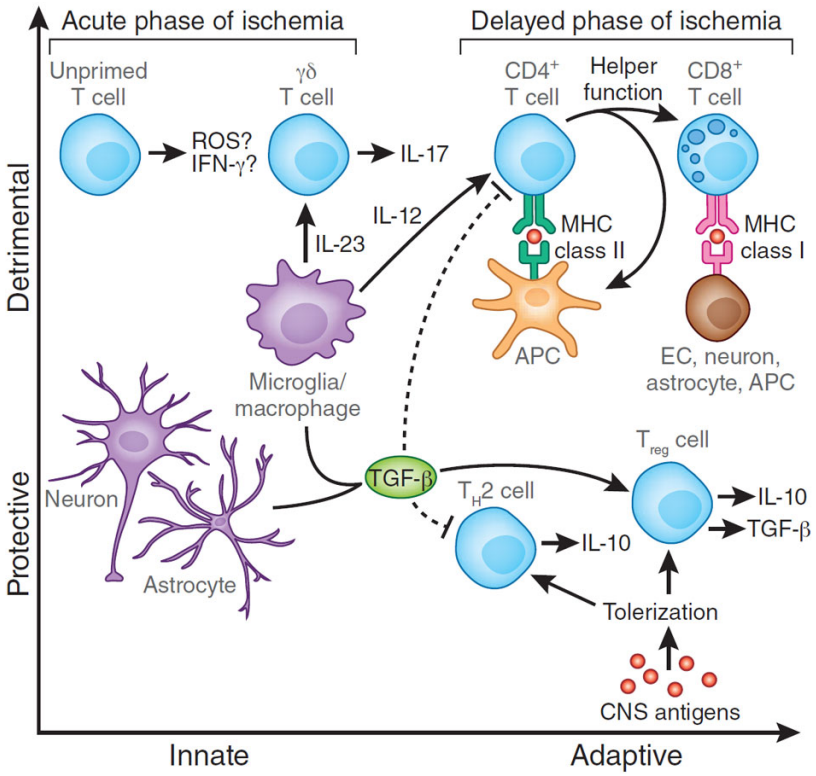

Figure 3. Pro and anti-inflammatory roles of T cells in stroke.
In the acute phase of cerebral ischemia, unprimed T cells and activated microglia/macrophages contribute to tissue damage in an antigen-independent manner (innate immunity). In the delayed phase of ischemia, naïve T cells are activated by APCs and produce inflammatory cytokines which damage the CNS. However, subsets of T cells can also be protective. Adapted from Iadecola, C. and Anrather, J. (2011).

Antigen presentation leads to the development of not only cellular but also humoral immunity directed against the recognized antigens. Antibodies against CNS antigens develop after ischemic stroke (Dambinova, Khounteev et al. 2003). Intrathecal synthesis of immunoglobulins has also been reported in stroke patients (Pruss, Iggena et al. 2012). Data from investigating post-mortem brain slices from stroke patients indicate that activated lymphocytes can chronically accumulate in ischemic brain and are strongly involved in the synthesis of autoreactive immunoglobulins which potentially impairs cognition (Doyle, Quach et al. 2015). Besides stroke-induced autoantibodies, preexisting autoantibodies can also take part in the lesion evolution in ischemic stroke. For example, autoantibody against water channel aquaporin-4 (AQP4) plays a direct pathological role in neuromyelitis optica (NMO) patients. Purified NMO-IgG can exacerbate infarct size in rats treated with 30 min MCAo compared to treatment with immunoglobulins from healthy controls (Juenemann, Braun et al. 2015). A more complex situation is seen with preexisting autoantibodies against the N-methyl-D-aspartate-receptor NMDAR subunit NR1 (NMDAR1). The BBB integrity before an acute ischemic stroke can influence whether autoantibodies against NMDAR1 are beneficial or detrimental for modulating the evolution of infarct size (Zerche, Weissenborn et al. 2015). However the detailed kinetics of B cell infiltration into the ischemic brain and their functional interaction with innate immune cells and T cells have not been fully investigated.

2.4 Modulation of lymphocytes in animal model of ischemic stroke

Lymphocytes, in particular T cells, have been indicated as a key mediator of local inflammation and tissue remodeling in ischemic brain (Brait, Arumugam et al. 2012). Activated lymphocytes are increasingly recognized as a target for anti-inflammatory stroke therapies (Frenkel, Huang et al. 2003). Modulation of T lymphocytes can dramatically influence the outcome after stroke (Iadecola and Anrather 2011). Induction of 90 min MCAo in mice with severe combined immunodeficiency (SCID) lacking T and B cells results in reduction of total infarct volume at 22 hours compared to

WT mice (Hurn, Subramanian et al. 2007). Two papers (Yilmaz, Arumugam et al. 2006, Shichita, Sugiyama et al. 2009) similarly described that in recombination activating gene 1 (RAG1)-deficient mice, the absence of functional T and B cells reduces infarct volume and neurologic deficits at 24 hours after 60 min MCAo, and this protection can be reversed upon reconstitution of $RAG1^{-/-}$ mice with T cells from wild-type littermates. Detailed analysis of lymphocyte subsets revealed that B-cell-deficient mice failed to show improvement following ischemic stroke injury (Yilmaz, Arumugam et al. 2006). However, it was later demonstrated that B cells are critical in governing infarct size and that MCAo-induced changes are prevented in B-cell-deficient (μMT-/-) mice after transfer of highly purified WT B cells, but not IL-10-deficient B cells, implicating IL-10-secreting B cells as a major regulatory cell type in stroke (Ren, Akiyoshi et al. 2011, Chen, Bodhankar et al. 2012, Bodhankar, Chen et al. 2014).

A transgenic approach is quite convenient for an experimental setup but not applicable in clinical practice. Therefore immunomodulators, adoptive transfer and monoclonal antibodies have been tested as potential therapies. Anti-inflammatory Tregs have been targeted in several studies. The cerebroprotective role of Treg with dependence on IL-10 signaling was first reported in acute experimental stroke (Liesz, Suri-Payer et al. 2009). However, a more recent study demonstrated that Tregs might also have a detrimental effect on microvascular thrombus formation in cerebral ischemia (Kleinschnitz, Kraft et al. 2013). Additional research demonstrated that Tregs can accumulate and proliferate up to 30 days after 60 min MCAo but do not promote neurological recovery (Stubbe, Ebner et al. 2013). Modulation of lymphocyte entry into CNS parenchyma has also led to controversial conclusions. The inhibition of leukocyte very late antigen-4 (VLA-4) and endothelial vascular cell adhesion molecule-1 (VCAM-1)-mediated brain invasion by monoclonal antibody (anti-CD49d) against α4 integrin shields the brain against deleterious neuroinflammation after stroke (Liesz, Zhou et al. 2011). But a later study reported that blocking α4 integrin does not protect from acute ischemic stroke in mice (Langhauser, Kraft et al. 2014). Recently, a randomized controlled preclinical study involving several researching groups found that anti-CD49d treatment does not reduce lesion size or affect leukocyte invasion after transient proximal occlusion of the MCA, which induces large lesions (Llovera, Hofmann et al. 2015). These results suggest that infarct severity and localization may determine the benefits of immune-targeted approaches.

It is necessary to point out that earlier dynamic studies (Gelderblom, Leypoldt et al. 2009, Chu, Kim et al. 2014) addressed the infiltration of lymphocytes into ischemic brain occurring three hours after transient cerebral ischemia and reaching its peak around day 3. Therefore, the majority of previous studies in rodents required the modulation of T lymphocytes during the acute phase or even before onset of stroke. However, recent studies (Gronberg, Johansen et al. 2013, Stubbe, Ebner et al. 2013, Romer, Engel et al. 2015) support the fact that due to the prerequisite of CNS antigen drainage (van Zwam, Huizinga et al. 2009, Planas, Gomez-Choco et al. 2012, Urra, Miro et al. 2014) and presentation by APCs to activate naïve lymphocytes in the periphery, massive lymphocyte infiltration occurs during the delayed phase of stroke (between 7 and 14 days), while the early (24 hours) detrimental T cell effects on experimental stroke are related neither to adaptive immunity nor to thrombus formation (Kleinschnitz, Schwab et al. 2010). Along the same line, a new study demonstrated that the pharmacological ablation of B cells, beginning 5 days post injury using anti-CD20 antibody, prevents the appearance of delayed cognitive impairment following experimental stroke (Doyle, Quach et al. 2015). However, modulation of T cells in the delayed phase of stroke and its effects on tissue remodeling or functional recovery are not reported.

3. AIMS OF THE STUDY

$CD4^+$ T cell is the dominant subtype of T cells that infiltrates into the peri-infarct region, and it acts as the interface between cellular and humoral immune responses. $CD4^+$ T cell is also a necessary mediator of autoreactive immune responses and long-term consequences post ischemic stroke. To narrow down the spectrum of CNS antigens related autoreactivity and also use this autoreactivity to harvest more CNS-infiltrating $CD4^+$ T cells for further analysis, 60 min MCAo was induced mainly in 2D2 mice with the majority of $CD4^+$ T cells expressing TCR recognizing myelin oligodendrocyte glycoprotein (MOG) (Bettelli, Pagany et al. 2003). WT mice also received similar procedures since they have an almost normal immune system to investigate stroke-induced autoreactive responses, whereas 2D2 mice are more prone to CNS-autoreactivity. The scope of my doctoral thesis focuses on investigating whether delayed depletion of $CD4^+$ T cells affects tissue remodeling and functional recovery after ischemic stroke. To elucidate this, the following key questions were addressed:

1. When do $CD4^+$ T cells massively infiltrate into ischemic brain parenchyma following 60 min MCAo in 2D2 mice? Does the accumulation of $CD4^+$ T cells temporally correlate with deposition of fibrotic ECMs within infarction?

2. Is delayed $CD4^+$ depletion using monoclonal antibody able to prevent entry of $CD4^+$ T cells into the ischemic brain? Does $CD4^+$ depletion influence tissue remodeling and motor recovery after stroke, and if so, how?

3. Does delayed CD4 depletion affect local phagocytes and CNS infiltrating immune cells in stroke-induced 2D2 mice? Does the same effect exist in WT mice after ischemic stroke?

4. When and how do B cells infiltrate the ischemic brain? Is there an autoreactive antibody-response in the ischemic brain after stroke? Does B cell accumulation have any impact on cognitive impairment following ischemic stroke?

4. MATERIALS AND METHODS

4.1 Materials

4.1.1 Animals

Strain	Provider
C57Bl/6J	Charles River Laboratories, Sulzfeld, Germany
2D2 TCR strain name: C57BL/6-Tg (Tcra2D2,Tcrb2D2)1Kuch/J stock number: 006912	The Jackson Laboratory, Bar Harbor, ME, USA

4.1.2 Veterinary drugs and chemicals for in vivo application

Name	Provider
2% Xylocain gel	AstraZeneca GmbH, Wedel, Germany
2.5% enrofloxacin	Baytril, Leverkusen, Germany
Bromdesoxyuridin (BrdU), 10mg/ml	BD Biosciences, Franklin Lakes, NJ, USA
Heparin-Rotexmedica 25000 I.E./5 ml	ROTEXMEDICA GmbH, Trittau, Germany
*InVivo*MAb anti-mouse CD4 (Clone: GK1.5)	Bio X Cell, West Lebanon, NH, USA
*InVivo*MAb Rat IgG2b Isotype control (Clone: LTF-2)	Bio X Cell, West Lebanon, NH, USA
Isoflurane	Forene, Abbott, Wiesbaden, Germany
Isotonic saline (0.9%)	Fresenius Kabi Deutschland GmbH, Bad Homburg, Germany
Ketamine	Deltaselect, Dreieich, Germany
MARBOCYL 10%	Vetoquinol GmbH, Ravensburg, Germany
Xylazine	Bayer Vital, Leverkusen, Germany

4.1.3 Chemicals

Name	Provider
1,4-Diazabicyclo[2.2.2]octane (DABCO)	Carl Roth GmbH-Co. KG, Karlsruhe, Germany
2-methylbutan	Carl Roth GmbH-Co. KG, Karlsruhe, Germany
2-propanol	Carl Roth GmbH & Co. KG, Karlsruhe, Germany
4',6-diamidino-2-phenylindole (DAPI)	Invitrogen, Life Technologies GmbH, Darmstadt, Germany
Agarose	Carl Roth GmbH & Co. KG, Karlsruhe, Germany

BD FACS™ Lysing Solution	BD Pharmingen, Franklin Lakes, NJ, USA
Bovine serum albumin (BSA) fraction V	Sigma-Aldrich, St Louis, MO, USA
Chloroform	Carl Roth GmbH-Co. KG, Karlsruhe, Germany
Diethyl pyrocarbonate (DEPC)	ThermoFisher Scientific Inc., Waltham, MA USA
Disodium phosphate	Sigma-Aldrich, St Louis, MO, USA
D(+)-sucrose	Carl Roth GmbH-Co. KG, Karlsruhe, Germany
Ethanol	Rotipuran, Carl Roth GmbH & Co. KG, Karlsruhe, Germany
Ethylene glycol	Sigma-Aldrich, St Louis, MO, USA
Glycerol	Merck, Darmstadt, Germany
Paraformaldehyde (PFA)	Sigma-Aldrich, St Louis, MO, USA
Red blood cell (RBC) lysis buffer	QIAGEN GmbH, Hilden, Germany
Sodium azide	Carl Roth GmbH-Co. KG, Karlsruhe, Germany
Sodium dihydrogen phosphate monohydrate	Sigma-Aldrich, St Louis, MO, USA
Tissue-Tek O.C.T Compound	Sakura Finetek Europe B.V. KvK, Leiden, V.A.T., Netherlands
Triton X	LABORAT GmbH, Germany
Tween-20	Carl Roth GmbH-Co. KG, Karlsruhe, Germany

4.1.4 Cell culture media and supplements

Name	Provider
Ampuwa distilled water	Fresenius Kabi Deutschland GmbH, Bad Homburg, Germany
Easycoll gradient	Biochrom AG, Berlin, Germany
Fetal calf serum (FCS Gold)	PAA Laboratories, Pasching, Austria
Gibco® PBS (10X), without Ca & Mg, pH 7.4	Thermo Fisher Scientific Inc., Waltham, Massachusetts, USA
L-alanyl-L-glutamine	Biochrom AG, Berlin, Germany
Normal goat serum	BIOZOL Diagnostica Vertrieb GmbH, Germany
Penicillin-streptomycin	Biochrom AG, Berlin, Germany
Dulbecco's PBS (1x), without Ca & Mg	PAA Laboratories, Pasching, Austria
Roswell Park Memorial Institute (RPMI) 1640 Medium, w/o L-Glutamine	Biochrom AG, Berlin, Germany

Dulbecco's MEM (DMEM) Liquid Medium With 1.0 G/L D-Gluocose, w/o L-Glutamine	Biochrom AG, Berlin, Germany
Trypan blue 0.5%* in physiol. saline	Biochrom AG, Berlin, Germany

4.1.5 Polymerase chain reaction (PCR) primers and reagents

Name	Provider
PCR primers	
β-actin 5': ACCCACACTGTGCCCATCTA	EuroFins MWG Operon, Ebersberg, Germany
β-actin 3': GCCACAGGATTCCATACCCA	EuroFins MWG Operon, Ebersberg, Germany
BDNF 5': GGCTAAGTGGAGCTGACATAC	EuroFins MWG Operon, Ebersberg, Germany
BDNF 3': CACTGTTAGGTAATGTAGGCAC	EuroFins MWG Operon, Ebersberg, Germany
ColI 5': CCTCCAGGTCCCAAGGGTAAC	EuroFins MWG Operon, Ebersberg, Germany
CXCL13 5': TACGCCCCCTGGGAATGGCT	EuroFins MWG Operon, Ebersberg, Germany
CXCL13 3': AGTGGCTTCAGGCAGCTCTTCT	EuroFins MWG Operon, Ebersberg, Germany
ColI 3': GGCTCCTCGTTTTCCTTCTTCTCC	EuroFins MWG Operon, Ebersberg, Germany
CCR2 5': GATCCTGCCTCCACTCTACTC	EuroFins MWG Operon, Ebersberg, Germany
CCR2 3': GCATAGTGAGCCCAGAATG	EuroFins MWG Operon, Ebersberg, Germany
NGF 5': GGTTTTGCCAAGGACGCAGC	EuroFins MWG Operon, Ebersberg, Germany
NGF 3': GCTGAAGTTTAGTCCAGTGGG	EuroFins MWG Operon, Ebersberg, Germany
PDGFRβ 5': GGGAGACACTGGGGAATAC	EuroFins MWG Operon, Ebersberg, Germany
PDGFRβ 3': GTCTCAGTGACATCCGTGAC	EuroFins MWG Operon, Ebersberg, Germany
Reep5 3': CTGATAGGT TTC GGATACCCAG	EuroFins MWG Operon, Ebersberg, Germany
Reep5 5': GACTCGTGCTTGAGGAAGATAG	EuroFins MWG Operon, Ebersberg, Germany
TGFβ1 5': CGTTACCTTGGTAACCGGCTG	EuroFins MWG Operon, Ebersberg, Germany
TGFβ1 3': GCTGATCCCG TTGATTTC	EuroFins MWG Operon, Ebersberg, Germany
VEGFa 5': GCTGTAACGATGAAGCCCTGG	EuroFins MWG Operon, Ebersberg, Germany
VEGFa 3': GGTCTGCATTCACATCTGC	EuroFins MWG Operon, Ebersberg, Germany
PCR reagents	
2-Log DNA ladder (0.1-10.0 kb)	NEB, Frankfurt am Main, Germany
dNTPs	Roche, Mannheim, Germany
LightCycler® 2.0	Roche, Mannheim, Germany
LightCycler® FastStart DNA Master SYBR Green I	Roche, Mannheim, Germany
NucleoSpin RNA clean-up KIT (740948.250)	Machery-Nagel GmbH&Co. KG, Düren, Germany

M-MLV-RT 200U/ul	Promgea, Madison, USA
M-MLV-RT reaction buffer 5x	Promgea, Madison, USA
RNA-Sin 40U/ul	Promgea, Madison, USA
RQ1 RNase-free DNase	Promgea, Madison, USA
RQ1 RNase-free DNase 10x reaction buffer	Promgea, Madison, USA
TRIzol® Reagent	ThermoFisher Scientific Inc., Waltham, USA

4.1.6 Fluorescence-activated cell sorting (FACS) staining panel for phenotyping 2D2 mice

Antibody	Conjugation	Clone	Per 100ul	Provider
IgG2α κ chain	APC	-	1ul	BD Pharmingen, Franklin Lakes, NJ, USA
IgG2β κ chain	PE	-	1ul	BD Pharmingen, Franklin Lakes, NJ, USA
Rat anti-Vβ11	PE	RR3-15	1ul	BD Pharmingen, Franklin Lakes, NJ, USA
Rat anti-CD4	APC	RM4-5	1ul	BD Pharmingen, Franklin Lakes, NJ, USA

4.1.7 FACS staining panel for proliferation study

Antibody	Conjugation	Clone	Per 100ul	Provider
Rat anti-CD45	PE-Cy7	30F11	0.5ul	BD Pharmingen, Franklin Lakes, NJ, USA
Rat anti-B220	PerCP	RA3-6B2	0.5ul	BD Pharmingen, Franklin Lakes, NJ, USA
Rat anti-CD4	A700	GK1.5	0.5ul	BioLegend, San Diego, CA, USA
Rat anti-CD44	APC-Cy7	IM-7	0.5ul	BD Pharmingen, Franklin Lakes, NJ, USA
Rat anti-CD8a	PB	53-6.7	0.5ul	BD Pharmingen, Franklin Lakes, NJ, USA
Rat anti-Vα3.2	APC	RR3-16	1ul	BD Pharmingen, Franklin Lakes, NJ, USA
Rat anti-Vβ11	PE	RR3-15	1ul	BD Pharmingen, Franklin Lakes, NJ, USA
Anti-BrdU	FITC	BU20A	1ul	eBioscience, San Diego, CA, USA

4.1.8 FACS staining panel for CD4 depletion study

Antibody	Conjugation	Clone	Per 100ul	Provider
Rat anti-CD45	PE-Cy7	30-F11	0.25ul	BD Pharmingen, Franklin Lakes, NJ, USA
Rat anti-CD19	FITC	1D3	0.25ul	BD Pharmingen, Franklin Lakes, NJ, USA
Rat anti-B220	PO	RA3-6B2	0.5ul	Life Technologies, Darmstadt, Germany

Rat anti-CD3ε	APC	145-2C11	0.5ul	BD Pharmingen, Franklin Lakes, NJ, USA
Rat anti-CD3ε	FITC	145-2C11	0.5ul	BD Pharmingen, Franklin Lakes, NJ, USA
Rat anti-CD3ε	PerCP-Cy5.5	17A2	1.25ul	BioLegend, San Diego, CA, USA
Rat anti-CD16/32	-	2.4G2	0.5ul	BD Pharmingen, Franklin Lakes, NJ, USA
Rat anti-CD11b	PE-TR	M1/70.15	0.25ul	Life Technologies, Darmstadt, Germany
Rat anti-CD4	A700	GK1.5	0.25ul	BioLegend, San Diego, CA, USA
Rat anti-CD44	APC-Cy7	IM7	0.25ul	BD Pharmingen, Franklin Lakes, NJ, USA
Rat anti-CD8α	APC-Cy7	53-6.7	0.5ul	BD Pharmingen, Franklin Lakes, NJ, USA
Rat anti-CD8α	PB	53-6.7	0.25ul	BD Pharmingen, Franklin Lakes, NJ, USA
Rat anti-CD138	PE	281-2	0.25ul	BioLegend, San Diego, CA, USA
Rat anti-Foxp3	PE	FJK-16s	1ul	eBioscience, San Diego, CA, USA
Mouse Anti-Human Ki67	FITC	MOPC-21	12ul	BD Pharmingen, Franklin Lakes, NJ, USA

*For surface staining of blood samples, amount of antibody was doubled.

4.1.9 FACS staining panel for B cell kinetic study

Antibody	Conjugation	Clone	Per 100ul	Provider
Rat anti-CD45	AF 700	30F11	1ul	BioLegend, San Diego, CA, USA
Rat anti-CD19	FITC	6D5	1ul	BioLegend, San Diego, CA, USA
Rat anti-CD93	PE	AA4.1	2ul	eBioscience, San Diego, CA, USA
Rat anti-CD23	PE-Cy7	B3B4	1ul	eBioscience, San Diego, CA, USA
Rat anti-CD21	PB	4E3	1ul	eBioscience, San Diego, CA, USA
Rat anti-CD138	V605	281-2	0.5ul	BioLegend, San Diego, CA, USA
Rat anti-IgD	APC-Cy7	11-26C	1ul	eBioscience, San Diego, CA, USA
Rat anti-IgM	PerCP-Cy5.5	RMM-1	1ul	BioLegend, San Diego, CA, USA
Rat anti-CD3ε	APC	17A2	1ul	eBioscience, San Diego, CA, USA
Rat anti-CD11b	APC	M1/70	1ul	eBioscience, San Diego, CA, USA
Rat anti-Gr1	APC	RM6-8C5	1ul (1:40 predilution)	DRFZ, Berlin, Germany

4.1.10 Antibodies for immunofluorescent microscopy

Antibody	Clone	Dilution	Provider
Primary antibodies			
Goat anti-CXCL 13	AF470	1:50	R&D, Minneapolis, MN, USA
Mouse anti-NeuN	A60	1:200	Merck, Darmstadt, Germany
Rabbit anti-CD3	Polyclonal	1:200	Abcam, Cambridge, UK
Rabbit anti-collagen type I	Polyclonal	1:200	Merck, Darmstadt, Germany
Rabbit anti-laminin 1+2	Polyclonal	1:400	Abcam, Cambridge, UK
Rabbit anti-Ki67	Polyclonal	1:200	Abcam, Cambridge, UK
Rat anti-CD4	L3T4	1:200	BD Biosciences, Franklin Lakes, NJ, USA
Rat anti-CD140b PDGF Receptor b)	APB5	1:200	eBioscience, San Diego, CA, USA
Rat anti-CD13	ER-BMDM1	1:200	Bio-Rad, Puchheim, Germany?
Rat anti-CD68	FA-11	1:200	Bio-Rad, Puchheim, Germany
Rat anti-CD45RO/B220, Alexa Fluor® 488 conjugated	RA3-6B2	1:200	BioLegend, San Diego, CA, USA
Secondary antibodies			
Donkey anti-goat, Alexa Fluor® 594		1:400	Life Technologies, Darmstadt, Germany
Goat anti-rat, Alexa Fluor® 488		1:400	Life Technologies, Darmstadt, Germany
Goat anti-rat, Alexa Fluor® 594		1:400	Life Technologies, Darmstadt, Germany
Goat anti-rabbit, Alexa Fluor® 488		1:400	Life Technologies, Darmstadt, Germany
Goat anti-rabbit, Alexa Fluor® 568		1:400	Life Technologies, Darmstadt, Germany
Goat anti-rabbit, Alexa Fluor® 594		1:400	Life Technologies, Darmstadt, Germany
Goat anti-mouse Oregon Green® 488		1:400	ThermoFisher, Waltham, MA USA

4.1.11 Commercial kits

Name	Provider
Anti-Mouse/Rat Foxp3 Staining Set PE	eBioscience, San Diego, CA, USA
FITC BrdU Flow Kit	BD Biosciences, Franklin Lakes, NJ, USA
Mouse CXCL13/BLC/BCA-1 DuoSet ELISA	R&D, Minneapolis, MN, USA
Mouse on Mouse (M.O.M. ™) Fluorescein Kit	Vector Laboratories, Burlingame, CA, USA

4.1.12 Laboratory consumables

Name	Provider
0.19±0.01 mm diameter silicon-rubber-coated monofilament	Doccol Corporation, MA, USA
100-µm, 70-µm, 40-µm cell strainer	BD Falcon, Franklin Lakes, NJ, USA
14ml BD Falcon™ round-bottom tube, snap cap	BD Falcon, Franklin Lakes, NJ, USA
15ml, 50ml BD Falcon™ tube, dome-seal screw cap	BD Falcon, Franklin Lakes, NJ, USA
1ml, 2ml, 5ml syringe	BD Discardit, Franklin Lakes, NJ, USA
35x10 (mm) tissue culture dish	BD Falcon, Franklin Lakes, NJ, USA
48-well cell culture plate	Falcon (Franklin Lakes, NJ, USA)
5ml, 10ml, 25ml BD Falcon™ serological pipets, individually wrapped	BD Falcon, Franklin Lakes, NJ, USA
BD Falcon™ 12x75(mm) tube with and without cell strainer cap	BD Falcon, Franklin Lakes, NJ, USA
BD Vacutainer® spray-coated K_2EDTA tube, 13x75 (mm)	BD Biosciences, Franklin Lakes, NJ, USA
BD Vacutainer® Plus Plastic Serum Tubes, 13x75 (mm)	BD Biosciences, Franklin Lakes, NJ, USA
CountBright™ Absolute Counting Beads, for flow cytometry	ThermoFisher Scientific Inc., Waltham, MA USA
Fuchs-Rosenthal chamber (depth 0.200mm, area 0.0625mm^2)	Paul Marienfeld GmbH & Co. KG; Lauda-Königshofen, Germany
Eppendorf® Safe-Lock microcentrifuge tubes, 1.5 mL	Eppendorf, Köln, Germany
LightCycler® Capillaries (20ul)	Roche, Mannheim, Germany
Low Profile 819 Disposable Blades	Leica, Wetzlar, Germany
Microscope slides (SuperFrost Plus)	R. Langenbrinck, Emmendingen, Germany
Pur-Zellin cotton pads	Paul Hartmann AG, Heidenheim, Germany
Sterile scalpel #21	B.Braun AESCULAP, Tuttlingen, Germany
Stainless Steel Beads, 5 mm	QIAGEN GmbH, Hilden, Germany
Transfer pipette 3.5ml, individually wrapped, sterile	Sarstedt AG & Co, Nümbrecht, Germany

4.1.13 Laboratory equipment

Name	Provider
1H (300 MHz) mouse head surface radiofrequency (RF) coil	RAPID Biomedical GmbH, Rimpar, Germany
20 mm diameter quadrature transmit/receive mouse head volume resonator	RAPID Biomedical GmbH, Rimpar, Germany
7T Bruker PharmaScan 70/16 magnet	Bruker BioSpin, Ettlingen, Germany
CasyTon cell counter	Casy-Technology, Innovatis AG, Reutlingen, Germany
CatWalk^{TM} XT system	Noldus Information Technology, Wageningen, The Netherlands
Centrifuge, Universal 30 RF	Thermo Electron, Oberhausen, Germany
Centrifuge 5804 R	Eppendorf, Köln, Germany
Electrophoresis chamber Criterion	Bio-Rad, Munich, Germany
Fluorescence microscope, DMRA2	Leica, Wetzlar, Germany
Eppendorf 5810R centrifuge	Eppendorf, Köln, Germany
Fluorescence microscope, DMI 6000B	Leica, Wetzlar, Germany
FACSCanto II flow cytometer	BD Pharmingen, Franklin Lakes, NJ, USA
Homoeothermic blanket system	Harvard Apparatus, Holliston, MA, USA
LC Carousal centrifuge 2.0	Roche Diagnostics, Indianapolis, IN, USA
Lightcycler 2.0	Roche, Mannheim, Germany
Leica confocal microscope	Leica TCS SPE, Nussloch, Germany
LSR II flow cytometer	BD Pharmingen, Franklin Lakes, NJ, USA
Mastercycler gradient	Eppendorf , Köln, Germany
Microtome MICROM HM 330	Thermo Scientific, Waldorf, Germany
Mini Rocking Platform, Biometra WT 17	Biometra GmbH, Göttingen, Germany
NanoDrop ND2000 spectrophotometer	Thermo Scientific, Asheville, NC, USA
pH 522 pH-meter	Wissenschaftlich-Technische Werkstätten GmbH, Weilheim, Germany
SpectraMax 190 Microplate Reader	Molecular Devices, LLC., Sunnyvale, CA, USA
Recovery box	MediHEAT PecoServives Ltd. Brough, Cumbria, UK
RET-3 rectal probe for mice	Physitemp Instruments Inc., Clifton, NJ, USA
Rodent Brain Matrix – Mouse, Adult 30g, Coronal Sections	ASI Instruments, Inc., Warren, MI, USA

Sliding microtome	Leica SM2000R, Nussloch, Germany
Thermomixer 5436 heating block	Eppendorf Vertrieb Deutschland GmbH, Hamburg, Germany
TissueLyser LT	QIAGEN GmbH, Hilden, Germany
TissueLyser Bead Dispensers	QIAGEN GmbH, Hilden, Germany
Vet ABC Animal blood counter	scil animal care company GmbH, Viernheim, Germany

4.1.14 Analytical software

Name	Provider
Bruker Paravision 6.0	Bruker BioSpin, Ettlingen, Germany
CasyTon cell counter and analyser system	Innovatis AG, Reutlingen, Germany
FACSDiva 6.1.3	BD Pharmingen, Franklin Lakes, NJ, USA
FlowJo 10.0.8r1	Tree Star, Ashland, OR, USA
ImageJ	ImageJ 1.42q Wayne Rasband, NIH, Bethesda, USA
LightCycler Software (build 4.1.1.21)	Roche Molecular Biochemicals, Basel, Switzerland
LEICA LAS AF Lite	Leica, Wetzlar, Germany
Mayo Clinic Analyze 5.0	Biomedical Imaging Resource, Analyze Direct, Overland Park, KS, USA
Noldus software for CatWalk	Noldus Information Technology, Wageningen, The Netherlands
Stereo Investigator software®	MBF Bioscience, VT, USA
GraphPad Prism 6.0	GraphPad, San Diego, CA, USA
IBM SPSS Statistics 25 for Windows	IBM Somers, NY, USA

4.2 Methods

4.2.1 Animal experiments

4.2.1.1 Animals and Housing

Gender-mixed WT C57BL/6J mice (10-12 weeks old) and MOG TCR transgenic 2D2 mice (see 4.1.1) with C57BL/6J background (10-16 weeks old) were used in this study. Animals were randomly assigned either to a control group or CD4 depletion group. Animals with different treatments were mixed in a cage and housed at the Charite animal facility with a 12 h light/dark cycle (lights on between 6:00 and 18:00). Cages were lined with chip bedding, enriched with a mouse tunnel and igloo (Plexx BV). Mice had ad libitum access to food (standard chow) and water (where study design indicates, water was replaced with an antibiotic solution). After MCAo surgery, enrichment was removed and for the first three post-operative days soft pellet food (standard chow softened with water/antibiotic solution) was given in addition. All animal experiments were conducted in accordance with the European Community Council Directives 86/609/EEC and German national laws and approved by the local authority (Landesamt für Gesundheit und Soziales, Berlin, Germany).

4.2.1.2 Middle cerebral artery occlusion

MCAo was performed adhering to the standard operating procedures of the laboratory (Engel, Kolodziej et al. 2011). In brief, anesthesia was induced with 2.5% isoflurane (Forene, Abbott) in 1:2 mixtures of O_2 / N_2O and maintained at 1.0%–1.5% isoflurane. Silicon rubber-coated monofilament with a diameter of 0.19 ± 0.01 mm (Doccol) was introduced into the common carotid artery, advanced along the internal carotid artery towards the origin of the MCA, and either withdrawn immediately to allow instant reperfusion (sham operation) or left there for 60 min. For reperfusion, the inserted filament was withdrawn and the internal carotid artery was ligated in mice under anesthesia. Body temperature was maintained with a heating pad. A drop of 2% Xylocain gel was applied to the wound for pain relief. Success of MCAo was verified using the modified Bederson score (Bederson, Pitts et al. 1986). Animals were randomly allocated into different operators. After surgery, animals were allowed to recover in a heated cage before returning to their home cages. Animals with unsuccessful stroke, as confirmed by MRI assessment or death on the day of operation, were excluded.

4.2.1.3 T2-weighted Magnetic Resonance Imaging (MRI) for infarct size determination

To quantify the ischemic lesion, animals were subjected to a T2-weighted MRI at 24 h and 7 days after MCAo. Anesthesia was induced at 2.0% isoflurane in O_2 / N_2O mixture (1:2) and maintained at 1.0%-1.5% isoflurane through a vaporizer and delivered through a face mask. Body temperature was kept stable at 36.5±0.5 °C with a heating pad. Respiratory rate was monitored with the Small Animal Monitoring and Gating System. The mouse's head was fixed in a magnet bore. Axial T2-weighted images were obtained using a 7T Bruker PharmaScan 70/16 magnet with a 20 mm diameter quadratum transmit/receive mouse head volume resonator radiofrequency coil and Bruker Paravision 6.0 software using Rapid Acquisition with Relaxation Enhancement (RARE) sequence (TE 36 ms, TR 4200 ms, FOV 28 mm, 20 contiguous slices with a thickness of 500 µm and interslice distance 500 µm, matrix=256 × 256, field of view=25.6 mm x 25.6 mm, repetition time=4200 ms, echo time=36 ms, RARE factor=8, 6:43 min). Axial slices covered the distance between the olfactory bulb and the cerebellum. Acquired images were analyzed semi-automatically with Mayo Clinic Analyze software version 5.0. The volume difference between the contralateral hemisphere and non-infarcted ipsilateral hemisphere was divided by the volume of the whole ipsilateral hemisphere. The calculated percentage was expressed as edema-corrected infarct size. Mice with an infarct size less than 5% were excluded from the final analysis.

4.2.1.4 Drug and antibody treatment

To minimize the influence of infection on stroke-induced autoreactivity and outcome parameters (Hetze, Engel et al. 2013), preventive antibiotic marbofloxacin (5mg/kg, diluted in saline to 1mg/ml, prepared fresh daily) was administered 24 h before and until day 6 after MCAo. Alternatively, in some experiments preventative antibiotic enrofloxacin (diluted in drinking water at 0.35 mg/ml) was administered 24 h before and until day 7 after MCAo. In addition, mice received 10 mg/kg of enrofloxacin injected intraperitoneally (i.p.) once a day for the first 3 days after MCAo. On day 3, mice were randomly allocated into either the CD4 depletion (clone GK1.5) group or the isotype control (clone LTF-2) group. On the same day, mice in the CD4 depletion group received intraperitoneal (i.p.) injection of 200ug CD4 depleting antibody (diluted in sterile PBS at 1mg/ml). Three more injections were administered on days 5, 7 and 9 after MCAo. In total, one mouse received 800ug CD4 depleting antibody to eliminate $CD4^+$ T cells in the blood circulation and

secondary lymphoid organs. The control group received only the same amount of isotype control antibody (diluted in sterile PBS at 1mg/ml) according to the same injection scheme.

For mice undergoing analysis of cellular proliferation, 100ul 10mg/mL solution of BrdU diluted in sterile 1X DPBS (BD) was injected i.p. into each animal 2 hours before sacrifice.

4.2.1.5 Neurological Deficit Score (De Simoni)

The Neuroscore was performed blindly as described (Orsini, Villa et al. 2012), 3 days before and 3, 7 and 13 days after MCAo or sham surgery when necessary. This test was used to evaluate the general health status and focal neurological malfunction after MCAo. The score ranges from 0 (no deficits) to 56 (representing the worst performance in all items). The Neuroscore results include the following general deficits: fur (0-2), ears (0-2), eyes (0-4), posture (0-4), spontaneous activity (0-4), and epileptic behavior (0-12); and the focal deficits: body symmetry (0-4), gait (0-4), climbing on a surface inclined at 45° (0-4), circulating behavior (0-4), front-limb symmetry (0-4), compulsory circulating behavior (0-4) and whisker sensation to light touch (0-4). The sum of all items was calculated to measure the general and focal deficits of each animal.

4.2.1.6 Catwalk and gait analysis

Quantitative gait analysis is useful for objective assessment of walking ability and exploring new parameters as targets for neuroprotective treatment. Catwalk^{TM} XT is a computer-assisted automated gait analysis system which was originally developed as a tool to enhance assessment of functional outcome in spinal cord injury (SCI) models (Hamers, Koopmans et al. 2006). It has also been reported as a promising tool to assess mid to long-term outcome in experimental stroke (Hetze, Romer et al. 2012). Animals were trained on three consecutive days before baseline measurement. They acquired a minimum of 3 compliant runs, fulfilling a minimum run duration of 0.5s, maximum run duration of 5s, and a maximum speed variation of 60%. Runs were excluded if an animal turned, and the animal was given another try. A second measurement was carried out at 10 days after MCAo to monitor mid-term recovery. Data was analyzed using the Catwalk XT software according to the manufacturer's instructions.

Gait parameters can be classified into three main categories (Hamers, Koopmans et al. 2006): parameters related to (a) individual paws, such as width and length of a paw print, duration of paw

contact, the pressure caused by a paw, etc. (b) the position of footprints, for instance relative print position, stride length and base of support and (c) the time-dependent relationship between footprints, such as phase dispersion and support formula. A summary of impairments in the right hind limb was designed post hoc. Reductions in maximal contact area, normalized swing speed, stand and stride length of the right hind limb were summed as an overall impairment score. For each item, only reduction got one point.

4.2.1.7 Y maze and memory evaluation

Spatial working memory performance of mice was assessed using the Y maze test (Maurice, Hiramatsu et al. 1994). This test is based on the natural tendency of mice to explore novel environments more than familiar ones. Accordingly, mice with intact working memory alternate among different arms of the maze during subsequent entries. Spontaneous alternation behavior during an 8-minute session was recorded on day -1, day 13 and day 48 after 60 min MCAo. The wooden maze, painted black, consisted of three arms positioned at 120° to each other (arm dimensions: 40cm long, 10.5 cm high and 3 cm wide). The test was performed in a testing room with diffused dim light (35 lux) to provide a less anxiogenic environment. Each mouse was placed at the end of one arm and allowed to move freely throughout the duration of the test. An entry was considered complete when all four limbs crossed a line located 6.5 cm from the arm entrance. The series of arm entries were recorded by video camera (Panasonic, CCTV camera), and alternation was defined as successive entries into three different arms in overlapping triplet sets. The percentage of alternation was calculated as a ratio of performed to total possible alternations multiplied by 100. Before and after testing each animal, the maze was cleaned thoroughly with Decosept AF to minimize influence of odor trails from previous animal.

Induction of stroke with extensive lesions can reduce mice's overall locomotor activity, which can be a confounding factor in a memory test that requires motor activity. For this reason, mice that performed less than 12 entries during an 8-minute session were excluded from the final analysis.

4.2.1.8 Multiple collections of blood from living animals

Methods for obtaining blood samples from mice are generally difficult. In order to get multiple blood samples from living animals, submandibular bleeding of mice using a lancet (Golde, Gollobin et al. 2005) was used in this study. The blood collection tubes, either with anti-coagulant

ethylenediaminetetraacetic acid (EDTA) (blood sample for harvesting leukocytes) or without EDTA (blood sample for harvesting serum), were used to collect approximately 100ul blood. After blood collection, a sterile gauze pad was simply applied with a little compression for less than a minute to stop the bleeding. After release, the mice groomed themselves and within a short time showed no evidence of the blood draw.

Blood was left to clot undisturbed at room temperature. 30 minutes later, the clot was removed by centrifuging at 1000g for 10 minutes in a refrigerated centrifuge. Following centrifugation, the liquid component (serum) was immediately transferred to a clean 1.5ml polypropylene tube. The samples were maintained at 4°C while handling. If the serum was not analyzed immediately, the serum was stored at –20°C.

4.2.1.9 Perfusion and tissue processing

At the endpoint of the study, mice were deeply anesthetized with an intraperitoneal injection of ketamine (150mg/kg, Deltaselect) and Xylazine (15mg/kg, Bayer Vital) diluted with 0.9% NaCl. Mice were laid on their back and fixed on a board. Body and fur were cleaned with 70% ethanol before abdominal incision. Under sterilized condition, up to 500ul whole blood was collected from the inferior vena cava using a 1ml syringe and placed into a blood collection tube without anticoagulants. Spleen, thymus, lymph nodes (cervical, lumbar and mesenteric) were removed and kept in Phosphate Buffered Saline (PBS, dilute 10x stock solution with sterilized water, GIBCO^{TM}) on ice.

Each animal was then transcardially perfused with 20ml of ice-cold PBS at 80cm water height. After careful removal of the skull, the whole brain was dissected without the cerebellum and kept in ice-cold complete Roswell Park Memorial Institute (RPMI) 1640 medium (medium supplemented with 10% fetal calf serum (FCS), 50U/ml penicillin, 50ug/ml streptomycin, 2mM L-alanyl-L-glutamine). The tissue was processed immediately. For the experiment designed for immunohistochemistry, perfusion was first done with 20ml ice-cold saline, followed by 20ml ice-cold 4% paraformaldehyde (PFA) in 0.1 M Sörensen buffer (consisting of 80 mM disodium phosphate, 20 mM sodium dihydrogen phosphate monohydrate in distilled water; pH 7.4) per animal. Brains were collected and post-fixed overnight in 4% PFA. After a short rinse in PBS, the fixed brains were transferred to 30%

D (+)-sucrose solution in 0.1M Sörensen buffer for cryoprotection. After 3 days, when the brains had totally sunk to the bottom, they were snap-frozen using 2-methylbutan (Carl Roth) and dry ice.

4.2.2 Molecular, immunological and immunohistochemistry methods

4.2.2.1 Isolation of leukocytes from spleen, lymph node, brain and blood

Brains, stored in complete RPMI 1640 medium, were transferred to 35 mm-diameter tissue culture dishes containing the same medium. Brains were separated into the ipsilateral and contralateral hemispheres using a sterile scalpel. Each hemisphere was pressed through a 70 µm pore-size cell strainer into a 50 ml Falcon tube filled with complete RPMI 1640 medium using a 2-ml syringe stamp. The same procedure was repeated until the medium, refilled in strainer, became clear. Cell suspension was washed once with complete RPMI 1640 medium by centrifugation at 1500 rpm at room temperature (RT) for 10 min. 6 ml single-cell suspension with 35% Easycoll gradient prepared in complete RPMI 1640 medium was cautiously pipetted using only gravity onto 4 ml 70% Easycoll gradient. After centrifugation at 2400 rpm and RT without brake for 30 min, the interface with mononuclear cells (MNCs) between two gradients was isolated. After washing isolated cells once again with complete medium, a small portion of MNCs were stained with Trypan Blue dye and counted under a light microscope using a Fuchs-Rosenthal chamber.

Spleens and lymph nodes were forced through a 100 µm pore-size cell strainer with a 2-ml syringe stamp and washed once with complete RPMI 1640 medium. Erythrocytes in the spleen were lysed during 2 min incubation of cell pellets with RBC lysis solution and occasional shaking with fingers. After resuspension with complete medium, splenocytes and lymphocytes were pipetted through a 40 µm pore-size cell strainer and washed once again. Splenocytes were quantified with automated CasyTon cell counter (with a program configured for counting mice splenocytes). Lymphocytes from lymph nodes were counted using the Trypan Blue method described above.

The peripheral blood was collected either by submandibular bleeding, as described, (Golde, Gollobin et al. 2005) from living animals (baseline and any intermediate time points) or from the inferior vena cava in deeply anesthetized mice at the endpoint. In both cases, whole blood was immediately collected into K_2EDTA-coated blood collection tubes with occasional shaking to prevent coagulation and placed at RT until FACS staining on the same day. All cells were washed

once again with FACS buffer containing 2% FCS in sterile PBS before following staining procedure for flow cytometry.

4.2.2.2 FACS analysis

4.2.2.2.1 FACS analysis of peripheral blood for phenotyping 2D2 mice

Blood samples from 2D2 mice were collected into EDTA-coated tubes and transferred at RT from the animal facility to the lab. Phenotyping using FACS was done on the same day. Erythrocytes were lysed with 1ml 1x Pharm Lyse lysis buffer (diluted in distilled water) per 50 ul blood sample using vortex. After 10 min of incubation at RT, samples were centrifuged at 1500rpm at RT for 5 min. After removal of supernatant, cell pellets were resuspended in 200 ul FACS buffer (PBS with 2% FCS + 15.4 mM sodium azide) and transferred to a new FACS tube filled with 2 ml FACS buffer. After centrifugation at 1500 rpm at 4°C for 5 min and removal of supernatants, blood leukocytes were stained with 50 ul 1:100 mixture of monoclonal antibodies containing APC conjugated anti-CD4 and PE conjugated anti-TCR Vβ11 (detecting MOG TCR transgenic $CD4^+$ T cells). Antibodies were incubated on ice for 30 min with light protection. Isotype control was stained with APC-rat IgG2α κ chain and PE-rat IgG2β κ chain. Samples were washed once again with FACS buffer and centrifuged to remove unbound antibodies. Final acquisition was done on FACSCanto II flow cytometer and analyzed with FlowJo software V10. Animals with over 80% of $CD4^+$ T cells positively expressing TCR Vβ11 were considered transgenic 2D2 mice and allowed into further experiments.

4.2.2.2.2 FACS analysis of leukocytes proliferation by flow cytometry

10^6 BrdU-pulsed splenocytes, thymocytes, leukocytes from lymph nodes and whole brain MNCs from each hemisphere were added to 12x75-mm FACS tubes, washed in FACS buffer and centrifuged at 260 g at 4 °C for 5 min. Cells were resuspended in 50 ul FACS buffer. Fluorescent antibodies specific for cell-surface markers (CD45-PE-Cy7, CD4-A700, CD8a-PB, B220-PerCP, TCR Vα3.2-APC, and TCR Vβ11-PE) diluted with 50 ul staining buffer were added per tube and mixed well. Cells were incubated with an antibody mixture in the dark for 15 min on ice and later washed with 1ml staining buffer with centrifugation at 260 g at 4 °C for 5 min.

After discarding supernatants, cells were fixed, permeabilized and intracellularly stained following the protocol supplied with the staining kit (BD BrdU Flow Kit). At the end of incubation, cells were washed once and resuspended with 1 mL of 1x BD Perm/Wash Buffer before acquisition on BD LSR II flow cytometer with gating strategy illustrated below (Figure 4). For optimal resolution, acquisition was run at a rate no greater than 400 events per second. Cells from the thymus were used as a positive control for successful BrdU labeling.

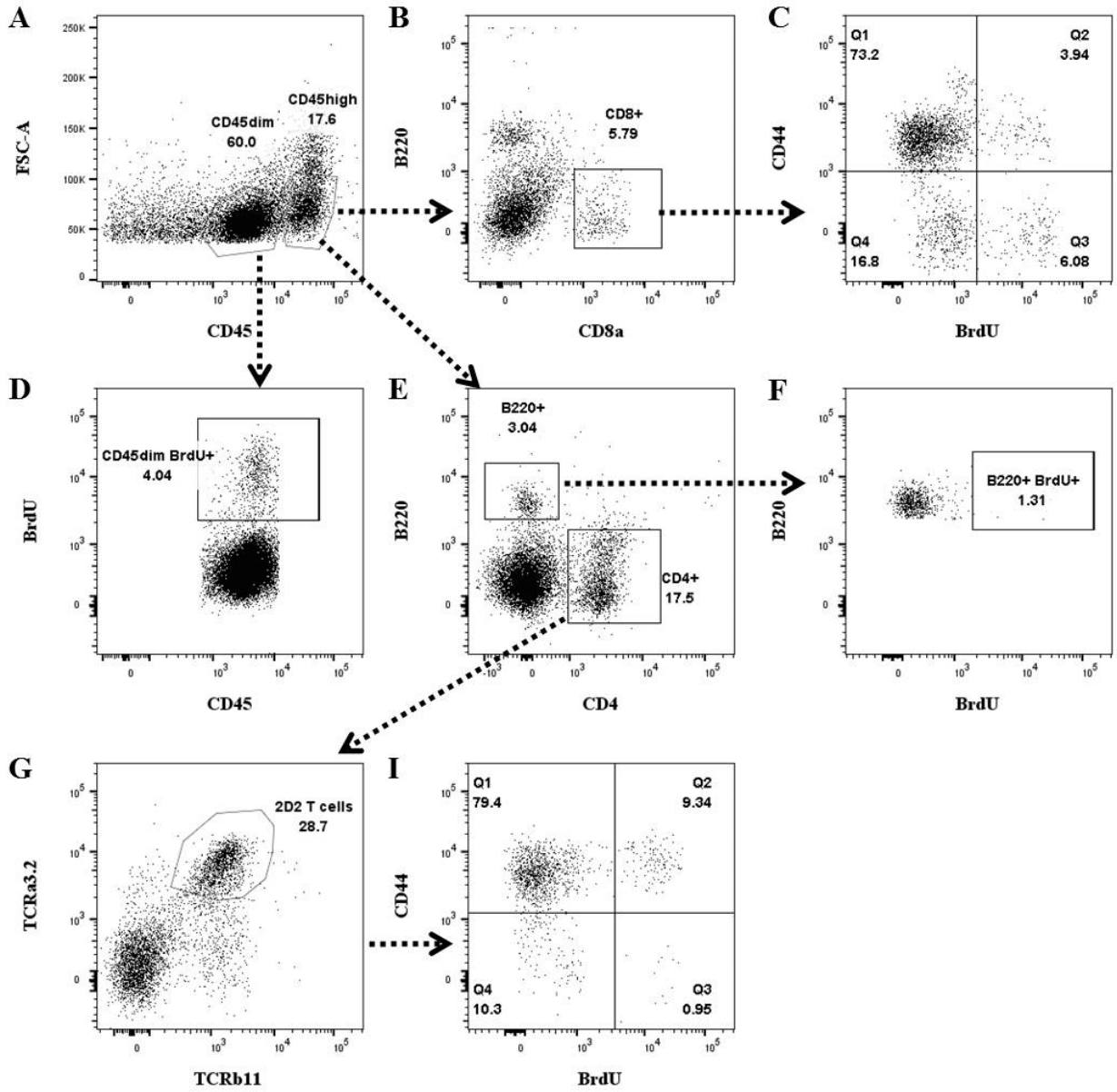

Figure 4. Gating strategy for FACS analysis of proliferating leukocytes in ischemic brain.
After gating out debris and doublets, the mononuclear cells were divided into $CD45^{hi}$ peripheral leukocytes and $CD45^{dim}$ local microglia (A). Within the $CD45^{hi}$ leukocytes, $CD8^+$ T cells were gated out (B) and their activation and proliferation were analyzed based on their expression of CD44 and labeling of BrdU (C). Similarly, proliferative microglia was labeled with BrdU (D). $B220^+$ B cells and $CD4^+$ T cells (E) were also gated out from the $CD45^{hi}$ leukocytes. The proliferation of B cells was gated in (F). 2D2 T cells were double labeled with TCRα3.2 and TCRβ11 (G) within the CD4 compartment. The activation and proliferation of 2D2 T cells were analyzed by staining with CD44 and BrdU (I).

4.2.2.2.3 FACS analysis of blood leukocytes following CD4 depletion

0.5 ul of each antibody (CD11b-APC, NK1.1-PE, CD19-FITC, CD3- PerCP-Cy5.5, CD4-PE-Cy7 and CD8a-PB) was added to 50 ul of EDTA whole blood. The mixtures were vortexed for 10 seconds and incubated in the dark for 15 min at RT. After adding 0.5 ml of 1x lysing solution (10x BD FACS Lysing Solution diluted with Millipore water), the mixtures were incubated in the dark for another 15 min at RT. Lysis of each sample was stopped by adding 0.5 ml of PBS and centrifuged at 300 g for 5 min at 4 °C. All supernatants were carefully removed and vortexed again. 3 ml of FACS buffer (PBS with 2% FCS + 15.4mM sodium azide) was added and samples were centrifuged again at 300 g for 5 min at 4°C. After removal of supernatants, samples were vortexed and 100 ul of FACS buffer were added. The samples were immediately put on ice and protected from light. In order to improve the accuracy of estimating cell counts, 20ul of CountBright Absolute Counting Beads (0.55 * 10^5 beads/50 ul) were added to the cell suspensions. Each mixture of cells and counting beads was vortexed and measured immediately on FACSCanto II flow cytometer.

4.2.2.2.4 FACS analysis of leukocytes in ischemic brain with or without CD4 depletion

Brain MNCs and 10^6 splenocytes were resuspended in a FACS buffer and centrifuged at 260 g at 4°C for 6 min. Samples were treated with anti-CD16/32 antibody to block unspecific binding of immunoglobulins and Fc receptors at 4°C for 15 min. Cellular surface markers were stained with a mixture of monoclonal antibodies: CD45-A700, CD11b-PE-TR, CD19-FITC, CD3-PerCp-Cy5.5, CD4-PE-Cy7, CD8a-PB, CD138-PE (only brain MNCs). Samples were incubated on ice for 30 min with light protection. Excessive unbound antibodies were washed away by washing with FACS buffer. After centrifugation, cell pellets were re-suspended in 100 ul FACS buffer and measured

immediately on BD LSR II flow cytometer using FACSDiva software version 6.1.3. Data were analyzed with FlowJo software 10.0.8r1 and subpopulations were gated as below (Figure 5).

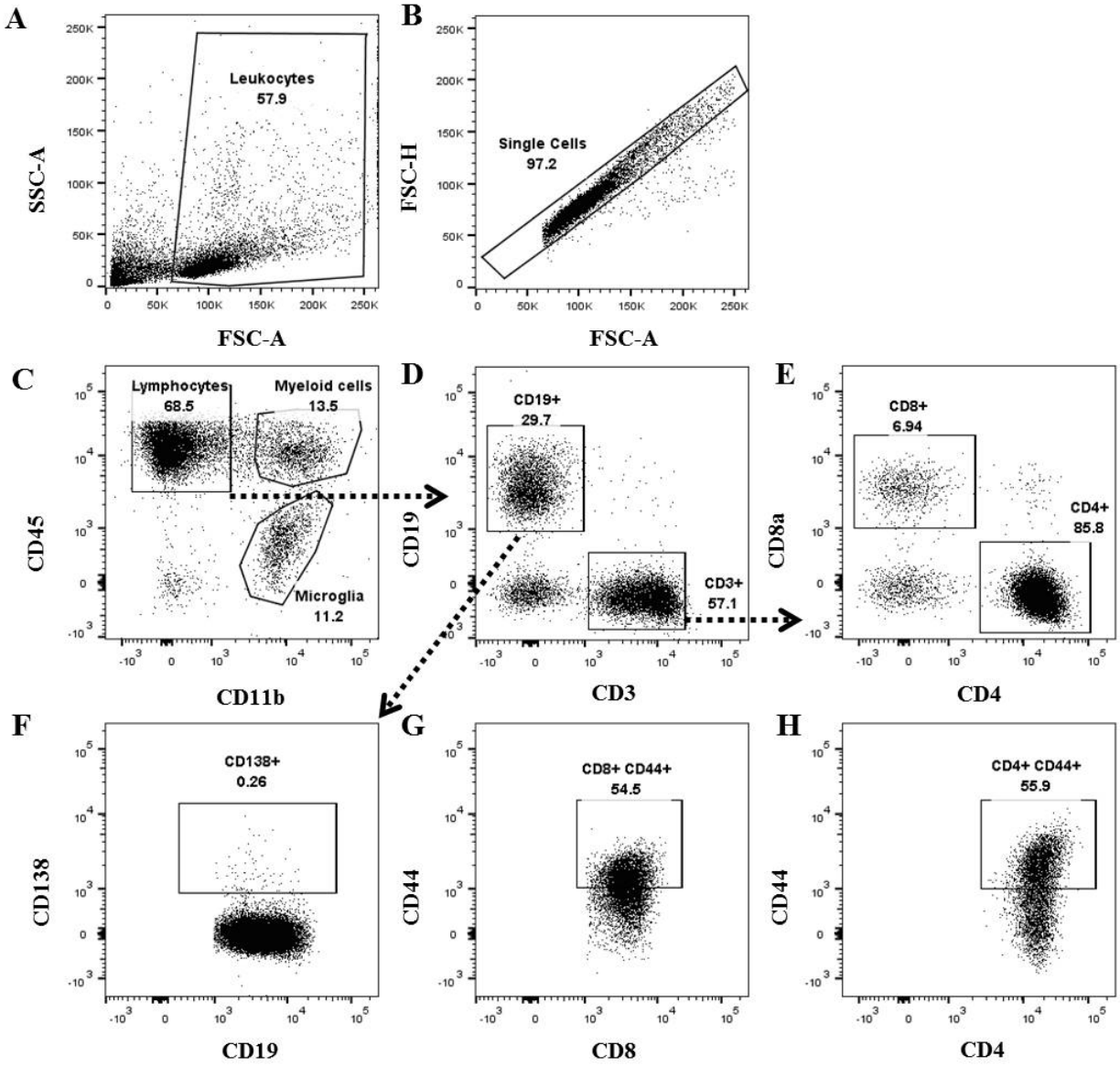

Figure 5. Gating strategy for FACS analysis of immune cells infiltrating ischemic brain.

A. Potential leukocytes with proper size (forward scatter, FSC) and granularity (side scatter, SSC) were separated from debris. B. Single cells were separated from doublets by cross-checking FSC-area (A) and FSC-height (H). C. Resting microglia cells expressing a low level of CD11b were separated from $CD45^{hi}$ infiltrating leukocytes. Within the $CD45^{hi}$ population, $CD11b^{+}$ myeloid cells were separated from $CD11b^{-}$ lymphocytes. D. Lymphocytes were further divided into $CD19^{+}$ B cells and $CD3^{+}$ T cells. E. $CD8^{+}$ and $CD4^{+}$ T cells are two main subpopulations within $CD3^{+}$ T cells. F. Within B cells, a small population of naïve B cells can differentiate into $CD138^{+}$ plasmablasts/plasma cells upon activation. 2D2 mice have far more $CD4^{+}$ T cells than $CD8^{+}$ T cells. Activated $CD8^{+}$ T cells (G) and activated $CD4^{+}$ T cells (H) upregulate expression of CD44.

4.2.2.2.5 FACS analysis of B cell subsets in WT mice after ischemic stroke

Brain MNCs and 10^6 splenocytes were washed with 1 mL FACS buffer and stained using standard techniques (see 4.2.2.3.4.). The fluorescence-conjugated monoclonal antibodies were used to stain different subsets in the B cell compartment (Table 1). The same antibody mixture was used to stain blood samples following a suitable staining protocol (see 4.2.2.3.3.). Finally, samples were resuspended in 100 ul FACS buffer and immediately acquired on BD LSR II flow cytometer using FACSDiva software version 6.1.3. Data were analyzed with FlowJo software 10.0.8r1. The detailed gating strategy for distinguishing B cell subsets based on differential expression of combined surface markers is illustrated in Figure 6.

Table1. Differential expression of surface markers by $CD19^+$ B cell subsets.

$CD19^+$ B cell subpopulation	Surface markers
Follicular	$CD138^-$, $CD93^-$, $CD21^{mid}IgM^{lo-hi}$, $CD23^+$, IgD^+
Marginal zone (MZ)	$CD138^-$, $CD93^-$, $CD21^+$, IgM^+
-MZ mature	$CD138^-$, $CD93^-$, $CD21^+$, IgM^+, $IgD^{-/low}$, $CD23^-$
-MZ progenitors	$CD138^-$, $CD93^-$, $CD21^+$, IgM^+, IgD^{hi}, $CD23^+$
Memory	$CD138^-$, $CD93^-$, $CD23^-$, IgD^-, IgM^-
Transitional	$CD138^-$, $CD93^+$, $CD23^+$, IgM^+
Immature	$CD138^-$, $CD93^+$, $CD23^-$, IgM^+, IgD^-
Plasmablasts/plasma cells	$CD138^+$

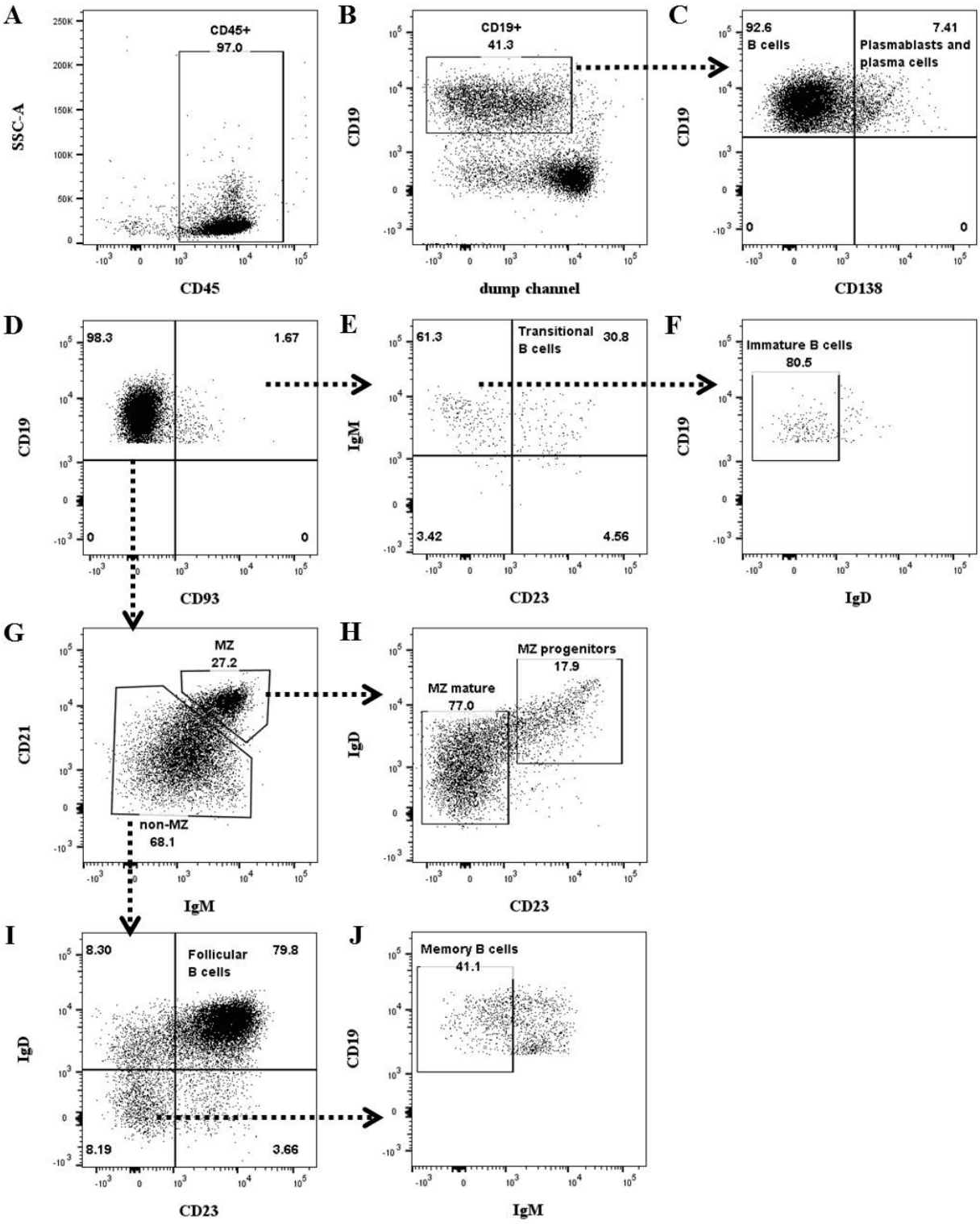
A
CD45+
97.0
SSC-A
CD45
B
CD19+
41.3
CD19
dump channel
C
92.6
B cells
7.41
Plasmablasts and plasma cells
CD19
0
0
CD138
D
98.3
1.67
CD19
0
0
CD93
E
61.3
Transitional B cells
30.8
IgM
3.42
4.56
CD23
F
Immature B cells
80.5
CD19
IgD
G
MZ
27.2
non-MZ
68.1
CD21
IgM
H
MZ progenitors
17.9
MZ mature
77.0
IgD
CD23
I
8.30
Follicular B cells
79.8
8.19
3.66
IgD
CD23
J
Memory B cells
41.1
CD19
IgM

Figure 6. Gating strategy for FACS analysis of B cell subsets in ischemic brain and spleen.
Similarly, leukocytes prepared from brains or spleens were separated from debris and doublets. $CD45^+$ leukocytes were selected (A) and $CD19^+$ B cells (B) were grouped together. The dump channel was prepared by three antibodies with the same conjugation so that $Gr1^+$ granulocytes, $CD11b^+$ myeloid cells and $CD3^+$ T cells were all excluded from analysis with a focus only on B cells. $CD138^+$ plasmablasts/plasma cells were gated out from the B cell population (C). Non-plasma B cells expressing CD93 (D) were gated by CD23 and IgD. CD23 and IgD double positive cells were gated as transitional B cells (E). Within the IgM^+ $CD23^-$ population (E) and with the absence of IgD, $CD19^+$ immature B cells (F) were gated. Marginal zone (MZ) B cells and non-MZ B cells were separated from non-plasma B cells with no expression of CD93 (D) by differential expression of CD21 and IgM (G). $CD21^+IgM^+$ MZ B cells are composed of IgD^{hi} $CD23^+$ MZ progenitors and $IgD^{-/low}$ $CD23^-$ mature MZ B cells (H). Follicular B cells (I) express $CD21^{mid}IgM^{lo-hi}$ IgD^+, $CD23^+$. (J) Memory B cells (J) are negative for IgD, CD23 and IgM.

4.2.2.3 Gene expression with quantitative real-time polymerase chain reaction

Quantitative real-time polymerase chain reaction (qRT-PCR) was used to analyze mRNA expression of growth factors in both the ipsilateral and contralateral hemispheres. All qPCR were run with LightCycler 2.0 (Roche). At the endpoint, mice were perfused with 20 ml ice-cold saline. Whole brain tissue including olfactory bulb and cerebellum was placed in brain matrix. Brain was sliced into four 2mm sections with five microtome blades that were pushed through every two notches between bregma 3.14mm and -5.46mm. The third and fourth sections were cut into two hemispheric parts. Brain sections from each hemisphere were harvested in Trizol (1ml per hemispherical sample).
Tissue homogenates were prepared with TissueLyzer LT (QIAGEN). Following chloroform extraction, pellets containing RNA were solved in DEPC-treated water. After DNase digestion, a NucleoSpin RNA clean-up Kit (Macherey Nagel) was used to remove PCR inhibitors. Total RNA concentration was determined with NanoDrop (Thermo Scientific), and probes were uniformly diluted. RNA was reversely transcribed to complementary DNA (cDNA) with M-MLV reverse transcriptase and random hexamers. LightCycler-FastStartDNA-Master SYBR-Green-I Kit (Roche) was used for qRT-PCR. Amplification and detection were supported by LightCyclerRelative Quantification Software (Roche Molecular Biochemicals). All PCRs were repeated twice. The relative expression of each gene of interest (GOI) was calculated compared to the reference gene (ref) by the delta Cp (crossing point) method with efficiency correction using the equation: E (GOI)

–Cp (GOI) / E (ref) –Cp (ref) (Pfaffl, Horgan et al. 2002). Mean values of duplicates were determined. The gene β-actin was chosen as a reference because it exhibits the most stable expression pattern in ischemic brain. In all experiments, amplification efficiencies (E) were determined for each primer pair by a serial dilution curve and calculated using LightCycler 2.0 software. Polymerase chain reaction (PCR) was performed on LightCycler 2.0 using the following program: 1) initial denaturation at 98°C for 30 seconds (1 cycle); 2) denaturation at 98°C for 10 seconds, annealing at the primer-specific temperature for 30 seconds, extension at 72°C for 1 min (45 cycles); 3) final extension at 72°C for 5 min and holding at 4°C (1 cycle). Specificity of PCR products was confirmed with melting curve analysis (LightCycler Software) and electrophoresis using 1.5% agarose gel.

4.2.2.4 Immunohistochemistry and fluorescent microscopy

4.2.2.4.1 Immunohistochemistry with cryosections

Frozen brains without cerebellums were embedded in Tissue-Tek ® O.C.T™ Compound. 8-10 um, coronal sections were collected from a +1.5 to 2.0 mm area around bregma using LEICA Cryostats. All brain slices were thaw-mounted on SuperFrost plus slides. Areas with slices in the middle were outlined using oil slide marker. Sections were then air-dried at RT for 30 min and later washed with PBS. Unspecific binding was blocked from incubation with blocking solution (PBS with 5% BSA) for 30 min. Primary antibodies (rat anti-mouse CD4, rabbit anti-mouse collagen type I, rat anti-mouse PDGFRβ) were diluted in blocking solution and incubated with the sections overnight in a moisture chamber at 4°C. The next day, slides were washed 3 times with PBS and incubated further with secondary antibodies (goat anti-rat Alexa 594 and goat anti-rabbit Alexa 488) for one hour in a dark moisture chamber at RT. After the final washing step, slides were mounted with DABCO anti-fading mounting medium reagent (25 mg/mL of 1, 4-diazabicyclo [2.2.2] octane in 50% glycerol/PBS, pH 8.6) and carefully covered with coverslips. The slides were left to air-dry for 30 min in the dark, and the edges were sealed with nail polish. Staining with omission of primary antibodies served as a negative control. Microscopical analysis of thin sections was performed with a Leica DMI 3000 fluorescent microscope.

4.2.2.4.2 Immunohistochemistry with floating sections

Brain tissues were fixed on the plate using Tissue-Tek of a sliding microtome and sectioned into 30 um slices. For long-term storage, floating sections were stored in cryoprotectant (25% ethylene glycol, 25% glycerol, 50% 0.1M PBS, v/v %) at -20°C. After washing with PBS, free-floating sections were blocked against unspecific binding with blocking solution (PBS with 10% normal goat serum and 0.3% Triton) for one hour at RT on a shaker. Primary and secondary antibodies were diluted in the same antibody diluent (PBS with 1% NGS and 0.3% Triton). Sections were incubated with primary antibodies at 4°C overnight on a shaker. Primary antibodies were specific for B220 (B cells), CD4 ($CD4^+$ helper T cells), CD68 (activated microglia/macrophages), CD13 (endothelial/periendothelial cells), NeuN (neurons), Iba-1 (microglia and macrophages), Ki67 (proliferating cells), Laminin 1+2 (basement membrane), and Collagen IV (basement membrane). After thorough washing with PBS, sections were incubated at RT with secondary antibodies for two hours on a shaker. Nuclei were counterstained with DAPI. Sections were transferred onto SuperFrost Ultra Plus® slides and air-dried until slices were firmly attached. Several brain slices were mounted together with DABCO anti-fading mounting medium. The specificity of primary staining was confirmed by comparing it with control staining, omitting primary antibody.

Fluorescent pictures were taken with a confocal microscope (Leica TCS SPE). 20um Z stack scanning with 5 steps for cells and 10 steps for vasculature were collected to generate maximal projection. Quantification of neurons, activated microglia/macrophages, infiltrating $CD4^+$ helper T cells and B cells in 2D2 mice were performed by counting 9 frames (173um×173um) per hemisphere using LEICA LAF software. One slice around bregma including striatum and cortex lesions was chosen to represent each animal. Quantification of B cells in WT mice was performed using a stereology workstation equipped with a fluorescence microscope (LEICA DMRE Fluorescence Microscope) and Stereo Investigator Software (MBF Bioscience). Two slices at the level of bregma and hippocampus were chosen to represent each animal. The hemispheres were outlined beforehand to limit the area of interest. A meander scan was used to count all positive-labeled cells in the ischemic hemisphere.

4.2.2.5 Enzyme-linked Immunosorbent Assay (ELISA)

At endpoint and before deep anesthesia, 200ul whole blood was collected into spray-coated K_2EDTA blood collection tubes by bleeding from the submandibular vein (see 4.2.1.8.). Cells were separated from plasma by centrifugation for 10 minutes at 1000x g using a refrigerated centrifuge. The resulting supernatants were apportioned into 50ul aliquots, and stored at –20°C until measurement. Mouse CXCL13/BLC/BCA-1 DuoSet (R&D Systems, DY470) was used for quantification of CXCL13 in mouse plasma. The manufacture's manual was followed exactly while performing this assay.

4.2.2.6 Serum Staining

Rat brain tissue was perfused and frozen as previously described (see 4.2.1.9.). Frozen brain tissue was sectioned at 20 um with a LEICA Cryostats. After blocking unspecific staining with blocking solution (PBS with 2% BSA, 5% NGS and 0.1% Triton) at RT for one hour, serum samples with 1:50 dilution were used as the primary antibody and incubated overnight in a moisture chamber at 4°C. After washing with PBS, secondary goat anti-mouse antibody (Oregon Green® 488 dye) was applied for two hours at RT in a moisture chamber with light protection. Baseline control was obtained by comparing staining with paired serum samples collected before MCAo (submandibular bleeding) or serum samples from naïve or sham-operated mice. Gut tissue was stained in parallel to serve as negative control for CNS antigen. Fluorescent pictures were taken with a confocal microscope (Leica TCS SPE).

4.2.3 Statistics

Examinations of mice in the control treatment and with CD4 depletion were all conducted in a blinded manner. Data analyzed with non-parametric tests were expressed either as median only (N<=5) or median with interquartile range (IQR) (N>5). Data for Catwalk (N=10-20) were expressed as mean ± standard deviation (SD) because it was analyzed by a parametric test. Data in figures were presented as scatterplot using Prism 6.0 software (GraphPad). Normality of data distribution was verified with the Kolmogorov-Smirnov test using IBM SPSS Statistics 25 software for windows. Parametric data were analyzed with Student's *t*-test (unpaired) or one-way analysis of variance (ANOVA) for s with Bonferroni correction. Non-parametric analysis was performed with the Mann Whitney *U*-test or one-way ANOVA on ranks (Kruskal-Wallis) with Dunn's multiple-

comparison test. Non-parametric paired data were analyzed with Wilcoxon matched-pairs signed rank test. Spearman's *rho* correlation coefficient (non-parametric data) was used for correlations. Survival rate was analyzed by comparing the survival curves (Kaplan-Meier) with the log-rank (Mantel-Cox) test. All tests were two-sided and a significance level of $\alpha=0.05$ was applied. P values <0.05 were considered significant (*$p<0.05$, **$p<0.001$, ***$p<0.001$). This was an exploratory study (Kimmelman, Mogil et al. 2014), hence no further adjustments were done for multiple testing.

5. RESULTS

This doctoral thesis is comprised of three experimental parts, each with its own focus:

1) Data were summarized from experiments where 60 min MCAo were induced to either 2D2 or WT mice in order to demonstrate the influence of transgenic MOG TCR on behavior of CNS-infiltrating $CD4^+$ T cells in ischemic stroke (5.1.1). Moreover, results from a kinetic study of lymphocyte proliferation following ischemic stroke were presented to support the notion that autoimmune responses can be induced in the peripheral lymphoid organs prior to entry of autoreactive lymphocytes into the ischemic brain (5.1.2 and 5.1.3)

2) In order to investigate the modulatory role of infiltrating $CD4^+$ T cells on tissue remodeling and functional recovery, 2D2 mice following 60 min MCAo were treated either with isotype control antibody or anti-CD4 depleting antibody plus preventative antibiotic. The correlation between infiltration of $CD4^+$ T cells and production of fibrotic fibers and growth factors that might be involved in tissue remodeling was summarized (5.2.1 and 5.2.2). Careful evaluation was then conducted of the effects of delayed CD4 depletion on infarct maturation as well as mid-term survival (5.2.3), accumulation of neuronal cells and activated microglia/macrophages (5.2.4), proliferation of periendothelial cells and activated microglia/macrophages (5.2.5), infiltration of B cells and patterns of B cell accumulation in ischemic brain (5.2.6), and motor functional recovery (5.2.7).

3) I aimed to investigate whether CD4 depletion can induce similar effects in WT mice. The aforementioned experimental procedure in 2D2 mice was also given to WT mice. The effects of delayed CD4 depletion on infiltration of other lymphocytes, and the neurological score were compared between 2D2 and WT mice (5.3.1).

4) Data presented were from experiments focusing on CNS infiltration (5.3.2) and phenotypical changes in B cell subpopulations both in ischemic brain and spleen (5.3.3) in WT mice. In order to investigate whether stroke can induce cognitive impairment, data collected from a Y maze at both day 13 and day 48 post stroke were analyzed (5.3.4). To further explore whether cognitive impairment post stroke might be related to the production of autoantibodies, I summarized the autoreactive patterns of antibodies in serum samples from WT mice before and after stroke (5.3.5).

5.1 CNS antigen-dependent activation of lymphocytes following stroke

5.1.1 More pronounced infiltration of $CD4^+$ T cells into the ischemic hemispheres of 2D2 mice than WT mice

The transgenic CNS antigen-specific T cell receptor (TCR) recognizing MOG provides 2D2 mice with enhanced potential for fostering autoreactive immune responses (Bettelli, Pagany et al. 2003). Therefore, compared to WT littermates (72 (18-526.00) cells, data was expressed as median plus interquartile range), 2D2 mice (2159 (1619-3186) cells) exhibited significantly more infiltration of $CD4^+$ T cells at 14 days post stroke (Figure 7A and 7B) and worse survival even with preventative antibiotic treatment (Figure 7C). The infarct volumes of 2D2 mice (36.61% (20.71-42.40) %) were also significantly larger than those of WT mice (16.00% (7.00-29.00) %) (Figure 7D). Larger infarction and stronger autoreactive potential in our experiments jointly promoted delayed (7-14 days) but massive infiltration of $CD4^+$ T cells into the ischemic brain of 2D2 mice. Hence, 2D2 mice were the main choice of animal model in this thesis to study the influence of autoreactivity from $CD4^+$ T cells on outcomes following experimental stroke.

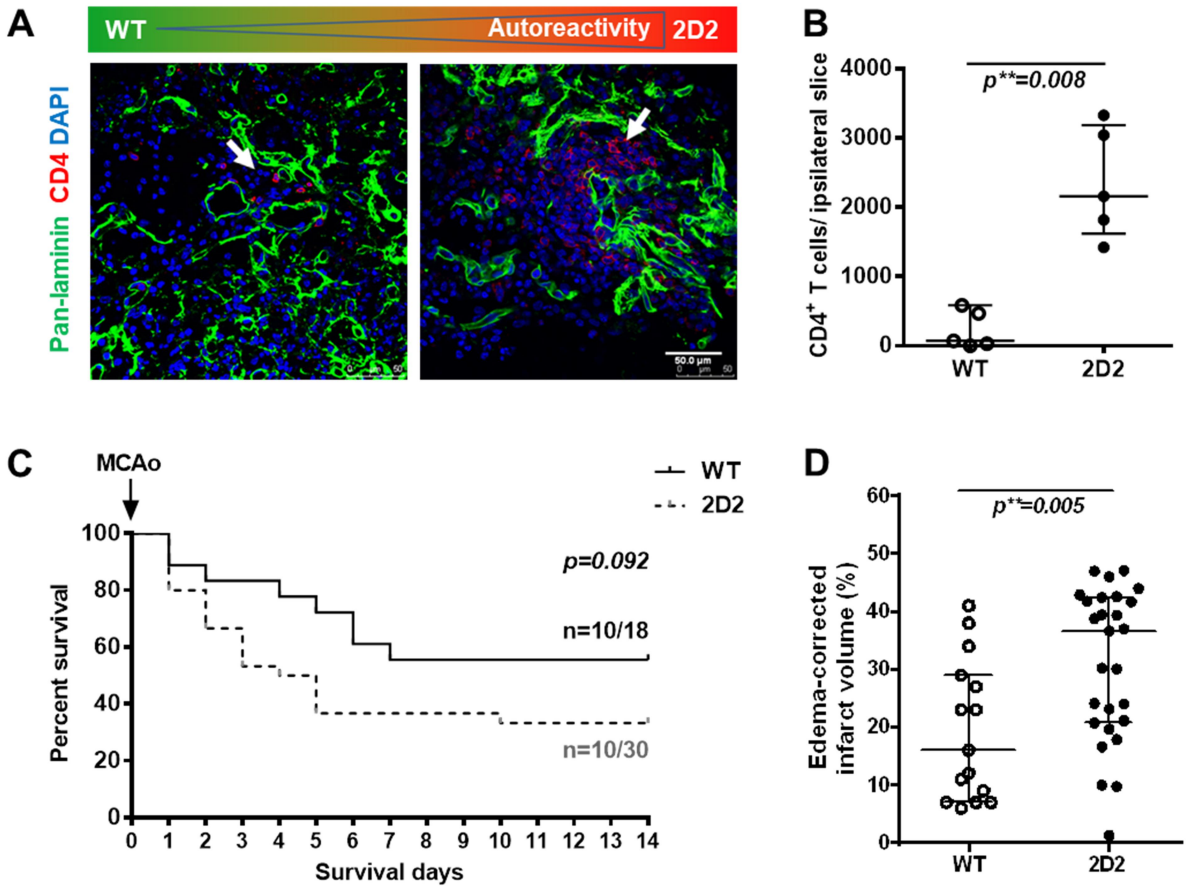

Figure 7. Autoreactivity linked with animal model and stroke outcome.

(**A**) The significantly different amounts of $CD4^+$ T cells infiltrating into ischemic brain were indicated with arrows in fluorescent staining of both WT and 2D2 brain slices from ipsilateral side. CD4 in red: surface marker for helper T cells; Pan-laminin in green: marker for basement membrane; DAPI in blue: marker for nuclei. Scale bar: 50µm. (**B**) Quantification of CNS-infiltrating $CD4^+$ T cells in ischemic brain on day 14 after stroke. A significantly higher number of $CD4^+$ T cells accumulated in the ischemic brains of 2D2 mice than in WT mice (N=5 per group, p=0.008, Mann-Whitney U Test). (**C**) 14 days of survival among 2D2 mice (N=30) with 60 min MCAo and preventative antibiotic treatment was worse than in WT mice (N=18) with the same procedures. However, no significant difference was found (p=0.092, Log-Rank (Mantel-Cox) Test). (**D**) 2D2 mice (N=27) had significantly larger infarction compared to WT mice (N=15) at one day after MCAo (N=15, p=0.005, Mann-Whitney U Test). Three animals died in each group before quantification of infarct volumes by MRI on day 1 after stroke. Significance level was marked as: *p<0.05, **p<0.01.

5.1.2 Ischemic stroke-induced proliferation of lymphocytes in secondary lymphoid organs

To prove stroke-induced proliferation of lymphocytes in vivo, 60 min MCAo was induced in 2D2 mice. The kinetic proliferation of BrdU-labeled lymphocytes was analyzed separately in CNS draining lymph nodes (superficial and deep cervical lymph nodes, lumbar lymph nodes), non-CNS draining lymph nodes (mesenteric lymph nodes), and spleens on day 1, 3 and 7 after MCAo compared to controls (naïve and sham-operated mice). Brain tissues were collected only on day 7 after MCAo. Edema-corrected average infarct sizes measured by MRI did not change significantly from days 1 to 7 after MCAo (Figure 8A). A significant decrease in the total count of splenocytes was detected in mice at 3 days (7.20×10^7 cells) after stroke compared to naïve mice (27.42×10^7 cells) (Figure 8B).

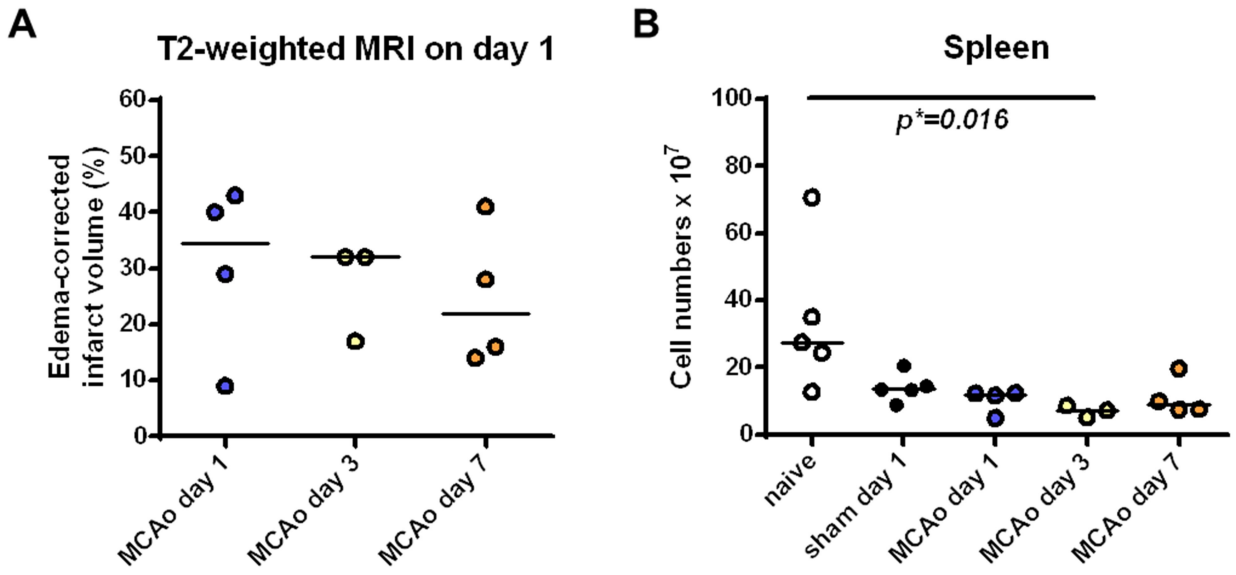

Figure 8. Quantification of infarct volume and kinetic cell counts of splenocytes before and after ischemic stroke.

(A) Edema-corrected infarct volume was measured with T2-weighted MRI at 24 hours post stroke. As expected, infarct volume of mice allocated into groups with indicated survival days revealed no significant differences. **(B)** Stroke-induced immunodepression down-regulated cell counts in spleen. Compared to naïve mice, splenocytes from mice on day 3 post stroke significantly decreased (Kruskal-Wallis, p=0.011; corrected for multiple comparisons, p=0.016). Sham-operated mice were sacrificed on day 1 after MCAo. All data from different groups were analyzed with Kruskal-Wallis test with Dunn's multiple comparisons test. Each p value was adjusted to account for multiple comparisons. Data analyzed with non-parametric tests were expressed as median. Significance level was marked as: *p<0.05, **p<0.01; N=3-5.

In contrast, proliferation of all $CD4^+$ T cells was reduced in sham-operated mice (sacrificed on day 1 after surgery) compared to naïve controls, while no difference was detected between sham and MCAo groups (Figure 9A). Data from pooled lymph nodes suggested that proliferation of $CD8^+$ T cells was transiently induced in mesenteric lymph nodes, spleen and superficial lymph nodes on day 1 post stroke (Figure 9B). The highest percentage of proliferating $CD8^+$ T cells on day 1 after stroke was seen in superficial cervical lymph nodes. Proliferation of $CD4^+$ T cells on day 1 after sham-operation, day 1 and day 3 after ischemic stroke remained unchanged. Further analysis with lymphocyte subsets showed that B cell proliferation in spleen was significantly impaired on day 3 (median=0.47%) compared to naïve control (median=7.08%) and day 1 post stroke (median=9.03%) (Figure 9C). The B cell population in all lymph nodes proliferated at a lower rate than in spleens at all time points except on day 3 after stroke. This data indicates that different lymphocytes responded differently to stroke and stroke-induced immunodepression. Compared to $CD8^+$ T cells and B cells, $CD4^+$ T cells maintained partial capacity to proliferate after stroke. It is also noteworthy that proliferation of B cells took place exclusively in spleen and not in lymph nodes.

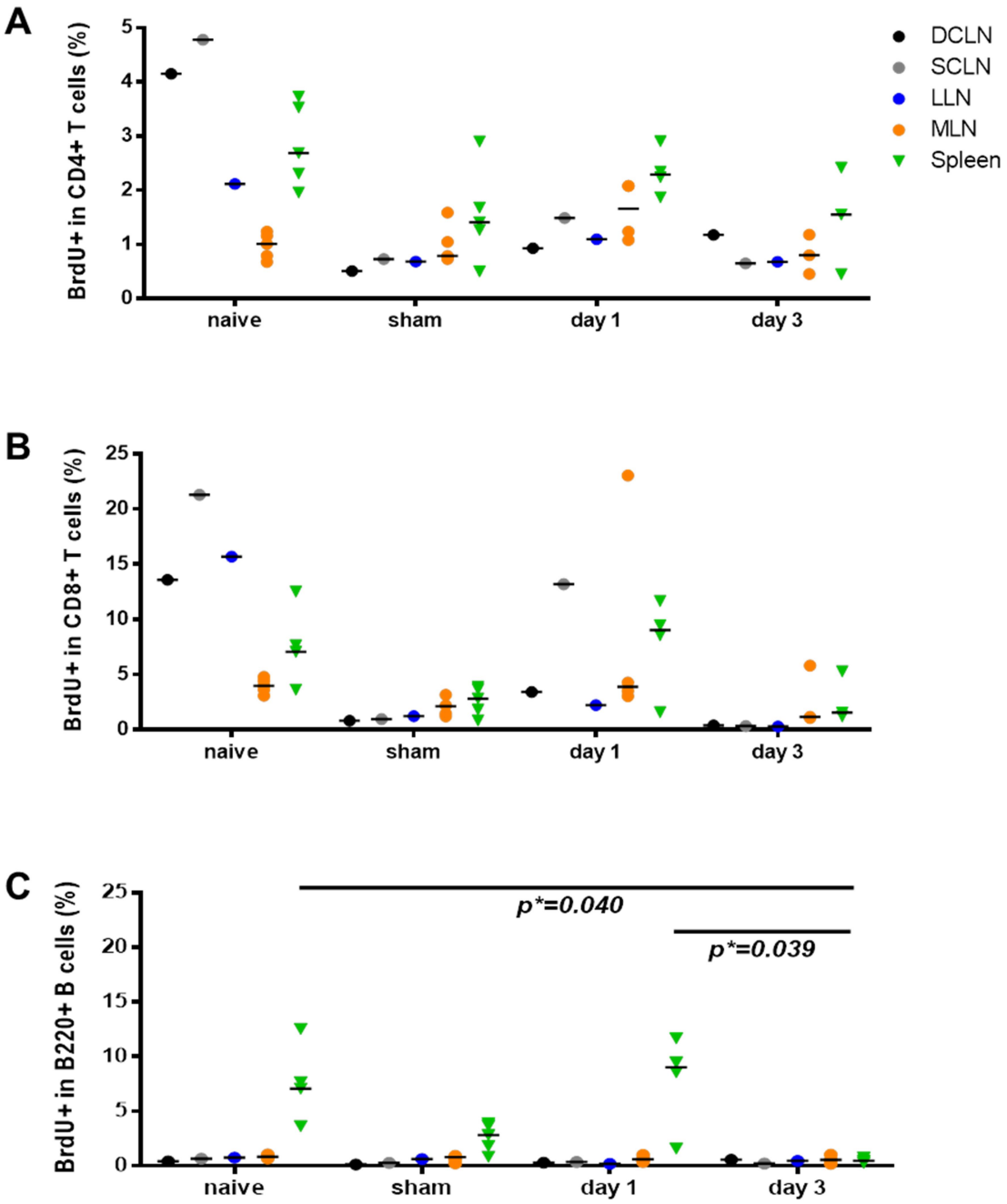
A
BrdU+ in CD4+ T cells (%)
0
1
2
3
4
5
naive
sham
day 1
day 3
DCLN
SCLN
LLN
MLN
Spleen
B
BrdU+ in CD8+ T cells (%)
0
5
10
15
20
25
naive
sham
day 1
day 3
C
BrdU+ in B220+ B cells (%)
0
5
10
15
20
25
p*=0.040
p*=0.039
naive
sham
day 1
day 3

Figure 9. Dynamic changes in proliferation of lymphocyte subsets in secondary lymphoid organs of 2D2 mice after ischemic stroke.

(**A)** Proliferation of $CD4^+$ T cells reduced slightly in cervical lymph nodes but remained unchanged in other secondary lymphoid organs after stroke. (**B)** Proliferation of $CD8^+$ T cells was decreased in sham-operated mice compared with naïve mice. There was transiently upregulated proliferation of B cells in mesenteric lymph nodes, spleen and superficial cervical lymph nodes on day 1 post stroke. (**C)** Proliferation of B cells in spleen was higher than in lymph nodes. Proliferation of B cells was significantly reduced on day 3 compared with day 1 (Kruskal-Wallis, p=0.006; corrected for multiple comparisons, p=0.040) and sham operation (Kruskal-Wallis, p=0.006; corrected for multiple comparisons, p=0.039). Abbreviations: deep cervical lymph node (DCLN), superficial cervical lymph node (SCLN), lumbar lymph node (LLN), mesenteric lymph node (MLN). All data from different groups (due to small sizes of LNs, lymphocytes from DCLN, SCLN and LLN at each time point were pooled together) were analyzed with Kruskal-Wallis test with Dunn's multiple comparison test. Each p value was adjusted to account for multiple comparisons. Data analyzed with non-parametric tests were expressed as median. Significance level was marked as: *p<0.05, **p<0.01; N=3-5.

Since there was no differential regulation of the overall proliferation of $CD4^+$ T cells, proliferation of MOG TCR^+ T cells ($CD4^+$ T cells expressing MOG TCR $V\alpha3.2^+$ $V\beta11^+$) among all proliferating lymphocytes was further investigated. Though the percentage of MOG TCR^+ T cells among all $CD4^+$ T cells was not affected by MCAo (Figure 10A), the representation of MOG TCR^+ T cells in all proliferating $CD4^+$ T cells strongly increased on day 1 in all CNS-draining LNs and MLNs (median=81.00%) compared with that of sham-operated mice (median=12.70%) (Figure 10B). Proliferation of effector-memory ($CD44^+$) MOG TCR^+ T cells significantly increased on day 1 after stroke in MLNs (median=8.52%) compared with naive group (median=3.20%) and sham-operated group (median=3.70%) (Figure 10C). Generally speaking, only a small percentage of naïve MOG TCR^+ T cells did proliferate after stroke. In spleen, a trend of impaired proliferation of naïve MOG TCR^+ T cells on day 1 after stroke (median=0.30%) was detected compared with naïve group (median=0.38%), while MLNs had significantly more proliferation of naïve MOG TCR^+ T cells on day 1 after stroke (median=0.38%) compared with that on day 1 after sham operation (median=0.08%) (Figure 10D). In summary, effector-memory MOG TCR^+ T cells had higher proliferation than naïve MOG TCR^+ T cells in both naïve and mice with MCAo. Both cell types had significantly upregulated proliferation in MLNs on day 1 after stroke.

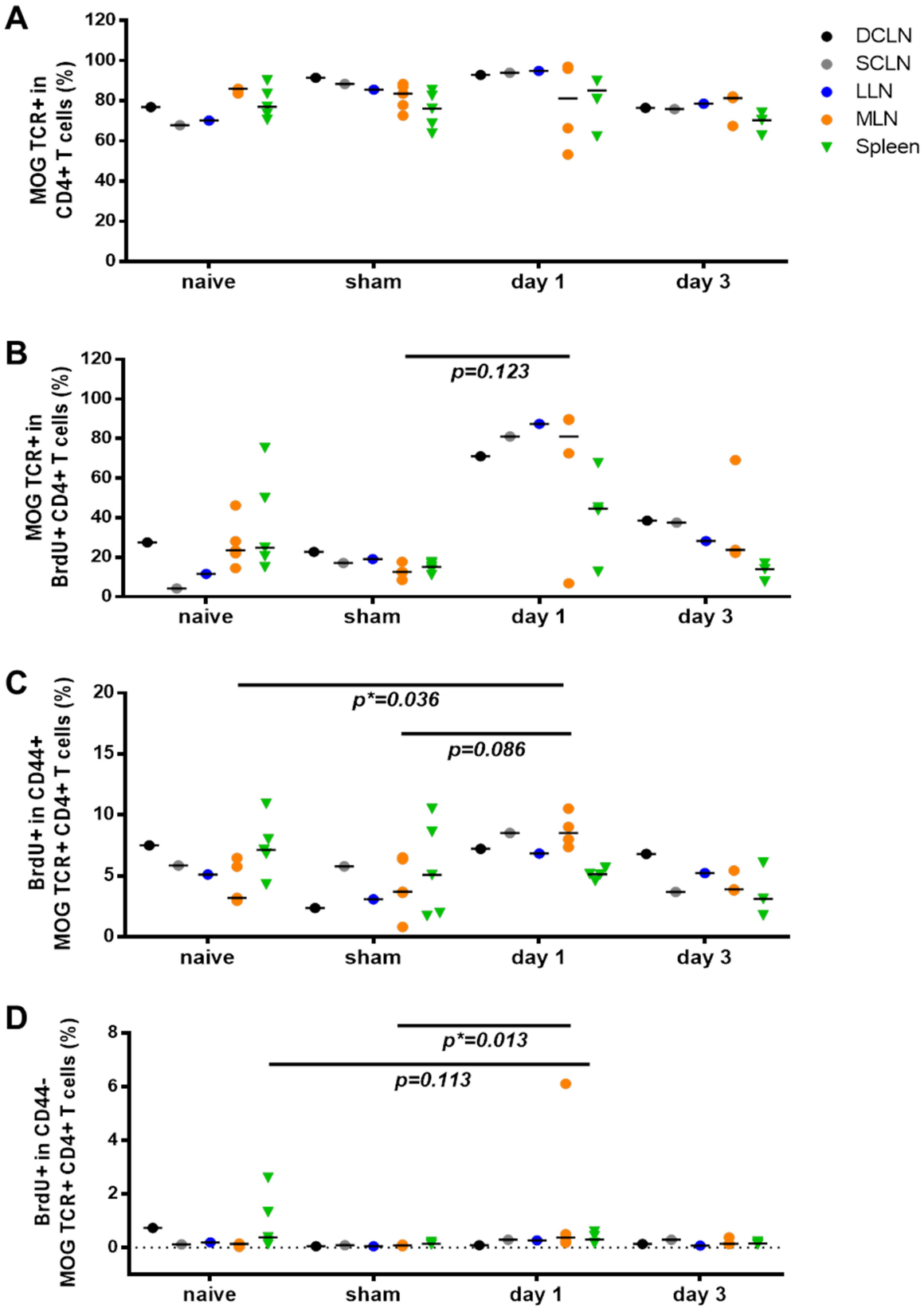
A
MOG TCR+ in CD4+ T cells (%)
120
100
80
60
40
20
0
naive
sham
day 1
day 3
DCLN
SCLN
LLN
MLN
Spleen
B
MOG TCR+ in BrdU+ CD4+ T cells (%)
p=0.123
C
BrdU+ in CD44+ MOG TCR+ CD4+ T cells (%)
p*=0.036
p=0.086
D
BrdU+ in CD44- MOG TCR+ CD4+ T cells (%)
p*=0.013
p=0.113

Figure 10. Dynamic changes in composition and proliferation of MOG TCR$^+$ T cells in secondary lymphoid organs of 2D2 mice before and after ischemic stroke.

(A) Percentage of MOG TCR$^+$ T cells in CD4$^+$ population did not change at different time points or in secondary lymphoid organs from the same time point. (**B)** Among all proliferative CD4$^+$ T cells, the percentage of MOG TCR$^+$ T cells generally increased on day 1 post stroke compared with other time points. Significantly more MOG TCR$^+$ T cells proliferated on day 1 after stroke than on 1 after sham operation (Kruskal-Wallis, p=0.078; corrected for multiple comparisons, p=0.123) (**C)** Proliferation of effector-memory MOG TCR$^+$ T cells (CD44$^+$) significantly increased in MLNs on day 1 post stroke compared with naive group (Kruskal-Wallis, p=0.015; corrected for multiple comparisons, p=0.036). A similar trend was detected in MLNs between day 1 after stroke and sham operation (p=0.086). (**D)** Proliferation of naïve MOG TCR$^+$ T cells (CD44$^-$) was significantly up-regulated in MLNs on day 1 after stroke compared with sham operation (Kruskal-Wallis, p=0.003; corrected for multiple comparisons, p=0.013). A trend of reduced proliferation of naïve MOG TCR$^+$ T cells in spleen was detected on day 1 after stroke compared to naïve group (Kruskal-Wallis, p=0.053; corrected for multiple comparisons, p=0.113). Abbreviations: deep cervical lymph node (DCLN), superficial lymph node (SCLN), lumbar lymph node (LLN), mesenteric lymph node (MLN). All data from different organ groups were analyzed with Kruskal-Wallis test and with Dunn's multiple comparison corrected for multiple comparison test. Each p value was adjusted to account for multiple comparisons. Data analyzed with non-parametric tests were expressed as median. Significance level was marked as: *p<0.05, **p<0.01; N=3-5.

5.1.3 Ischemic brain was the favored place for proliferation of CNS-antigen reactive lymphocytes following stroke

I investigated brain-infiltration by lymphocytes on day 7 post stroke and compared the proliferative capacity of lymphocytes between ischemic brain and peripheral lymphoid organs. Infiltration by lymphocytes was selective towards the ischemic hemisphere (ipsilateral side). Besides monocytes and macrophages, CD4$^+$ T cells constituted the largest population among all lymphocytes. The absolute count of CD45$^+$ leukocytes (median=27310 CD45$^+$ cells) and CD4$^+$ T cells (median=6367 cells) were much increased in the ipsilateral hemisphere compared with the contralateral hemisphere (median=2794 CD45$^+$ cells, median=458 CD4$^+$ T cells) (Figure 11A). Furthermore, the total proliferative CD4$^+$ T cells (median=287 cells) and MOG TCR$^+$ T cells (median=112 cells) in the ipsilateral hemisphere together were more than those in the contralateral hemisphere (median=19 proliferative CD4$^+$ T cells, median=6 proliferative MOG TCR$^+$ T cells) (Figure 11B). Although

$CD8^+$ T cell and B cell counts did not differ between the hemispheres, the proliferation of $CD8^+$ T cells (median=36 cells) and B cells (median=33 cells) tended to increase in the ischemic hemisphere compared with the contralateral hemisphere (median=9 proliferative $CD8^+$ T cells, median=6 proliferative B cells) (Figure 11B).

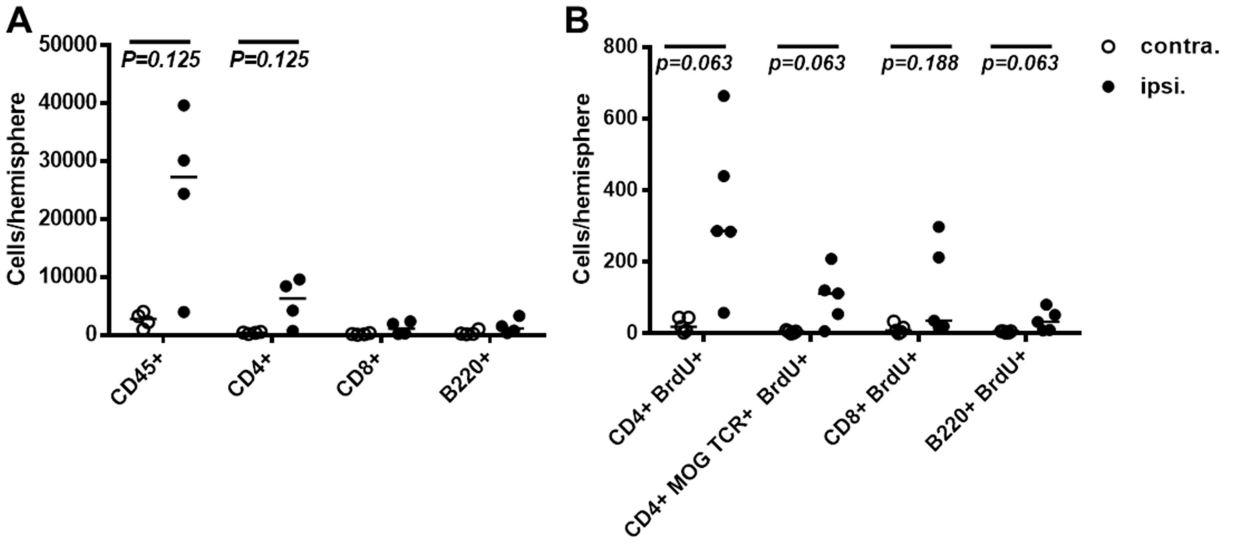

Figure 11. CNS-infiltrating leukocytes and proliferation of 2D2 mice on day 7 post ischemic stroke.
Absolute counts of leukocytes from the ipsilateral (ipsi.) and contralateral (contra.) hemispheres were presented separately. (**A)** Relatively more $CD45^+$ leukocytes (p=0.125) and $CD4^+$ T cells (p=0.125) infiltrated into the ischemic hemisphere. (**B)** Similar to subset comparison, more proliferative $CD4^+$ T cells (p=0.063), MOG TCR^+ T cells (p=0.063), $CD8^+$ T cells (p=0.188) and $B220^+$ B cells (p=0.063) were detected in the ipsilateral hemispheres than the contralateral hemispheres. All data were analyzed with Wilcoxon Signed Rank Test. Data analyzed with non-parametric tests were expressed as median. Significance level was marked as: *p<0.05, **p<0.01; N=4.

Next, proliferative capacity of lymphocytes in ischemic brain was compared to that in spleen and non-draining mesenteric lymph nodes on day 7 post stroke. In line with our previous finding showing significant inhibition of B cell proliferation in spleen (see 5.1.2), the proliferation of B cells was further inhibited in spleen and mesenteric lymph nodes until day 7 after stroke. In contrast, the CNS-infiltrating B cells (2.61% (0.60-6.49) %) had significantly higher proliferation than the B cells residing in spleens (0.26% (0.22-0.49) %) (Figure 12A). Proliferation of both $CD4^+$ (6.78% (5.57-

7.25) %) and $CD8^+$ T cells (8.13% (6.50-13.55) %) (Figure 12C) were also significantly up-regulated in ischemic brain compared with the same populations in mesenteric lymph nodes (0.79% (0.53-0.97) % for $CD4^+$ T cells, 1.57 % (0.89-2.67) % for $CD8^+$ T cells).

In addition, activation of $CD4^+$ T cells significantly increased in ischemic brain (median=93.72%) compared with cells in the mesenteric lymph nodes (median=15.88%) (Figure 12D). Effector-memory $CD8^+$ T cells uniformly maintained high activation in both CNS and peripheral lymphoid organs (Figure 12E). Interestingly, the dominant phenotype of MOG TCR^+ T cells within total $CD4^+$ T cells in periphery was not seen in ischemic brain. The percentage of MOG TCR^+ T cells was actually significantly decreased in ischemic brain (median=28.95%) compared with the percentage (median=76.35%) in the mesenteric lymph nodes (Figure 12F). Nevertheless, the percentage of proliferating MOG TCR^+ T cells in total proliferating $CD4^+$ T cells remained the same between ischemic brain and peripheral lymphoid organs (Figure 12G). After infiltrating into ischemic brain and being exposed to diverse CNS antigens, MOG TCR^- $CD4^+$ T cells (median=7.49%) could expand similar to MOG TCR^+ $CD4^+$ T cells (median=9.13%) (Figure 12H and 12I). In ischemic brain (median=7.49%) and spleen (median=9.05%), proliferation of MOG TCR^- $CD4^+$ T cells was higher than in MLNs (median=3.95%) (Figure 12H). The proliferation of MOG TCR^+ T cells was significantly higher in the ischemic brain (median=9.13%) compared with the proliferation in the MLNs (median=0.20%) and the spleen (median=0.63%) (Figure 12I). Within the MOG TCR^+ T cell compartment, the proliferation of $CD44^+$ effector-memory MOG TCR^+ T cells was significantly higher in the ischemic brain (median=9.58%) than in the MLNs (median=2.28%) (Figure 12J). The proliferation of naïve MOG TCR^+ T cells was also partially up-regulated in the ischemic brain (median=1.94%) compared with the spleen (median=0.25%) and MLNs (median=0.10%) (Figure 12K). In the ischemic brain, effector-memory MOG TCR^+ T cells proliferated much more than naïve MOG TCR^+ T cells. Although the majority of infiltrating $CD8^+$ T cells (almost 80%) had effector-memory phenotype ($CD44^+$), naïve $CD8^+$ T cells (median=10.18%) proliferated slightly more than effector-memory $CD8^+$ T cells (median=7.01%) (Figure 12L).

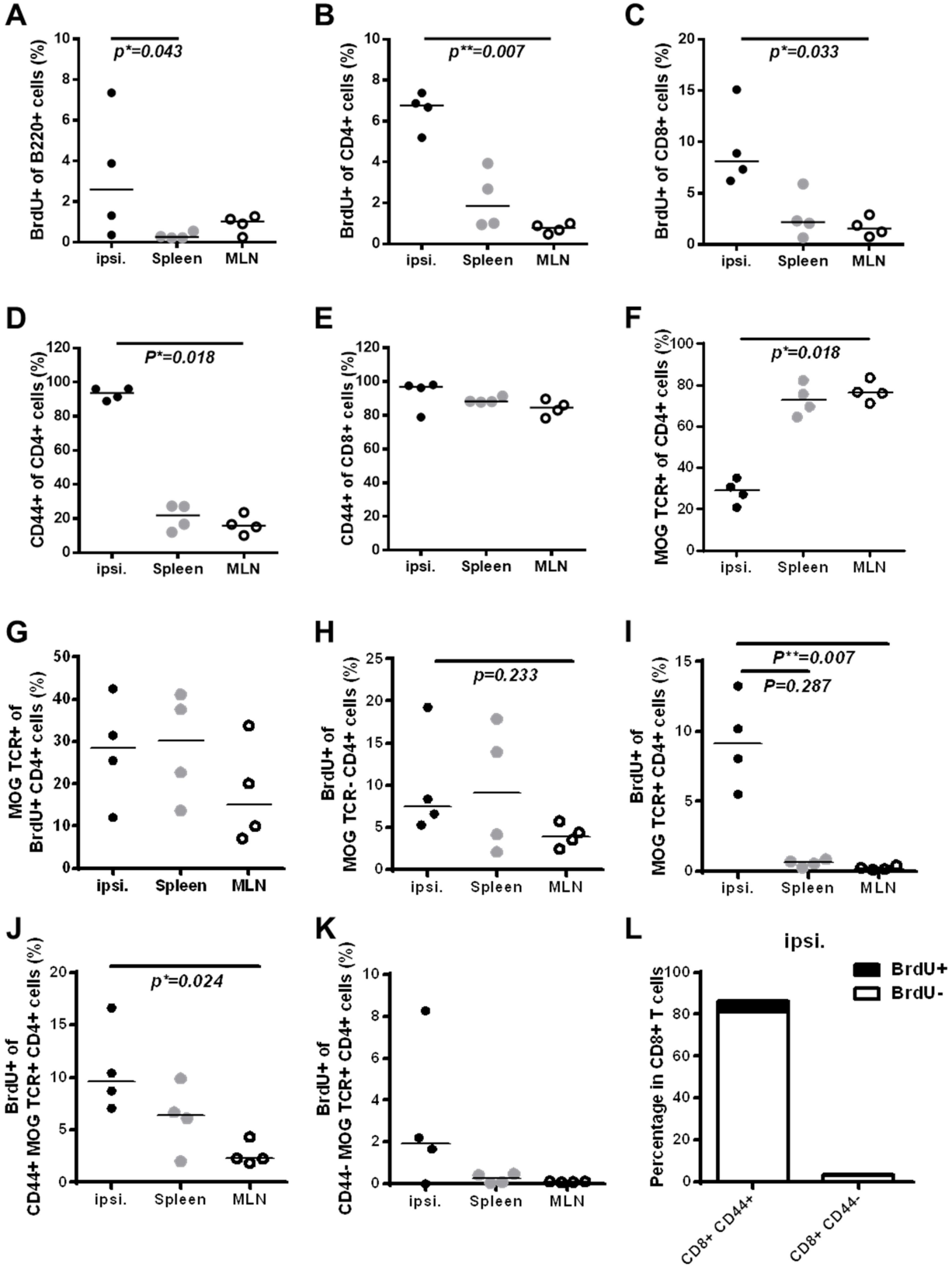
A
BrdU+ of B220+ cells (%)
p*=0.043
ipsi.
Spleen
MLN
B
BrdU+ of CD4+ cells (%)
p**=0.007
C
BrdU+ of CD8+ cells (%)
p*=0.033
D
CD44+ of CD4+ cells (%)
P*=0.018
E
CD44+ of CD8+ cells (%)
F
MOG TCR+ of CD4+ cells (%)
p*=0.018
G
MOG TCR+ of BrdU+ CD4+ cells (%)
H
BrdU+ of MOG TCR- CD4+ cells (%)
p=0.233
I
BrdU+ of MOG TCR+ CD4+ cells (%)
P**=0.007
P=0.287
J
BrdU+ of CD44+ MOG TCR+ CD4+ cells (%)
p*=0.024
K
BrdU+ of CD44- MOG TCR+ CD4+ cells (%)
L
ipsi.
BrdU+
BrdU-
Percentage in CD8+ T cells
CD8+ CD44+
CD8+ CD44-

Figure 12. Comparison of lymphocyte proliferation and activation in the ipsilateral hemisphere of brain, spleen and mesenteric lymph nodes on day 7 post ischemic stroke

(**A)** Compared to spleen, B lymphocytes in ischemic brain increased proliferation significantly (Kruskal-Wallis, p=0.037; corrected for multiple comparisons, p=0.043). Proliferation of both $CD4^+$ T cells (**B**, Kruskal-Wallis, p=0.001; corrected for multiple comparisons, p=0.007) and $CD8^+$ T cells (**C**, Kruskal-Wallis, p=0.011; corrected for multiple comparisons, p=0.033) was significantly higher in ischemic brain than in MLNs. (**D)** Activation of $CD4^+$ T cells in the ischemic brain was extremely higher compared to that of MLNs (Kruskal-Wallis, p=0.001; corrected for multiple comparisons, p=0.018). (**E)** However, activation of $CD8^+$ T cells did not differ among the ischemic hemisphere, the spleen or the MLNs (Kruskal-Wallis, p=0.197). **(F)** Percentage of $CD4^+$ MOG TCR^+ ($V\alpha3.2^+$ $V\beta11^+$) T cells was quite different among ischemic brain, spleen and MLNs (Kruskal-Wallis, p=0.005). Significant difference was seen between the ipsilateral hemisphere and the MLNs (Kruskal-Wallis, p=0.005; corrected for multiple comparisons, p=0.018). **G)** Among all proliferating $CD4^+$ T cells, a similar percentage of MOG TCR^+ T cells was seen in ischemic brain and secondary lymphoid organs (Kruskal-Wallis, p=0.348). **(H)** MOG TCR^- $CD4^+$ T cells had a trend to proliferate more in the ischemic brain compared with the MLNs (Kruskal-Wallis, p=0.219; corrected for multiple comparisons, p=0.233). **(I)** MOG TCR^+ $CD4^+$ T cells significantly increased their proliferation in the ischemic brain compared with the MLNs (Kruskal-Wallis, p=0.001; corrected for multiple comparisons, p=0.007) and showed a trend of upregulation over spleen (Kruskal-Wallis, p=0.001; corrected for multiple comparisons, p=0.287). (**J)** Proliferation of effector-memory $CD4^+$ MOG TCR^+ T cells ($CD44^+$) was significantly up-regulated in the ischemic brain compared to MLNs (Kruskal-Wallis, p=0.018; corrected for multiple comparisons, p=0.024). (**K)** Proliferation of naive $CD4^+$ MOG TCR^+ T cells ($CD44^-$) slightly increased in the ischemic brain compared to the spleen and MLNs (Kruskal-Wallis, p=0.419). **(L)** Although the population of naïve $CD8^+$ T cells was smaller, they proliferated slightly more than $CD44^+$ $CD8^+$ T cells in the ipsilateral (ipsi.) hemispheres. All data from different groups were analyzed with Kruskal-Wallis test with Dunn's multiple comparison test. Each p value was adjusted to account for multiple comparisons. Data analyzed with non-parametric tests were expressed as median. Significance level was marked as: *p<0.05, **p<0.01.

5.2 Effects of $CD4^+$ T cells on tissue remodeling and mid-term functional recovery after stroke

5.2.1 Kinetic infiltration of $CD4^+$ T cells temporally correlated with deposition of fibrotic fibers in ischemic brain of 2D2 mice

In accordance with the hypothesis that $CD4^+$ T cells play a key role in post-stroke autoreactivity, I aimed to explore their role in tissue remodeling during chronic inflammation. Co-staining of $CD4^+$ T cells and collagen type I fibers demonstrated that $CD4^+$ T cells massively accumulated in the peri-infarct area on day 14 (Figure 13B) compared to day 7 (Figure 13A) after stroke. $CD4^+$ T cells transmigrated through inflamed vessels surrounding the infarcted area where collagen type I fibers were also deposited (indicated by the white arrow in Figure 13A). Moreover, accumulation of CNS-infiltrating $CD4^+$ T cells was temporally correlated with deposition of collagen type I fibers between day 7 and day 14 after stroke.

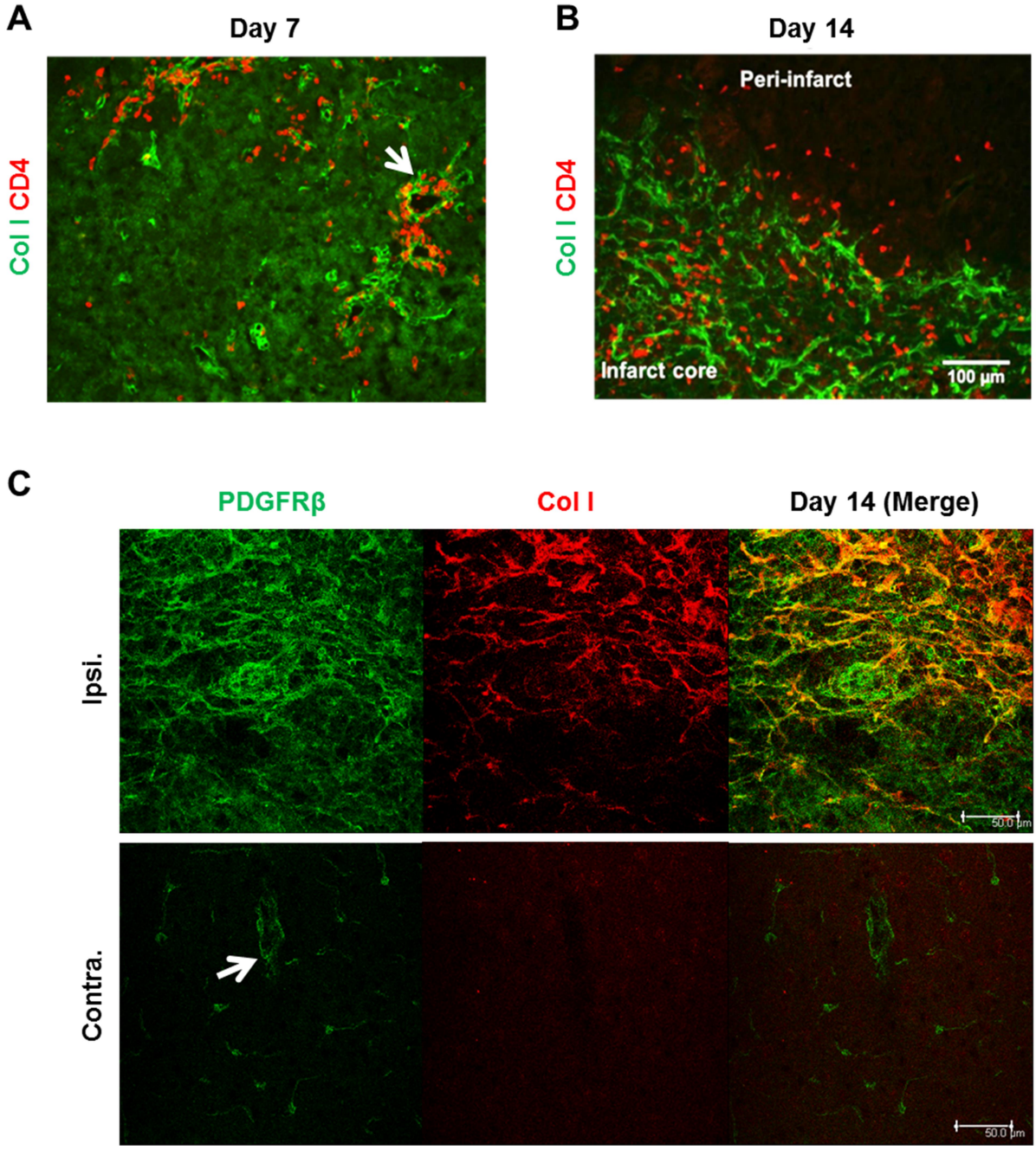
A
Day 7
Col I CD4
B
Day 14
Peri-infarct
Col I CD4
Infarct core
100 μm
C
PDGFRβ
Col I
Day 14 (Merge)
Ipsi.
Contra.
50.0 μm
50.0 μm

Figure 13. Infiltration of $CD4^+$ T cells temporally correlates with the deposition of fibrotic fibers in the ischemic brain.

(A) Infiltration of $CD4^+$ T cells and deposition of collagen type I fibers in inflamed brain vessels (indicated by white arrow) in the ischemic hemisphere on day 7 after stroke. **(B)** Increased accumulation of $CD4^+$ T cells and deposition collagen type I fibers in infarcted area on day 14 post MCAo. Scale bar: 100μm. **(C)** Stroke-induced deposition of collagen type I fibers co-localized with upregulation of PDGFRβ in the ipsilateral hemisphere (ipsi.) on day 14 after stroke. In the contralateral (contra.) hemisphere, PDGFRβ was expressed at low level in the area surrounding brain vessels (indicated by white arrow). Scale bar: 50μm. Abbreviations: Col I (collagen type I).

Collagen type I is not the basic component of the basement membrane (BM) of the blood-brain barrier, and there are no fibroblasts (main producer of collagen I in connective tissue or during tissue fibrosis) in the healthy brain parenchyma. It has been postulated that inflammation and autoreactive $CD4^+$ T cells might be responsible for the induction of such abnormal deposition of fibrotic fibers (personal communication with Prof. Lydia Sorokin). In addition, based on the evidence that expression of platelet-derived growth factor receptor β (PDGFRβ) was exclusively induced in the ischemic hemisphere and its expression co-localized with deposition of collagen type I fibers (Figure 13C), I further investigated whether $CD4^+$ T cells played a role in modulating the expression of PDGFRβ and in the deposition of fibrotic type I collagen fibers in the ischemic hemisphere.

5.2.2 TGFβ1 rather than PDGFRβ was positively correlated with the deposition of fibrotic fibers in the ischemic hemisphere of 2D2 mice while CD4 depletion did not affect mRNA expression of genes related to tissue remodeling

The role of $CD4^+$ T cells in tissue remodeling was investigated by depleting this cell type starting at 3 days after stroke using an antibody-based approach (Figure 14A). After four consecutive injections of $CD4^+$ T cell-depleting antibody on days 3, 5, 7, and 9 after MCAo, $CD4^+$ T cells were completely eliminated in the spleen. This phenotype was maintained at least until day 14 after stroke (Figure 14B). Accordingly, the entry of $CD4^+$ T cells into the ischemic brain was also successfully blocked by the anti-CD4 treatment (Figure 14C). I then compared kinetic mRNA expression of collagen type I and other relevant growth factors in the ischemic brain on days 3, 7, 10, and 14 after

MCAo. Moreover, mice with control treatment (isotype control antibody) were compared to mice with CD4 depletion on day 14.

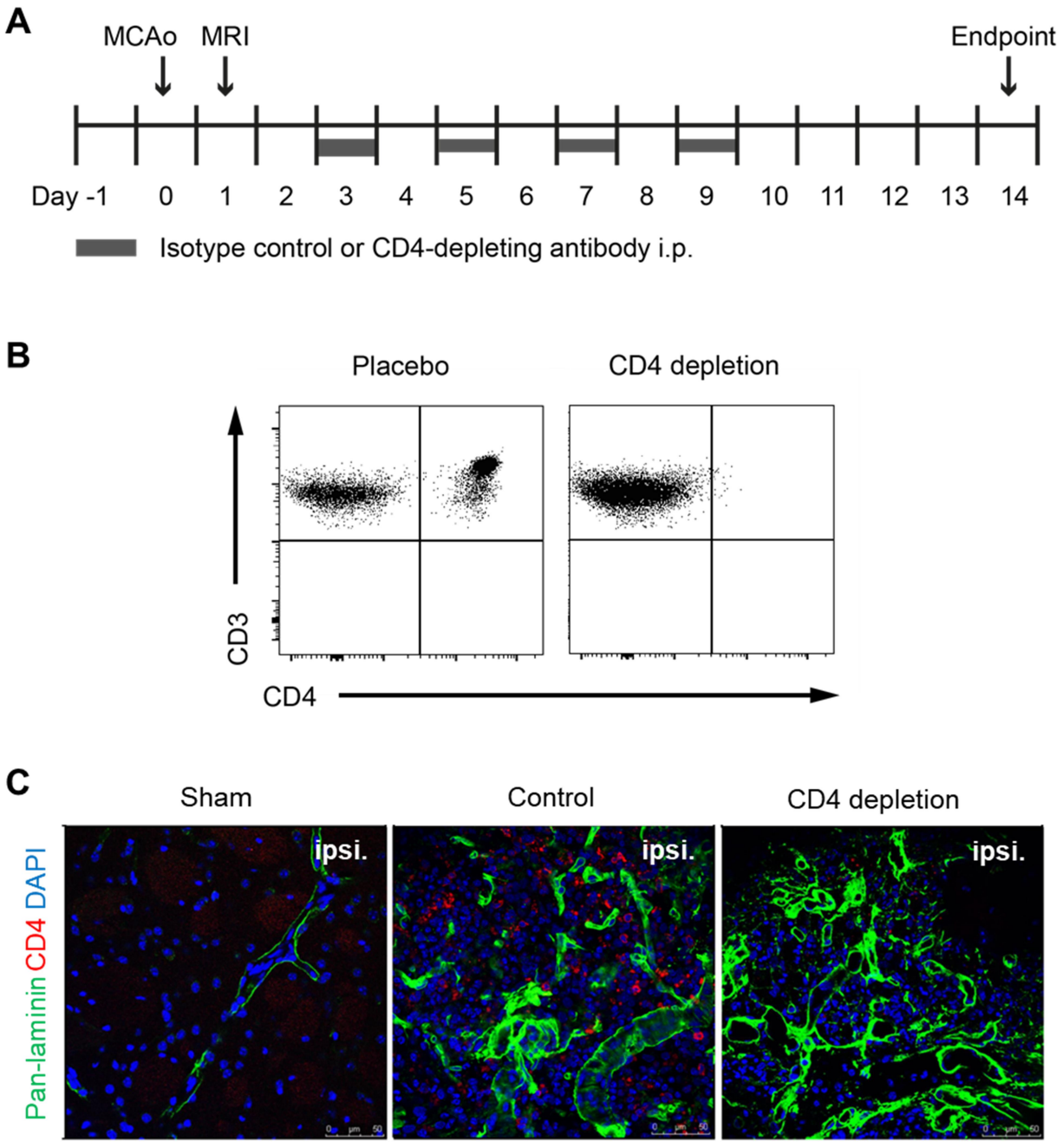

Figure 14. Experimental setups for 2D2 mice with anti-CD4 treatment and efficacy of depleting $CD4^+$ T cells in the periphery and the brain.

(A) 60 min middle cerebral artery occlusion (MCAo) was performed in 2D2 mice. Stroke-induced mice were monitored for 14 days. On day 1 after MCAo, infarct volume was measured by T2-weighted MRI. Isotype control antibody (control) or anti-CD4 antibody was intraperitoneally injected at four indicated time points. **(B)** At the endpoint (day 14), spleens were analyzed by flow cytometry to confirm success of CD4 depletion. **(C)** Infiltration of $CD4^+$ T cells into the ischemic brain was blocked by anti-CD4 treatment. Pan-laminin (green) was used to visualize basement membrane of brain blood vessels. In sham-operated mice and mice with CD4 depletion, there were no positive stainings for $CD4^+$ T cells (red) in the ipsilateral (ipsi.) hemisphere. Scale bar: 50μm.

Since infarct size determines the extent of tissue injury and inflammation, infarct volumes on day 1 were compared in all mice sacrificed at different time points after stroke. There were no significant differences between any of the groups (Figure 15A), although infarct volumes from one group (day 7) appeared slightly smaller compared to the groups sacrificed at other time points. Although deposition of collagen type I fiber (fibrotic extracellular matrix produced in connective tissue or during tissue fibrosis of damaged peripheral organs) is only limited to the infarct region in the ischemic hemisphere (see 5.2.1), no correlation between infarct volume and mRNA expression of collagen type I was detected (Figure 15B).

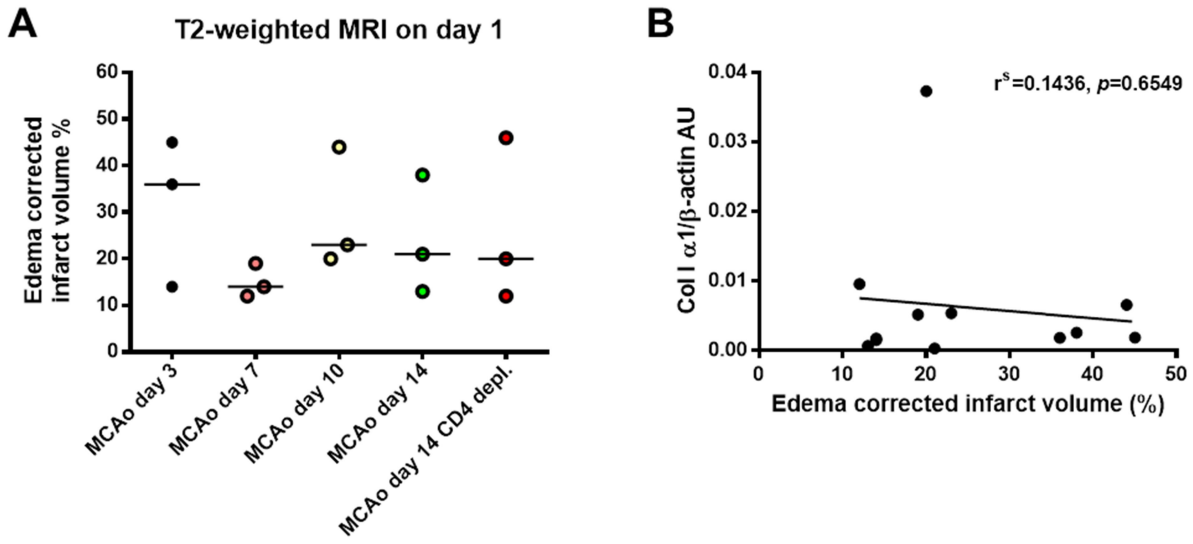

Figure 15. Quantification of infarct volume (day 1) and correlation between infarct volume and deposition of collagen type I fibrotic fibers in the ischemic hemisphere.

(A) Similarly, infarct volume was quantified on day 1 post stroke. Infarct volume of 2D2 mice with different survival days (N=3 per time point) had no significant differences. **(B)** No significant correlation was detected between infarct size and deposition of collagen type I in the ischemic hemisphere. Abbreviations: arbitrary unit (AU), collagen type I alpha 1 chain (Col I α1), CD4 depletion (CD4 depl.). All data from multiple groups were analyzed with Kruskal-Wallis test with Dunn's multiple comparison test. Each *p* value was adjusted to account for multiple comparisons. Data analyzed with non-parametric tests were expressed as median. Correlation was analyzed with nonparametric Spearman's *rho* correlation coefficient.

Firstly, mRNA expressions of collagen type I alpha subunit, transforming growth factor β type 1 (TGFβ1, a strong modulator for tissue remodeling and fibrosis after injury) (Iadecola and Anrather 2011) and C-C chemokine receptor type 2 (CCR2, chemokine for monocyte) (Gelderblom, Leypoldt et al. 2009) were investigated. At the mRNA level, expression of collagen type I expression was induced as early as day 7 after stroke, while in naïve mice it was not expressed at all (Figure 16A). However, CD4 depletion did not abolish the mRNA expression of collagen type I. The mRNA expression of TGFβ slightly increased on day 10 (median=0.020 AU) in the ischemic brain compared with that of naïve control (median=0.011 AU). Significant upregulation of CCR2 (median=0.044 AU) and TGFβ (median=0.020 AU) was measured in the ipsilateral hemisphere on day 10 compared with that of naïve control (median=0.009 AU and 0.006 AU, respectively) (Figure

16B and 16C). CD4 depletion did not affect expression of TGFβ1 and CCR2 in the ipsilateral hemisphere on day 14 post stroke. Nevertheless, plotting all paired data (without CD4 depletion) revealed a positive correlation between mRNA expressions of collagen type I and TGFβ1 in the ischemic hemispheres (Figure 16D and 16E).

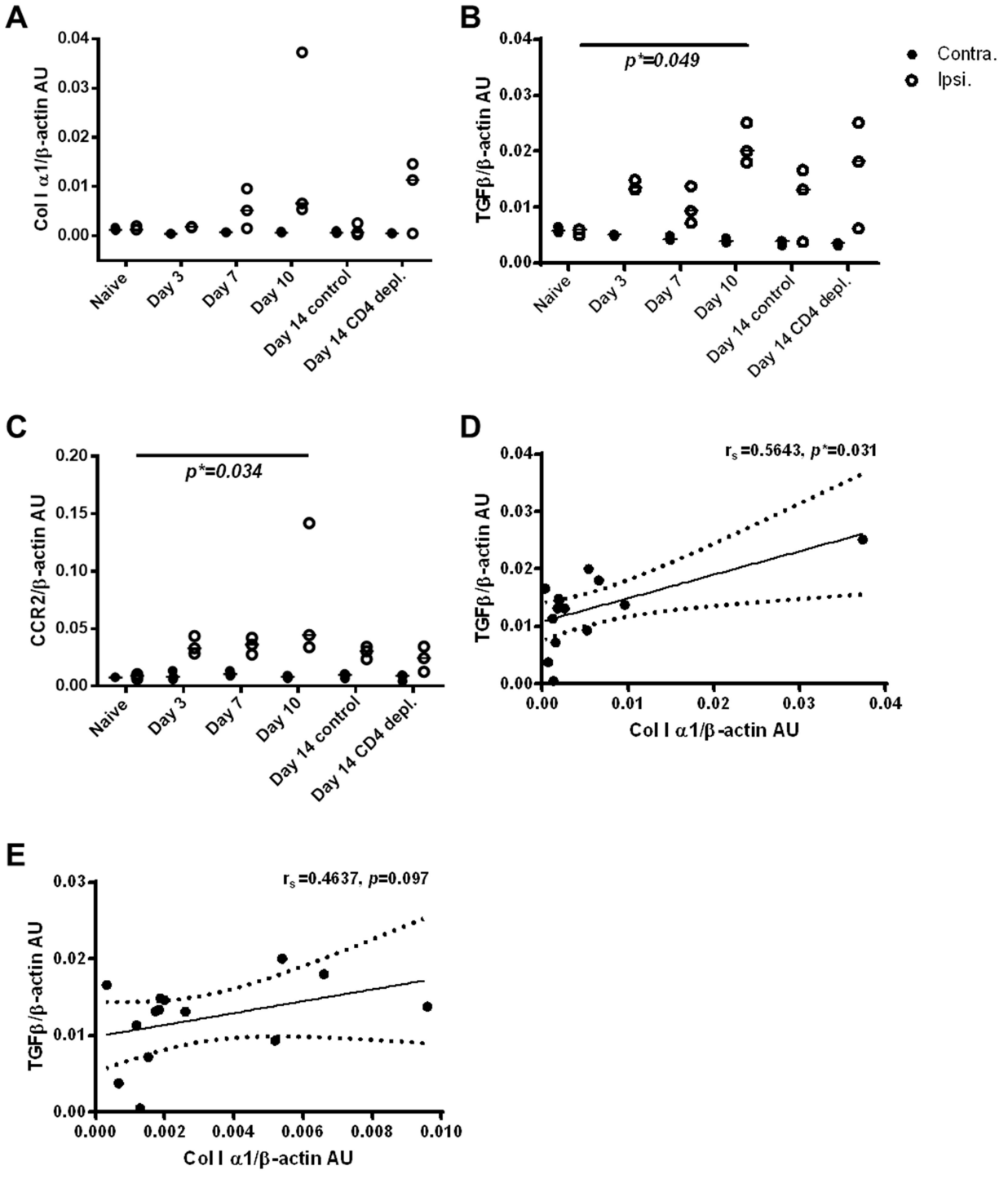

Figure 16. The relative expressions of mRNA in fibrosis-related fibrotic fibers, growth factor and chemokine receptor before and after ischemic stroke.

(A) Ischemic stroke induced slight upregulation of collagen type 1 in the ischemic hemisphere. **(B)** Expression of TGFβ1 significantly increased on day 10 after stroke in the ipsilateral hemispheres compared with that of naïve control mice (Kruskal-Wallis, p=0.064; corrected for multiple comparisons, p=0.049). **(C)** CCR2 was significantly upregulated on day 10 post stroke compared to naïve control (Kruskal-Wallis, p=0.025; corrected for multiple comparisons, p=0.034). **(D)** The mRNA expressions of collagen I and TGFβ1 positively correlated with each other (p=0.031). **(E)** There was an extreme value in the previous graph. To investigate how much this value would contaminate the real correlation between the mRNA expressions of collagen I and TGFβ1, data was analyzed again without that value. A strong correlation was still observed (p=0.097). Abbreviations: arbitrary unit (AU), collagen type I alpha 1 chain (Col I α1), transforming growth factor β type 1 (TGFβ1), C-C motif chemokine receptor 2 (CCR2), CD4 depletion (CD4 depl.), contralateral (contra.), and ipsilateral (ipsi.). Comparison of the two hemispheres was analyzed with Wilcoxon matched-pairs signed rank test. Comparison between control treatment and CD4 depletion in the ipsilateral hemisphere on day 14 were analyzed with Mann-Whitney U test. All data from multiple groups were analyzed with Kruskal-Wallis test with Dunn's multiple comparison test. Each p value was adjusted to account for multiple comparisons. Data analyzed with non-parametric tests were expressed as median. Correlation was analyzed with nonparametric Spearman's *rho* correlation coefficient. Significance level was marked as: *p<0.05, **p<0.01; N=3.

In contrast to inflammation-related growth factors (e.g. TGFβ1) or chemokines (e.g. CCR2) which were exclusively induced in the ischemic hemisphere, the mRNA expressions of CNS growth factors or receptors were simultaneously affected in both hemispheres after stroke. The expressions of NGF and VEGFa in whole brain were reduced over 50% after stroke compared with naïve control. In the contralateral hemispheres, the expressions of NGF, BDNF and VEGFa were significantly reduced in mice with control treatment on day 14 after stroke compared with that of naïve mice (Figure 17A-C).

PDGFRβ was evaluated to investigate whether pericytes and possibly fibroblasts are activated and contribute to the deposition of extracellular matrix (ECM) after stroke. In contrast to neuronal and vascular growth factors, mRNA expression of PDGFRβ did not undergo immediate reduction after stroke onset and showed a trend of upregulation in the ischemic hemispheres compared with the contralateral hemispheres (Figure 17D). Between the contralateral and the ipsilateral hemispheres,

no significant difference was detected. CD4 depletion also did not affect the expression of PDGFRβ. Data from qPCR indicated that stroke might modulate the genes related to tissue fibrosis and repairing. However, $CD4^+$ T cells do not have a significant effect on this process at the transcriptional level.

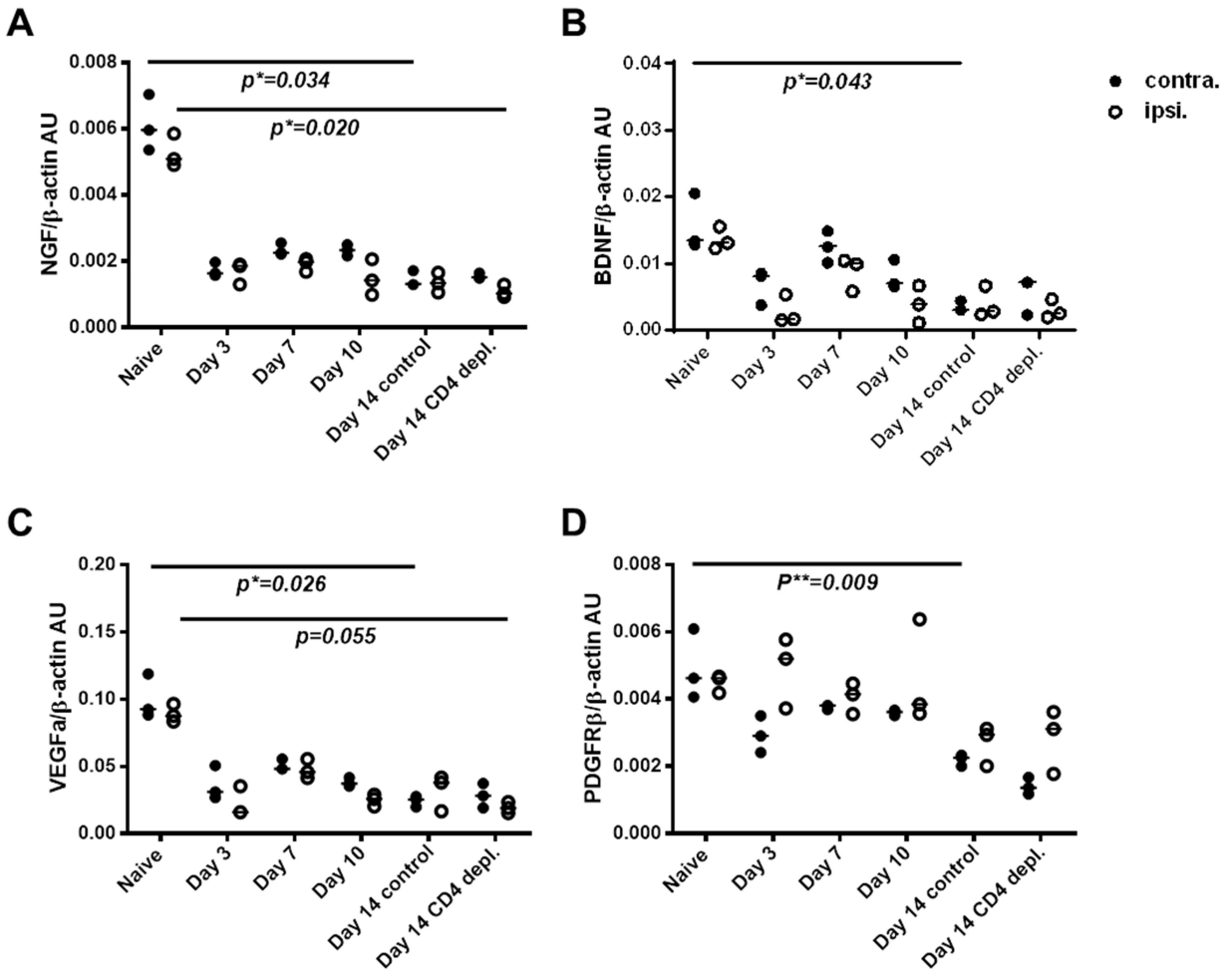

Figure 17. The relative mRNA expressions of CNS growth factors and pericyte-specific growth factor receptor before and after ischemic stroke.

(A) Ischemic stroke-impaired mRNA expression of NGF in both hemispheres. The expression of NGF in the ischemic hemispheres was reduced by over 80% on day 14 in mice with CD4 depletion compared with that of naïve controls (Kruskal-Wallis, p=0.012; corrected for multiple comparisons, p=0.034). There was a significant reduction of NGF on day 14 in the contralateral hemispheres of control animals compared with that of naïve controls (Kruskal-Wallis, p=0.028; corrected for multiple comparisons, p=0.020). **(B)** Significant reduction of BDNF in the contralateral hemispheres on day 14 with control treatment compared with that of naïve controls (Kruskal-Wallis, p=0.025; corrected for multiple comparisons, p=0.043). **(C)** Significantly impaired expression of VEGFa in the contralateral hemispheres of control animals on day 14 after stroke compare with that of naïve control (Kruskal-Wallis, p=0.022; corrected for multiple comparisons, p=0.026). The expression of VEGFa in the ischemic hemispheres was strongly reduced on day 14 in mice with CD4 depletion compared with that of naïve controls (Kruskal-Wallis, p=0.023; corrected for multiple comparisons, p=0.055). **(D)** The reduction of PDGFRβ was delayed after stroke. Significant reduction was only detected until day 14 in the contralateral hemispheres in mice with control treatment compared with that of naïve controls (Kruskal-Wallis, p=0.005; corrected for multiple comparisons, p=0.009). Abbreviations: arbitrary unit (AU), nerve growth factor (NGF), brain-derived neurotrophic factor (BDNF), vascular epithelial growth factor a (VEGFa), platelet-derived growth factor receptor β (PDGFRβ), CD4 depletion (CD4 depl.), central nervous system (CNS), contralateral (contra.), and ipsilateral (ipsi.). Comparison between control treatment and CD4 depletion on day 14 were analyzed with Mann-Whitney U test. All data from multiple groups were analyzed with Kruskal-Wallis test with Dunn's multiple comparison test. Each p value was adjusted to account for multiple comparisons. Data analyzed with non-parametric tests were expressed as median. Significance level was marked as: *p<0.05, **p<0.01; N=3.

5.2.3 Survival until 14 days after stroke and infarct maturation on day 7 were not affected by CD4 depletion in 2D2 mice

As mentioned previously (see 5.1.1), 2D2 mice generally have a lower survival rate than WT littermates. Since post-stroke infection influences survival, outcome and autoreactive immune responses after stroke (Romer, Engel et al. 2015), the preventative antibiotic treatment was given to all mice. In order to investigate the effect of $CD4^+$ T cells on mid-term functional recovery and tissue remodeling after stroke, an antibody-mediated $CD4^+$ T cell depletion experiment was designed (Figure 18A). To avoid bias, before any analysis at endpoint, infarct volumes on day 1 in

both groups were compared. In each experiment there was no significant difference in initial infarct size between two treatments (Figure 18B). At endpoint, survival rate was not significantly changed by depleting $CD4^+$ T cells after stroke (Figure 18C). Nevertheless, this also confirmed that neither control treatment nor CD4 depletion brought additional harm to the long-term survival of stroke-induced mice.

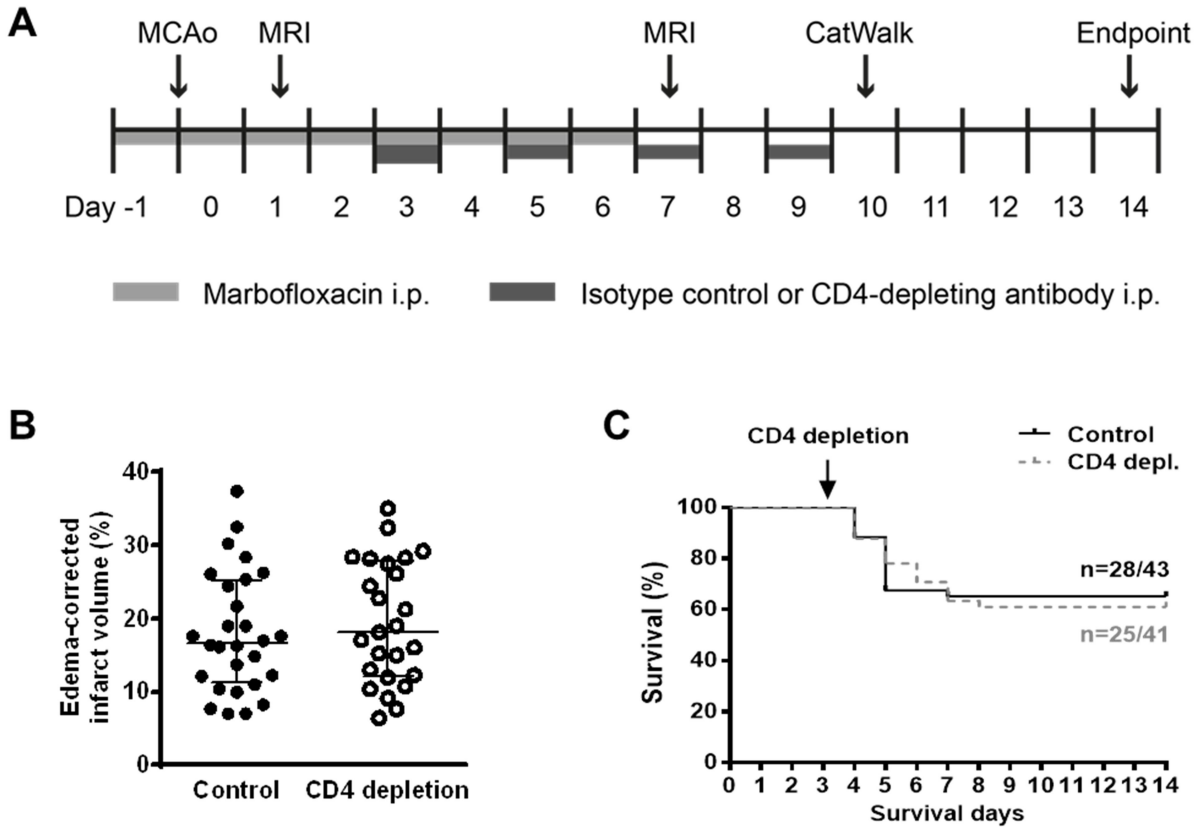

Figure 18. CD4 depletion has no effect on 14-day survival.

(A) CD4 depletion was performed as described before. Preventative antibiotic treatment with daily intraperitoneal injection of Marbofloxacin was used to prevent infection and related mortality. In all experiments, infarct size was measured on day 1 post stroke. In one experiment, infarct volume was measured once again on day 7 by T2-weighted MRI. Mid-term (day 10 after stroke) motor function was measured with Catwalk (see 5.2.7). Endpoint analysis included mainly immunofluorescent microscopy (see 5.2.4-5.2.6). **(B)** Animals with similarly averaged infarct size on day 1 post stroke were randomly allocated to either control treatment (N=28) or CD4 depletion (N=25). 2D2 mice that died before day 3 were not included. **(C)** Delayed CD4 depletion did not significantly influence 14-day survival in 2D2 mice with preventative antibiotic treatment. N indicates the number of mice that survived until day 14 and the number of mice that received at least one injection of antibody. Abbreviations: middle cerebral artery occlusion (MCAo); intraperitoneal (i.p.); CD4 depletion (CD4 depl.). Infarct size was analyzed with Mann-Whitney U Test. Data analyzed with non-parametric tests were expressed as median with interquartile range. Data were pooled from four experiments.

Delayed CD4 depletion starting on day 3 had no effect on infarct volume on day 7 after stroke (Figure 19A). In both treatment groups, infarct size significantly shrank on day 7 (control=15.00% (10.11-21.16)%, CD4 depletion=10.00% (7.69-17.00)%) compared with that of day 1 (control=19.00% (10.94-25.83)%, CD4 depletion=15.00% (10.79-19)%) (Figure 19B and 19C). There was no significant difference in infarct sizes on day 7 post stroke between control treatment and CD4 depletion.

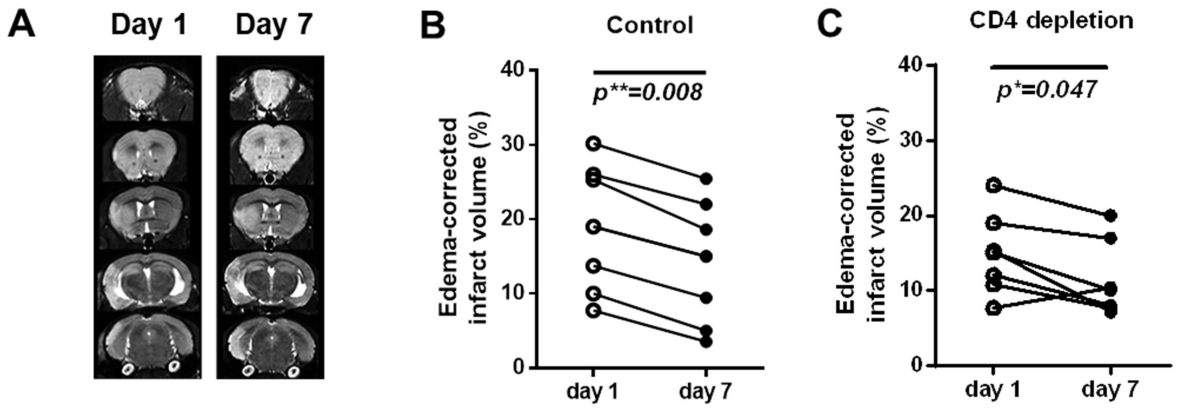

Figure 19. CD4 depletion did not significantly influence infarct maturation on day 7 after stroke.
(A) Representative T2-weighted images of infarction on day 1 and day 7 after stroke. **(B)** In control group (N=8, two mice had same infarct volumes at both time points), infarct size was significantly reduced on day 7 compared to day 1 post stroke (Wilcoxon Matched-pairs Signed Rank Test, p=0.008). **(C)** In CD4-depleted group (N=7), infarct size was also significantly reduced on day 7 compared to day 1 post stroke (Wilcoxon Matched-pairs Signed Rank Test, p=0.047). However, there was no significant difference in infarct size on day 7 after stroke between control treatment and anti-CD4 depletion. Data analyzed with non-parametric tests were expressed as median with interquartile range. Significance level was marked as: *p<0.05, **p<0.01.

5.2.4 CD4 depletion did not affect neuronal survival but does influence accumulation of myeloid cells in ischemic brain

Neurons were stained with NeuN and quantified in both hemispheres. Stroke induced severe loss of neurons in the ipsilateral hemispheres (Figure 20A). In both treatment groups, the counts of $NeuN^+$ neurons in the ischemic hemispheres (control=230 cells/slice, CD4 depletion=231 cells/slice) were significantly reduced compared with that of their correspondent contralateral hemispheres (control=347 cells/slice, CD4 depletion=340 cells/slice). However, there was no difference in the number of remaining neurons in the ischemic hemispheres between control treatment and CD4 depletion (Figure 20B). Moreover, microglia and macrophages selectively accumulated in the ipsilateral hemisphere (Figure 20C). In both treatment groups, the counts of $Iba1^+$ cells in the ischemic hemispheres (control=872 cells/slice, CD4 depletion=467 cells/slice) were significantly increased compared with that of their correspondent contralateral hemispheres (control=42 cells/slice, CD4 depletion=42 cells/slice). Even without significant difference, a trend towards reduced accumulation of activated microglia/macrophages in the ipsilateral hemisphere was detected in the CD4-depleted group (Figure 20D).

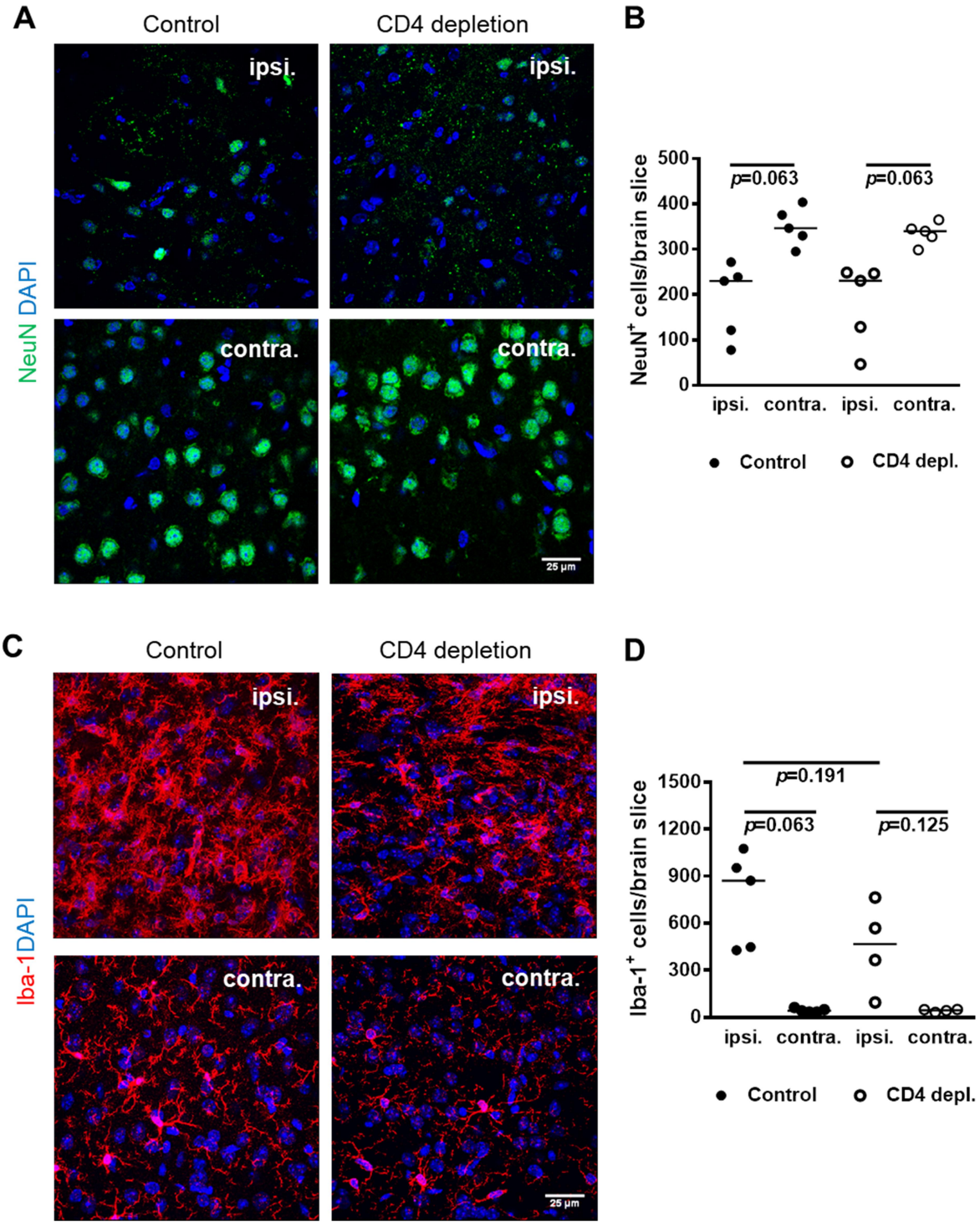
A
Control
CD4 depletion
ipsi.
ipsi.
contra.
contra.
NeuN DAPI
25 µm
B
NeuN+ cells/brain slice
500
400
300
200
100
0
p=0.063
p=0.063
ipsi.
contra.
ipsi.
contra.
Control
CD4 depl.
C
Control
CD4 depletion
ipsi.
ipsi.
contra.
contra.
Iba-1DAPI
25 µm
D
Iba-1+ cells/brain slice
1500
1200
900
600
300
0
p=0.191
p=0.063
p=0.125
ipsi.
contra.
ipsi.
contra.
Control
CD4 depl.

Figure 20. Reduced labeling of the neuronal marker and accumulation of Iba1$^+$ microglia and macrophages remained unchanged in the ischemic hemispheres with CD4 depletion compared to control treatment.

(A) Representative images from both hemispheres demonstrated lost immunoreactivity for neuronal marker (NeuN) exclusively in ischemic side. **(B)** Number of neurons were reduced in the ipsilateral hemisphere compared with the contralateral side (control p=0.063, CD4 depletion p=0.063, Wilcoxon Matched-Pairs Signed Rank Test). No significant difference was detected between control treatment and CD4 depletion regarding remaining neurons in the ipsilateral hemisphere (p>0.05, Mann-Whitney U Test). Scale bar: 25µm. **(C)** Representative images from both hemispheres demonstrated accumulation of Iba1$^+$ activated microglia and macrophages with thicker processes exclusively in ischemic side. Resting microglia cells in the contralateral hemisphere had typically ramified morphology. Scale bar: 25µm. **(D)** In both groups, more activated microglia/macrophages accumulated in the ischemic hemispheres (control p=0.063, CD4 depletion p=0.125, Wilcoxon Matched-Pairs Signed Rank Test). There was no significant difference in the number of microglia and macrophages in the ischemic hemispheres between the control treatment and CD4 depletion (p=0.191, Mann-Whitney U Test). Abbreviations: contralateral (contra.), and ipsilateral (ipsi.). Data analyzed with non-parametric tests were expressed as median. Significance level was marked as: *p<0.05, **p<0.01.

5.2.5 CD4 depletion significantly impaired proliferation of endothelial and periendothelial cells in peri-infarct area

Both resting and activated microglia express Iba-1. As a result, the differential accumulation of activated microglia and macrophages might be covered up by the larger number of resting microglia. Therefore activated microglia and macrophages were visualized by using specific marker CD68, which predominantly localizes to lysosomes and endosomes with a smaller fraction circulating to the cell surface. Activated microglia and macrophages were able to proliferate in the ischemic hemisphere on day 14 after stroke (Figure 21A). Though the number of CD68$^+$ activated microglia/macrophages was reduced in the CD4-depletion group (median=362 cells/slice) compared with that of the control group (median=534 cells/slice) (Figure 21B), the number of proliferating activated microglia and macrophages which double-labeled with CD68 and Ki67 (proliferating marker), showed a trend of reduced proliferation in mice with CD4 depletion (median=2 cells/slice) compared with that of the control treatment (median=20 cells/slice) (Figure 21C). This finding

suggests that the proliferation of activated microglia and macrophages during the delayed phase of inflammation in ischemic brain is partially regulated by $CD4^+$ T cells.

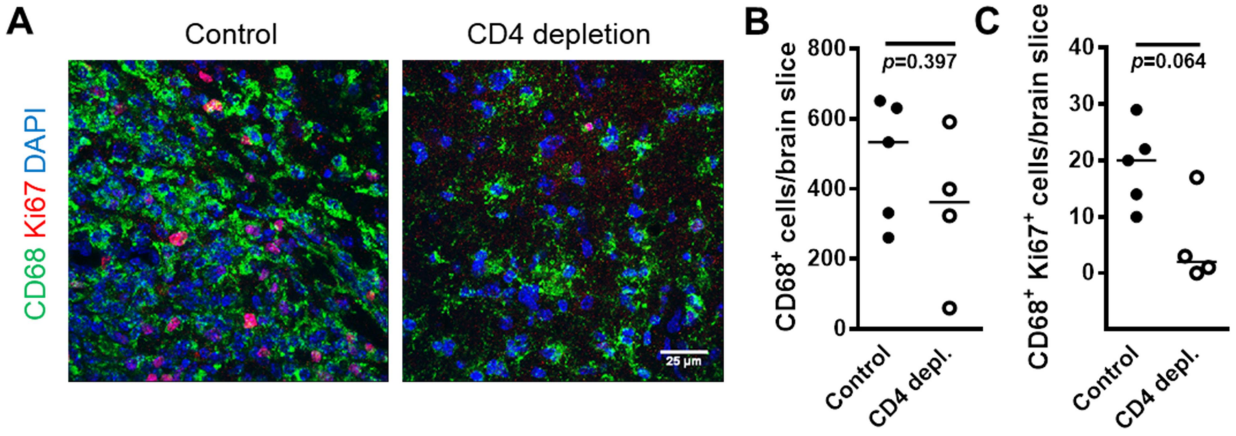

Figure 21. CD4 depletion-impaired proliferation of activated microglia and macrophages in the ischemic hemisphere during the delayed phase of post-stroke inflammation.

(A) Representative images from ischemic hemispheres demonstrated accumulation of $CD68^+$ activated microglia and macrophages as well as co-expression of Ki67 by proliferating cells. Scale bar: 25µm. **(B)** Number of activated microglia and macrophages did not differ much with CD4 depletion (p=0.397, Mann-Whitney U Test). **(C)** Proliferation of $CD68^+$ cells exhibited a trend towards reduction by CD4 depletion (p=0.064, Mann-Whitney U Test). Abbreviations: CD4 depletion (CD4 depl.). Data analyzed with non-parametric tests were expressed as median.

Besides inflammatory cells, the proliferation of endothelial and periendothelial cells, which can react to ischemia and contact with immune cells during their active transmigration through the blood-brain barrier (BBB), was carefully analyzed. CD13 was chosen to label endothelial and periendothelial cells (partially pericytes) of blood vessels in brain parenchyma (Alliot, Rutin et al. 1999). Macrophages can also express CD13. However by examining their morphology under immunofluorescent microcopy, staining of vessels can be easily distinguished from accumulation of macrophages within the infarct core. Similar to macrophages, there were also $Ki67^+$ proliferating cells within inflamed vasculature in peri-infarct area (Figure 22A). Interestingly, proliferation of

endothelial and periendothelial cells was significantly affected by CD4 depletion (control=41 cells/slice; CD4 depletion=11 cells/slice) (Figure 22B).

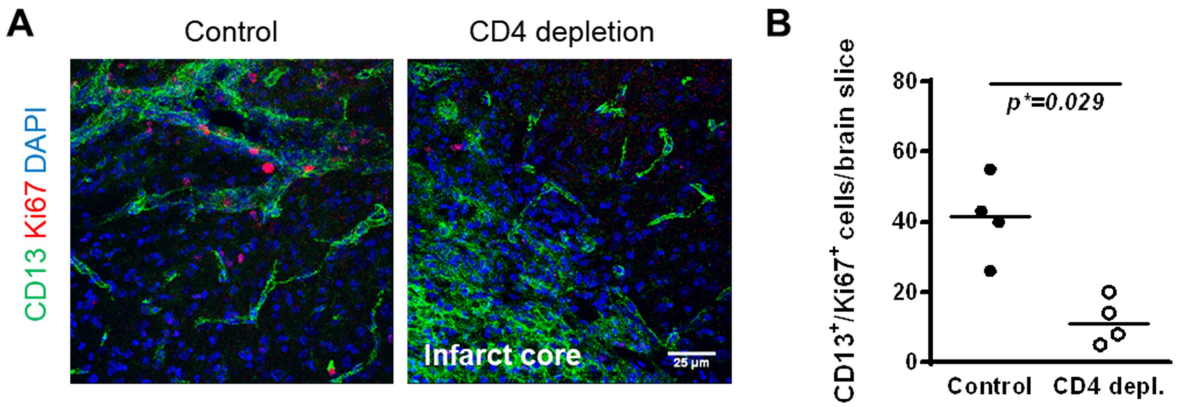

Figure 22. Proliferation of endothelial and periendothelial cells.

(A) Representative images from ischemic hemispheres showed proliferating endothelial and periendothelial cells in peri-infarct area. Image from CD4 depletion additionally included infarct core where immunoreactivity for CD13 was substantially up-regulated due to labeling of activated pericytes and macrophages. Scale bar: 25µm. **(B) The** number of proliferating endothelial and periendothelial cells significantly reduced with CD4 depletion compared to the control treatment **(***p*=0.029, Mann-Whitney U Test**).** Abbreviations: CD4 depletion (CD4 depl.). Data analyzed with non-parametric tests were expressed as median. Data analyzed with non-parametric tests were expressed as median. Significance level was marked as: *$p<0.05$, **$p<0.01$.

5.2.6 CD4 depletion significantly blocked CNS infiltration of B cells in 2D2 mice on day 14 after stroke

Since B cells also infiltrated ischemic brain and transiently proliferated at an early time point after stroke (see 5.1.2), the effect of CD4 depletion on the infiltration of B cells was evaluated. Compared with the control treatment (median=275 cells/slice), delayed CD4 depletion significantly blocked the infiltration of B cells into the ischemic hemispheres (median=0 cells/slice) in 2D2 mice

on day 14 after stroke (Figure 23A and 23B). Unlike $CD4^+$ T cells that disseminated in the peri-infarct area, $B220^+$ B cells formed condensed follicle-like aggregates near inflamed vasculature (Figure 23C and 23D).

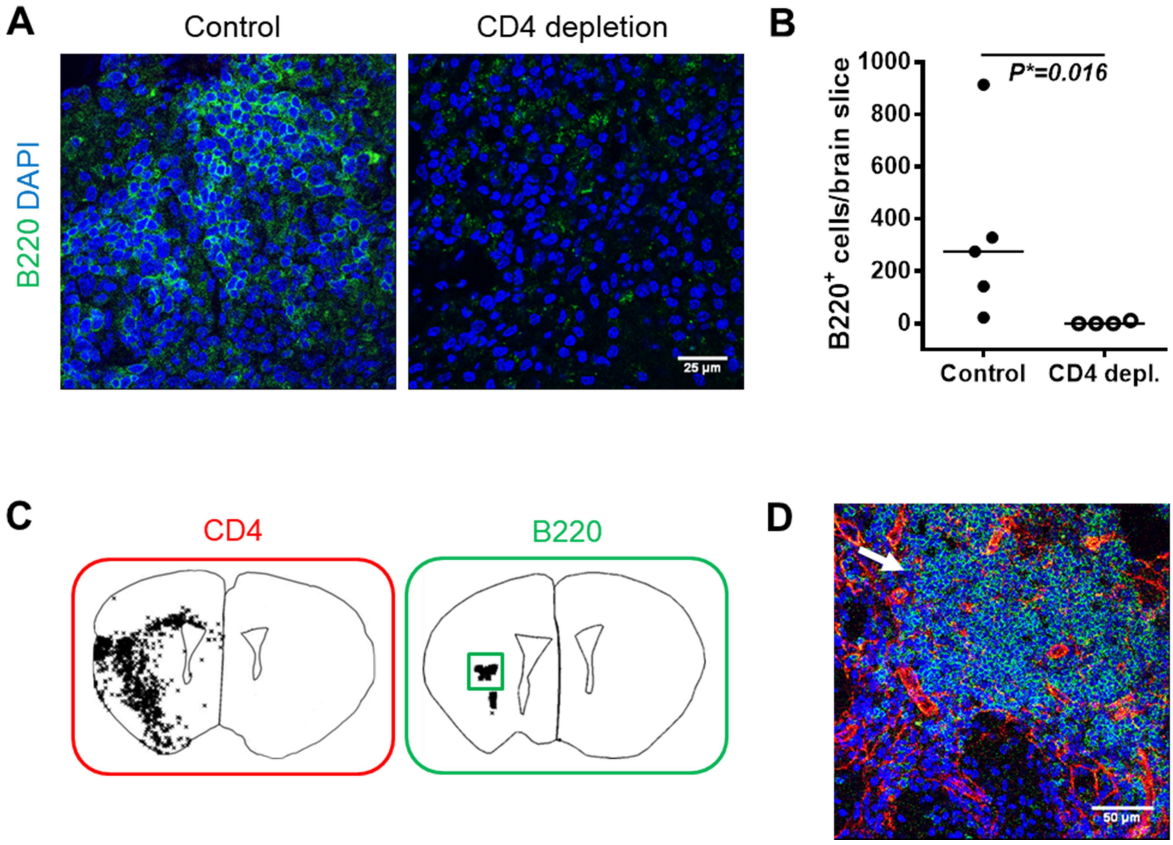

Figure 23. Follicle-like aggregates formed by infiltrating B cells is significantly blocked by CD4 depletion in 2D2 mice on day 14 after stroke.

(A) Representative images from ischemic hemispheres demonstrated accumulation of B cells in 2D2 mice with either control treatment or CD4 depletion. Scale bar: 25µm. **(B)** CNS infiltration by B cells was significantly blocked by delayed CD4 depletion (p=0.016, Mann-Whitney U Test). **(C)** Typical distribution of $CD4^+$ T cells and B cells in the ischemic hemisphere was obtained by counting all CD4 or B220 positively labeled cells in brain slice under fluorescent microscopy equipped with a Stereology workstation. **(D)** Representative image for B cell-rich follicle-like aggregates (indicated by white arrow) resided close to inflamed vasculature. Scale bar: 50µm. B cells (green) were labeled with $B220^+$ and basement membrane was labeled with collagen type IV. Nuclei (blue) were counterstained with DAPI. Data analyzed with non-parametric tests were expressed as median. Significance level was marked as: *p<0.05, **p<0.01.

5.2.7 Impact of CD4 depletion on functional outcome in 2D2 mice on day 10 after stroke

Cerebral ischemia induced via occlusion of left MCA with filament results in paralysis on the right side of the mouse body. Typical motor deficits detected by CatWalk include decreased maximum contact area and stride length, increased run duration as well as decreased normalized swing speed, increased stand time, altered base of support (distance between front or hind paws) at 10 days after MCAo in WT mice (Hetze, Romer et al. 2012). In our experiments, 2D2 mice with control treatment also showed similar motor deficits such as significantly decreased maximum contact area with the right hind paw, significantly increased run duration, decreased stride length, increased stand time and altered phase dispersion (Table 2). This indicated that 2D2 mice with $CD4^+$ T cells having transgenic MOG TCRs had similar patterns of gait impairments compared with WT littermates post stroke. Compared with control treatment, 2D2 mice with CD4 depletion had also significantly reduced maximal contact area and normalized swing speed in the right hind limb, but in general fewer gait parameters were significantly affected on day10 after stroke (Table 2).

Since several significant differences already existed in baseline between the two treatments, change from baseline was calculated to represent post-stroke functional status. This revealed significantly prolonged run duration and shortened stride length with left front limbs in the control group on day 10 after stroke (Table 2). Furthermore, the impairment score of the right hind limb was calculated to specifically detect stroke-induced deficits to the contralateral hind limb (Figure 24A). 2D2 mice with CD4 depletion had a lower impairment score of the right hind limb (median=2) compared with that of 2D2 mice with control treatment on day 10 after stroke (median=3) (Figure 24B).

Table 2. Gait analysis (CatWalk) of 2D2 mice with control or CD4-depletion treatment before and 10 days after MCAo.

Parameter	Definition	Paw	Control (N=26)		CD4 depletion (N=23)		Control	CD4 depletion
			Baseline	Day 10	Baseline	Day 10	Day 10 (Change from baseline)	Day 10 (change from baseline)
Spatial characteristics								
Max contact area (mm^2)	Maximal contact area of individual paws on glass plate	RF	20.60±4.10	19.35±4.39	18.07±4.18§	18.03±4.61	-1.26±5.67	-0.03±5.28
		RH	18.28±5.23	**13.57±7.41***	17.77±4.64	**12.62±4.77****	-4.71±9.04	-5.15±6.07
		LF	22.05±3.70	22.11±4.31	19.39±3.12§§	20.70±3.08	0.06±5.00	1.31±3.76
		LH	20.24±5.31	18.55±7.35	17.84±4.78	16.07±5.75	-1.69±8.21	-1.77±7.87
Kinetic characteristics								
Run durations (s)	Time for passing through the walkway		2.47±0.50	**3.12±0.63*****	3.11±0.69§§	3.09±0.52	0.65±0.83	**-0.01±0.83**$^{\#}$
Normalized swing speed (mm)	Swing speed (mm/s) x Run duration (s)	RF	806.38±153.02	**913.82±215.06***	1145.56±271.07§§§	1097.61±225.54	107.45±156.87-	**-47.95±233.92**$^{\#}$
		RH	721.73±178.05	675.93±225.65	1080.49±306.22§§§	**866.83±222.07***	-45.79±246.54	**-213.66±207.52**$^{\#\#}$
		LF	843.32±206.90	948.25±299.20	1174.16±271.85§§§	1120.70±234.47	104.93±235.99	**-53.46±234.02**$^{\#}$
		LH	772.78±144.17	847.95±276.76	1162.38±235.10§§§	996.67±192.81	75.18±236.48	**-65.70±226.52**$^{\#}$
Stand (s)	Duration of individual paws contacting glass plate	RF	0.17±0.03	**0.20±0.04*****	0.19±0.03§	0.21±0.04	0.04±0.04	0.02±0.05
		RH	0.15±0.02	0.15±0.05	0.18±0.04§§§	0.16±0.04	0.01±0.06	-0.02±0.05
		LF	0.17±0.03	**0.19±0.04****	0.20±0.04§	0.21±0.03	0.03±0.05	0.01±0.05
		LH	0.16±0.02	**0.18±0.05****	0.18±0.03§	0.19±0.05	0.02±0.05	0.01±0.05
Comparative statistics								
Regularity index (%)	Regularity of gait		91.78±5.30	86.93±16.35	88.77±7.64	89.65±10.21	-4.85±16.68	0.85±13.29
Base of support (mm)	Distance between both front paws or hind paws	RF-LF	10.15±6.98	10.47±8.09	11.83±7.63	10.70±7.62	0.32±11.72	-1.13±9.53
		RH-LH	19.83±14.77	19.18±15.00	23.04±15.90	17.15±11.61	-0.65±23.76	-5.89±15.59
Stride length (mm)	Distance between successive steps of the same paw	RF	41.35±7.91	37.89±5.80	47.10±9.64	47.88±8.18	-3.47±6.78	0.79±7.96
		RH	37.41±9.38	34.21±8.20	42.92±8.35§	43.87±9.72	-3.19±9.67	0.95±9.31
		LF	41.67±7.77	**37.57±6.08***	47.39±8.15§	47.90±7.86	-4.10±6.51	**0.51±7.03**$^{\#}$
		LH	38.50±8.57	**33.28±6.08***	43.13±9.93	43.40±9.52	-5.22±10.14	0.27±10.40
Phase dispersion (%)	Contact of a target paw in relation to step cycle of another paw	RF-LH	3.50±6.03	**7.74±7.22***	4.63±5.41	8.57±8.19	4.23±9.78	3.94±9.68
		LF-RH	6.79±7.46	9.64±6.71	7.18±6.29	9.58±6.26	2.86±10.68	2.40±8.15
		RH-LH	39.13±9.34	41.88±9.21	41.78±7.47	42.73±9.77	2.75±12.15	0.95±11.73
		RF-LF	51.07±2.76	49.79±4.41	49.30±5.04	50.71±2.93	-1.29±4.69	1.41±5.51
		RF-RH	46.36±5.69	**51.52±5.45****	46.44±5.61	**50.75±7.59***	5.16±8.64	4.31±9.10
		LF-LH	47.86±4.00	49.07±9.20	46.21±6.40	**50.64±6.09***	1.22±10.03	4.43±7.87

comparison between baselines and paired measurements on day 10 after MCAo: Wilcoxon Signed Rank Test (p<0.05, **p<0.01, ***p<0.001).
§comparison between baselines in either treatment: Mann-Whitney U Test (§p<0.05, §§p<0.01, §§§p<0.001)
#comparison of change from baseline between control and CD4 depletion treatments on day 10 after MCAo: Mann-Whitney U Test (#p<0.05, ##p<0.01)
Abbreviations: RF, right front paw; RH, right hind paw; LF, left front paw; LH, left hind paw. 2D2 mice: gender-mixed. Control N=26, CD4 depletion N=23.

A

Right Hind limb	↑ / -	↓
Max contact area (mm^2)	0	1
Normalized swing speed (mm)	0	1
Stand (s)	0	1
Stride length (mm)	0	1

B

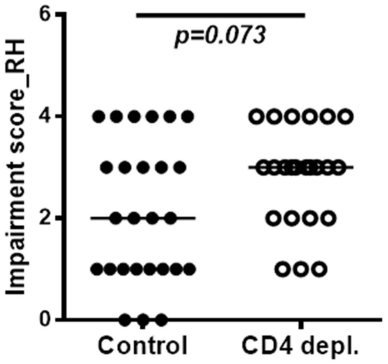

Figure 24. Functional deficits on day 10 after stroke in 2D2 mice measured by an impairment score are much reduced by CD4 depletion.

(A) Reduction in maximal contact area, normalized swing speed, stand and stride length of the right hind limb was summed as an overall impairment score. For each item, only reduction compared with baseline got one point. **(B)** In the CD4-depletion group, the impairment score of the right hind limb was lower than that in the control group (Control=26, CD4 depletion=23, p=0.073, Mann-Whitney U Test). Abbreviations: right hind limb (RH); CD4 depletion (CD4 depl.). Data analyzed with non-parametric tests were expressed as median.

5.3 B cells formed follicle-like aggregates in WT mice after stroke and were associated with autoantibody production and potential cognitive impairment

5.3.1 Significant blockage of B cell entry by delayed CD4 depletion in ischemic brain was only detected in 2D2 mice but not in WT mice on day 14 after stroke

Both T and B lymphocytes have been proven to infiltrate into ischemic brain, however the interdependence between $CD4^+$ T cells and B cells have not been reported in stroke. In order to confirm the significant impairment of B cell infiltration into ischemic brain of 2D2 mice seen with immunohistochemistry, I alternatively quantified CNS-infiltrating B cells and myeloid cells from control and CD4 depletion groups with flow cytometry. Moreover, I compared the effect of CD4 depletion additionally in WT mice to validate whether strong blockage of B cell infiltration by CD4 depletion seen in 2D2 mice was also effective in WT mice. Besides the same CD4-depletion procedure and preventative antibiotic treatment, a neurological Deficit Score (De Simoni) (Orsini,

Villa et al. 2012) was repeatedly performed to evaluate the general health status as well as focal deficits (Figure 25A). Functional deficits developed on day 3, and they showed a tendency to further deteriorate between day 7 and day 13 in the control group, while mice with CD4 depletion showed peak neurologic deficits on day 7 with subsequent recovery on day 13 compared with the earlier time points (Figure 25B). 2D2 mice with CD4 depletion had lower neurological scores (median=4.5) compared with that of the control group (median=20) on day 13 after stroke. WT mice developed a similar severity of functional deficits on day 3, compared to 2D2 mice, but experienced similar recovery on day 13 in both groups (control=9, CD4 depletion=7) (Figure 25C).

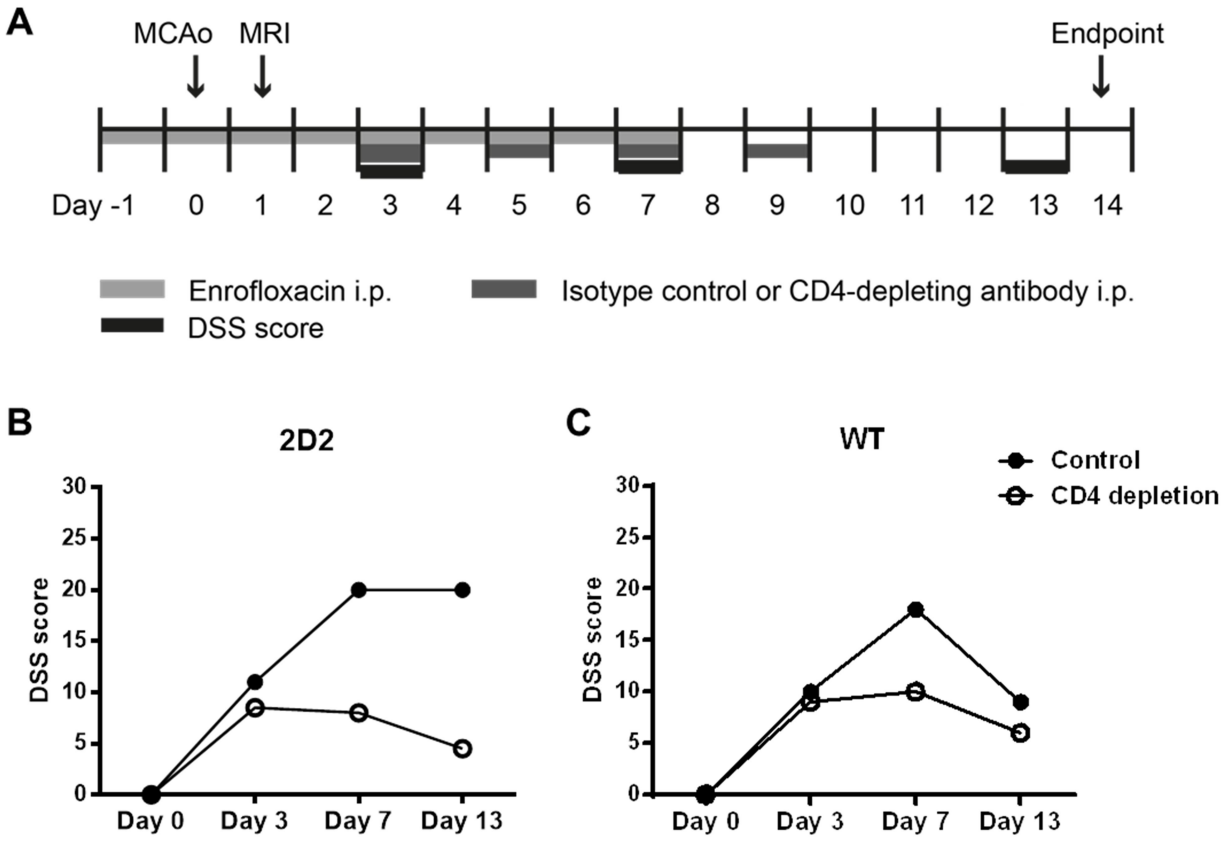

Figure 25. Comparison of neurological score between control treatment and CD4 depletion in 2D2 and WT mice following stroke.

(A) 60 min MCAo and CD4 depletion were performed. Preventative antibiotic (Enrofloxacin) was given one day before the operation and administered until day 7 after stroke. Mice with either treatment surviving until day 13 had similar initial infarct sizes on day 1 post stroke (data not shown, Mann-Whitney U Test, control vs. CD4 depletion in 2D2 mice, p=0.619; control vs. CD4 depletion in WT mice, p=0.994). The neurological deficit score was evaluated before operation and repeated on days 3, 7 and 13 after stroke. At endpoint (day 14), mononuclear cells from ischemic hemispheres were analyzed by flow cytometry**.** Serum samples were also prepared from peripheral blood for chemokine analysis. **(B)** 2D2 mice with CD4 depletion exhibited recovery on day 13 compared to the control treatment after stroke (Control=3, CD4 depletion=6, Mann-Whitney U Test, p=0.114). **(C)** CD4 depletion did not affect neurological recovery in WT mice compared to the control treatment on day 13 after stroke (Control=5, CD4 depletion=5). Data analyzed with non-parametric tests were expressed as median.

Even though CD4 depletion did not significantly promote neurological recovery in 2D2 mice, the strong blockage of B cells infiltrating into the ischemic hemisphere was reproducible with FACS analysis. Quantitatively speaking, our data reaffirmed that CD4 depletion during the delayed phase not only significantly blocked the entry of $CD4^+$ T cells (median=14 cells) but also significantly impaired the infiltration of B cells (median=1936 cells) and their follicle-like aggregation in the ischemic hemispheres compared with that of the control group ($CD4^+$ T cells=64599 cells; B cells=39658 cells) (Figure 26A). However, using the same experimental setup, there was no such significant blockage of the B cells' infiltration with CD4 depletion in WT mice (Figure 26B). Only $CD4^+$ T cells were successfully depleted in the ischemic hemispheres (control=1762 cells; CD4 depletion=7 cells).

The migration of B cells is strongly regulated by the B cell chemokine CXCL13 (Huber and Irani 2015). The expression of CXCL13 was detected surrounding follicle-like aggregates on day 14 after stroke (Figure 26C). The mRNA expression of CXCL13 was exclusively increased in the ischemic hemispheres (median=0.114 AU) of 2D2 mice on day 14 after stroke compared with that of contralateral sides (median=0.0043 AU) (Figure 26D). Since B cells were originally recruited from the periphery, the serum levels of CXCL13 in WT and 2D2 mice, both in control and anti-CD4-depletion groups were compared. While in 2D2 mice, the serum level of CXCL13 was slightly

reduced by CD4 depletion (median=572.7 pg/ml) compared with that of the control group (median=980.1 pg/ml) (Figure 26E), the serum level of CXCL13 was not affected by CD4 depletion in WT mice (Control=595.2 pg/ml, CD4 depletion=592.3 pg/ml) (Figure 26F).

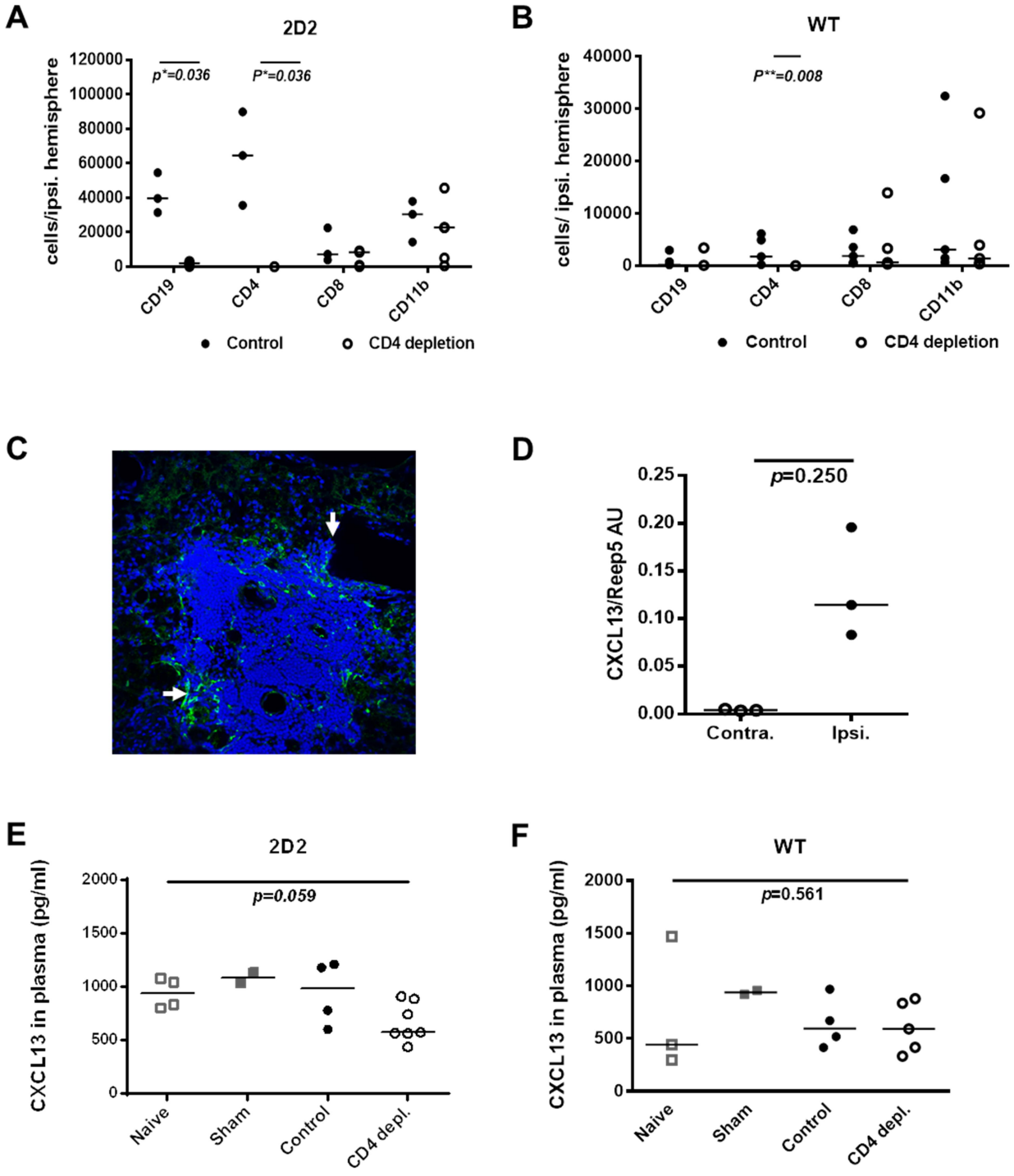

Figure 26. CD4 depletion significantly blocks CNS infiltration by B cells in 2D2 mice but not in WT mice on day 14 after stroke.

(A) CD4 depletion significantly depleted $CD4^+$ T cells (Mann-Whitney U Test, p=0.036) and impaired the entry of B cells into the ischemic hemisphere (Mann-Whitney U Test, p=0.036). Control N=3, CD4 depletion N=6. **(B)** CD4 depletion still worked effectively to deplete $CD4^+$ T cells (N=5 per group, Mann-Whitney U Test, p=0.008), but no significant difference was detected in B cell infiltration between the control and CD4-depletion group in WT mice. **(C)** Expression of CXCL13 surrounding follicle-like aggregates (indicated by white arrows) increased only in the ischemic hemisphere of 2D2 mice on day 14 after stroke. CXCL13: green. DAPI: blue. Magnification: 25X. **(D)** The mRNA expression of CXCL13 in the ischemic hemispheres of 2D2 mice on day 14 after stroke (N=3, Wilcoxon Matched-pairs Signed Rank Test, p=0.25). Reep5 served as a housekeeping gene. **(E)** Serum samples from two treatment groups collected at endpoint (day 14 after stroke) were compared with control serum samples from either naïve (N=4) or sham-operated (N=2) 2D2 mice. There was no significant difference among any groups in 2D2 mice (Kruskal-Wallis, p=0.059; corrected for multiple comparisons, not significant). But the serum level of CXCL13 was slightly reduced by CD4 depletion compared with the control group. (**F)** CD4 depletion did not influence the concentration of CXCL13 in serum samples in WT mice (naïve N=3, sham N=2, control N=5, CD4 depletion=5, Kruskal-Wallis, p=0.561; corrected for multiple comparisons, not significant). Abbreviations: ipsilateral (ipsi.); CD4 depletion (CD4 depl.). All data from multiple groups were analyzed with the Kruskal-Wallis test with Dunn's multiple comparison test. Each p value was adjusted to account for multiple comparisons. Data analyzed with non-parametric tests were expressed as median. Significance level was marked as: *p<0.05, **p<0.01.

5.3.2 Significantly more B cells accumulated in the ischemic brain of WT mice on day 49 compared to day 14 after stroke

Compared to 2D2 mice, WT littermates have limited potential to induce autoreactivity after stroke. Infiltration of $CD4^+$ T cells is significantly less pronounced and slower in WT mice compared to 2D2 mice (see 5.1.1). Moreover, comparing FACS data from the previous section showed that a similar number of B cells accumulated in the ischemic brain of WT mice compared with either control treatment or CD4 depletion on day 14 after stroke. However it was not clear whether relatively fewer B cells seen in WT mice could still form follicle-like aggregates. To address this question, kinetic B cell migration was carefully measured on day 14 and day 49 after stroke. Unlike 2D2 mice, WT mice had accumulation but no obvious follicle-like aggregates of B cells on day 14 after stroke (Figure 27A). Compared with day 14 (median=1237 B cells), significantly more B cells

with typical follicle-like organization accumulated in the ischemic brain on day 49 after stroke (median=7500 B cells) (Figure 27B). The delayed infiltration of $CD4^+$ T cells (see 5.1.1) and formation of B cell aggregates in WT mice perfectly indicated the link between autoreactive $CD4^+$ T cells and potential autoimmunity driven by B cells.

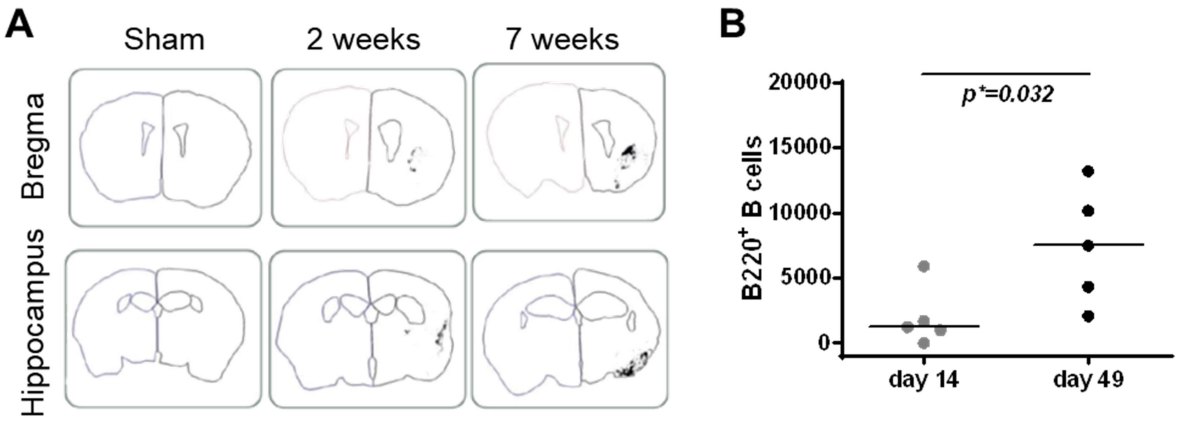

Figure 27. B cells continuously accumulate in the ischemic hemispheres in WT mice between day 14 and day 49 after stroke.

(A) Representative counting images of B cells in brains from sham-operated mice and stroke-induced mice. Cell counts from two slices at both bregma and hippocampus levels were chosen to represent each mouse. **(B)** Compared to day 14, the accumulation of B cells in the ischemic hemispheres was significantly up-regulated on day 49 after stroke (Mann-Whitney U Test, p=0.032). Data analyzed with non-parametric tests were expressed as median. Significance level was marked as: *p<0.05.

5.3.3 Stroke-induced expansion of plasmablasts/plasma cells and marginal zone B cells in ischemic brain and spleen of WT mice

In the FACS analysis, the total CNS-infiltrating leukocytes did not significantly decline between day 14 and day 49 after stroke in the ischemic brain of WT mice (Figure 28A), but the percentage of $CD19^+$ B cells in overall infiltrating leukocytes did significantly increase on day 49 (36.80% (20.46-44.93)%) compared with that of day 14 (7.93% (3.95-12.45)%) after stroke (Figure 28B). Follicular B cell was the main B cell subset residing in ischemic brain at both time points (Figure 28C). Both

plasmablasts/plasma cells and marginal zone B cells had their highest representations within B cell compartment on day 14 after stroke (Figure 28C). The percentage of plasmablasts/plasma cells significantly reduced on day 49 (13.91% (9.92-18.70) %) compared with day 14 (24.03% (20.86-44.79) %) after stroke (Figure 28D). The percentage of marginal zone B cells also significantly decreased on day 49 (0.60% (0.36-1.44) %) compared with day 14 (2.21% (1.42-4.22) %) after stroke (Figure 28E). However, the absolute counts of both cell types did not significantly change between day 14 and day 49 (data not shown).

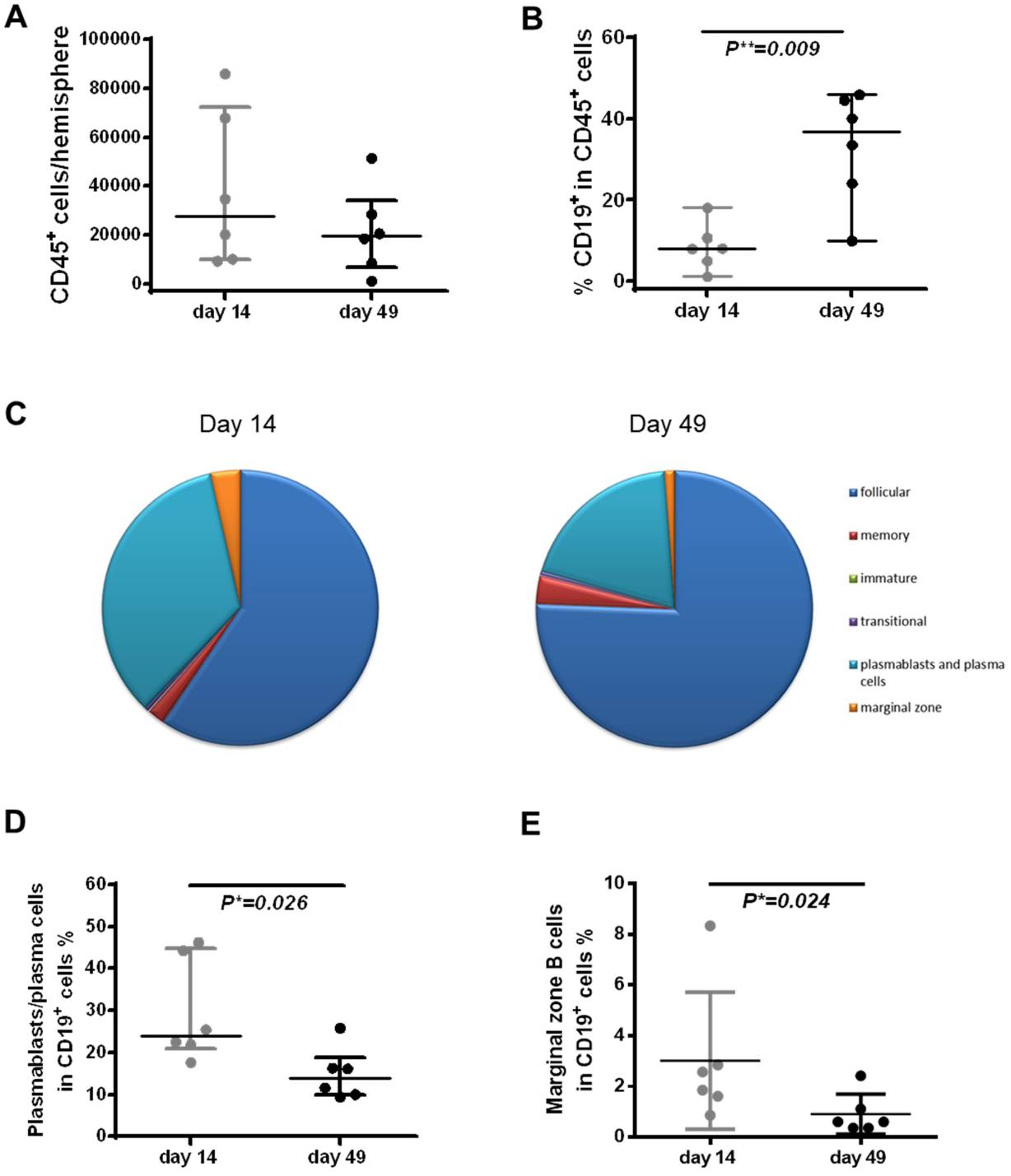
A
CD45+ cells/hemisphere
100000
80000
60000
40000
20000
0
day 14
day 49
B
% CD19+ in CD45+ cells
60
40
20
0
P**=0.009
day 14
day 49
C
Day 14
Day 49
follicular
memory
immature
transitional
plasmablasts and plasma cells
marginal zone
D
Plasmablasts/plasma cells in CD19+ cells %
60
50
40
30
20
10
0
P*=0.026
day 14
day 49
E
Marginal zone B cells in CD19+ cells %
10
8
6
4
2
0
P*=0.024
day 14
day 49

Figure 28. Ratios of plasmablasts/plasma cells and marginal zone B cells in ischemic brain are significantly higher on day 14 compared to day 49 after stroke.

(A) The overall infiltrating leukocytes slightly decreased on day 49 (N=6) compared with day 14 (N=6) after stroke (Mann-Whitney U Test, p=0.387). **(B)** FACS analysis showed significantly increased percentage of B cells among total infiltrating leukocytes on day 49 day compared with day 14 after stroke (Mann-Whitney U Test, p=0.009). CD45: pan leukocyte marker. CD19: B cell marker. **(C)** Summary of mean subset percentages within B cell compartment in the ischemic hemisphere on day 14 and day 49 after stroke. Infiltrating B cells were mainly composed of follicular B cells, while plasmablasts/plasma cells formed the second largest population. **(D)** A significantly higher percentage of plasmablasts/plasma cells were detected in the ischemic hemisphere on day 14 compared with day 49 after stroke (Mann-Whitney U Test, p=0.026). **(E)** A significantly higher percentage of marginal zone B cells were detected in the ischemic hemisphere on day 14 compared with day 49 after stroke (Mann-Whitney U Test, p=0.024). Data analyzed with non-parametric tests were expressed as median with interquartile range. Significance level was marked as: *p<0.05, **p<0.01.

Not only ischemic brain but also secondary lymphoid organs such as spleen could be involved in priming and early proliferation of B lymphocytes following stroke (see 5.1.2). Therefore B cell subsets in spleen were also analyzed by FACS at both time points. On day 14 after stroke, the influence of stroke-induced immunodepression on splenocytes was already weaker compared with that in the acute phase. Total counts of $CD45^+$ leukocytes did not differ between day 14 and day 49 post stroke compared with naïve mice (Figure 29A). The percentage of $CD19^+$ B cells was significantly reduced on day 14 (39.35% (30.13-43.03)%) and recovered on day 49 (46.00% (40.15-51.53)%) similar to the level in naïve control mice (median=52.00%) (Figure 29B). Furthermore, comparing percentages of different subsets within B cell compartment, it became clear that marginal zone B cells expanded more compared with plasmablasts/plasma cells on day 14 post stroke (Figure 29C). The percentage of plasmablasts/plasma cells (17.25% (12.95-24.61)%) prominently up-regulated on day 14 compared with naïve control (9.91% (7.73-11.15)%) and that of day 49 after stroke (10.89% (9.50-11.73)%) (Figure 29D). In addition, the percentage of marginal zone B cells also slightly increased on day 14 (22.27% (18.56-34.70)%) compared with naïve control (5.46% (4.46-10.35)%) (Figure 29E).

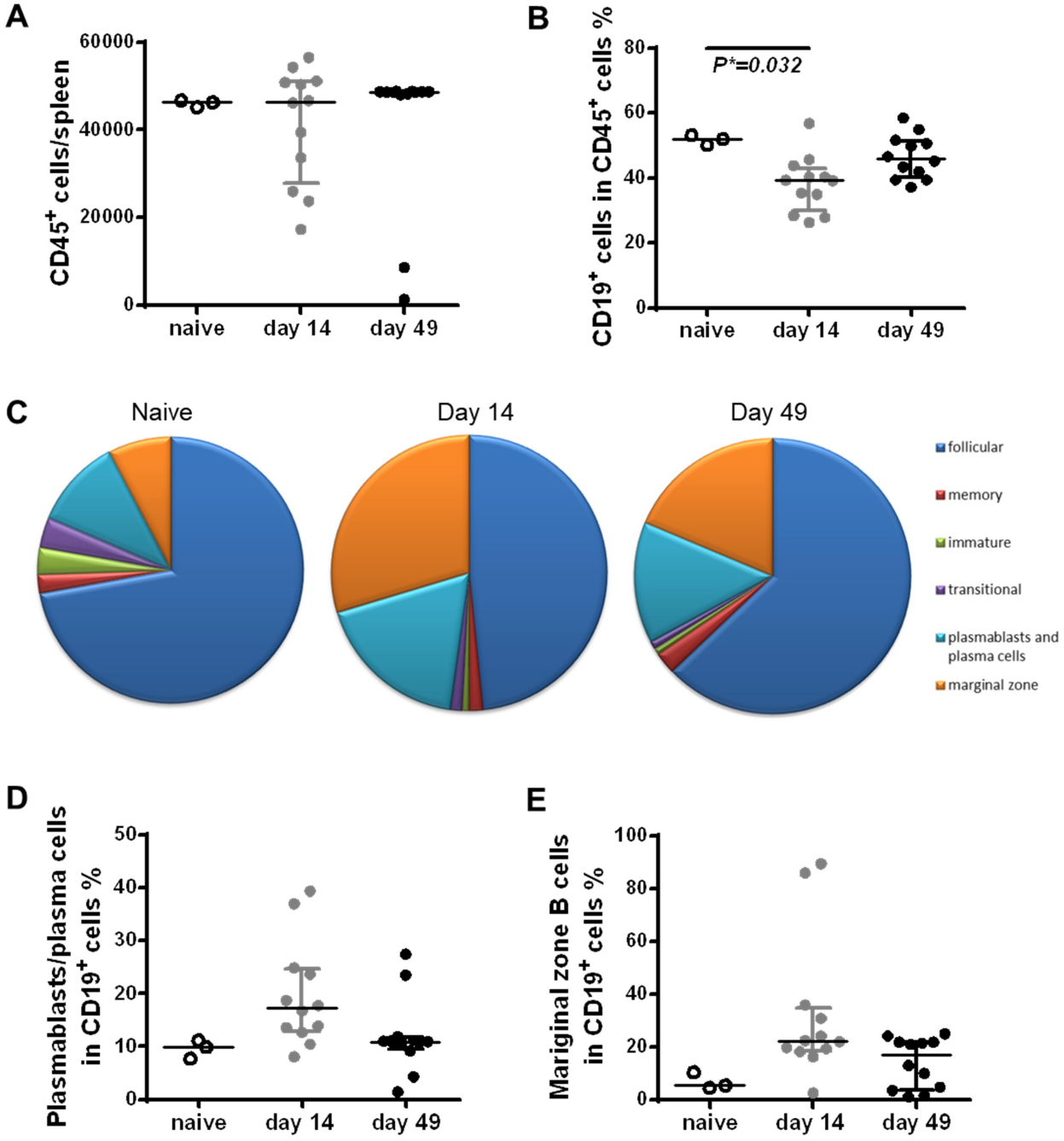
A
CD45+ cells/spleen
60000
40000
20000
0
naive
day 14
day 49
B
CD19+ cells in CD45+ cells %
P*=0.032
80
60
40
20
0
naive
day 14
day 49
C
Naive
Day 14
Day 49
follicular
memory
immature
transitional
plasmablasts and plasma cells
marginal zone
D
Plasmablasts/plasma cells in CD19+ cells %
50
40
30
20
10
0
naive
day 14
day 49
E
Mariginal zone B cells in CD19+ cells %
100
80
60
40
20
0
naive
day 14
day 49

Figure 29. B cells are significantly reduced in spleen on day 14 with normalization by day 49 after stroke.

(A) The overall $CD45^+$ leukocytes did not differ among naïve control mice (N=3) on day14 (N=12) or day 49 (N=12) after stroke. **(B)** The percentage of $CD19^+$ B cells significantly reduced on day 14 compared to naïve control mice (Kruskal-Wallis, p=0.011; corrected for multiple comparisons, p=0.032). **(C)** Summary of mean subset percentages within B cell compartment in spleens of naïve mice and mice on day 14 as well as day 49 after stroke. Infiltrating B cells were mainly composed of follicular B cells, while plasmablasts/plasma cells and marginal zone (MZ) B cells formed the second largest populations. **(D)** There was a trend that the percentage of plasmablasts/plasma cells prominently up-regulated on day 14 compared with naïve control mice (Kruskal-Wallis, p=0.021; corrected for multiple comparisons, p=0.085) and slightly decreased on day 49 (Kruskal-Wallis, p=0.021; corrected for multiple comparisons, p=0.062). **(E)** The percentage of marginal zone B cells also slightly up-regulated on day 14 compared with naïve control mice (Kruskal-Wallis, p=0.046; corrected for multiple comparisons, p=0.100). Abbreviation: marginal zone (MZ). All data from different groups were analyzed with Kruskal-Wallis test and with Dunn's multiple comparison test. Each p value was adjusted to account for multiple comparisons. Data analyzed with non-parametric tests were expressed as either median or median with interquartile range. Significance level was marked as: *p<0.05.

5.3.4 Delayed formation of follicle-like aggregates by B cells was associated with delayed cognitive impairment

Previous evidence of B cell follicular aggregates and expansion of plasmablasts/plasma cells as well as marginal zone B cells strongly suggested possible development of autoreactivity-induced functional impairment during the chronic phase of stroke. A Y maze (Figure 30A) was used in this thesis to evaluate spatial working memory. In line with the kinetics of brain-infiltrating B cells, there was no detectable memory deficit on day 13 after stroke (Figure 30B), when the accumulation of B cells was not yet as prominent as it was on day 48. The significant impairment of spatial working memory was detected only until day 49 after stroke (60.00% (43.25-67.00)% alternation) compared with naïve control mice (73.00% (60.00-80.00)% alternation) (Figure 30C), indicating a possible correlation between autoimmunity-driven B cells and a decline in cognitive function during the chronic phase of stroke.

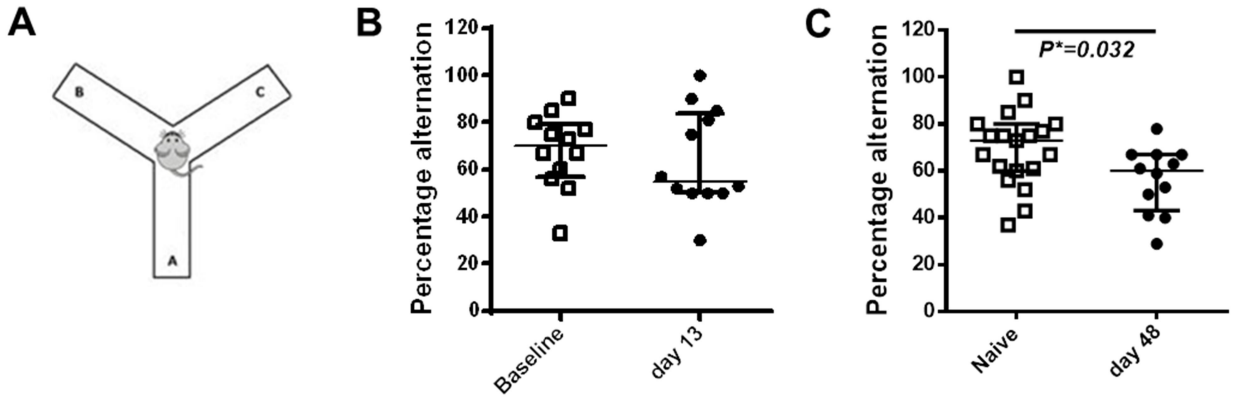

Figure 30. WT mice develop memory deficits at 48 days after stroke.

(A) Schematic representation of Y maze test of spatial working memory. The mouse was placed in the maze. Subsequent entries to different arms allowed the calculation of percentage alternation which reflects working memory performance. **(B)** On day 13, there was not yet evidence of memory deficits in stroke-induced mice compared with their own performance at baseline (N=12 per group, Wilcoxon Signed Rank Test, p=0.365). **(C)** Mice did develop significantly impaired working memory at 48 days after stroke compared with naïve mice (Mann-Whitney-U test, p=0.032). Data analyzed with non-parametric tests were expressed as median with interquartile range. Significance level was marked as: *p<0.05.

5.3.5 Induced production of autoantibody in serum from WT mice with cerebral ischemia

The expansion of marginal B cells and plasmablasts/plasma cells is a potential manifestation of antigen-specific autoimmune responses in secondary lymphoid organs. All mice were screened to explore whether there was stroke-induced synthesis of autoantibody in periphery, which could serve as indirect proof of chronic B cell activation and autoantibody synthesis similar to previous findings in spinal cord injury (Ankeny, Lucin et al. 2006). It is worthy of note that preexisting serum autoantibodies against multiple antigens such as cytoplasmic antigens, Purkinje cells, neuronal nuclear antigen (Figure 31A) and universal nuclear antigen beyond CNS location (Figure 31B) were detected in more than half of naïve mice (Table 3). When mice were stratified based on sera reactivity against autoantigen, there was a clear tendency that mice with preexisting autoantibody tended to suffer from larger infarction (33.50% (18.00-39.50)%) than mice with negative sera for self-antigens (18.00% (16.00-28.00)%) on day 1 after stroke (Figure 31C). Interestingly, regarding

the epitope recognized by autoantibody, reactivity against hippocampal neurons was mainly induced after MCAo (Figure 31D).

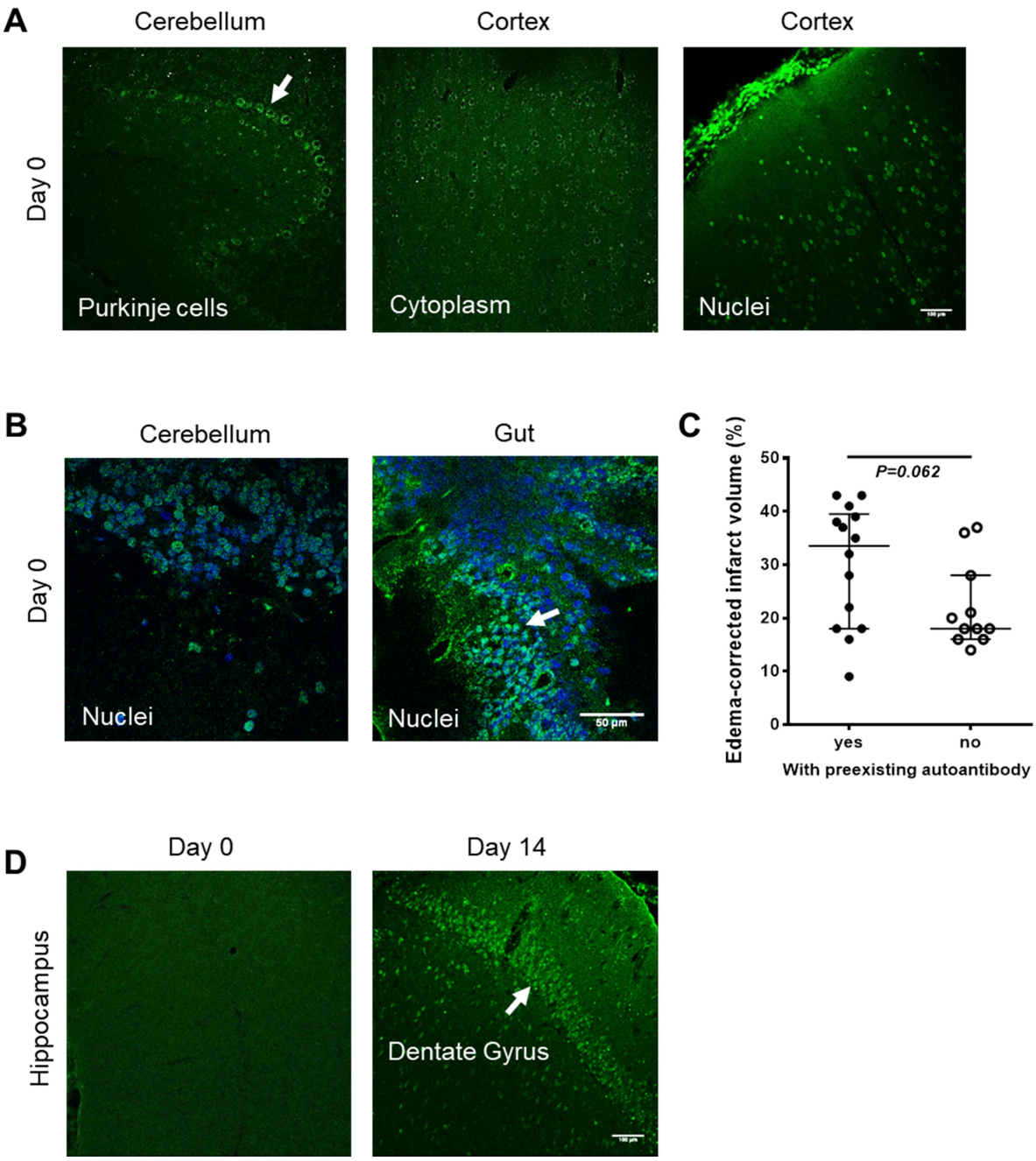

Figure 31. Screening of autoantibody in paired serum samples collected at baseline and endpoint.
(A) Preexisting autoantibody was detected in naïve WT mice. From serum samples collected before MCAo, three epitopes with potential localization to purkinje cells (indicated by white arrow) in cerebellum, cytoplasm and nuclear in cortex were shown in each representative image. Scale bar: 100µm**. (B)** Serum staining with gut tissue was compared with staining from brain tissue. In this example, it exemplified the universal reactivity of autoantibody against nuclear epitope not specific to CNS. The white arrow indicates the nuclear staining in epithelium of gut tissue. Scale bar: 50µm. (**C)** Mice with preexisting autoantibody tended to have larger infarction (Yes=14, No=11, Mann-Whitney U Test, p=0.062) compared with mice with no autoantibody at baseline. **(D)** Screening-paired serum samples revealed that small groups of mice had autoantibody induced only after stroke. A representative image from the same mouse showed a positive signal against dentate gyrus neurons (indicated by the white arrow) on day 14 after stroke while no reactivity was detected in baseline serum. Scale bar: 100µm**.** Data analyzed with non-parametric tests were expressed as median with interquartile range.

Table 3. Summary of autoantibody screening with paired serum samples.

Serum type	Day 14	Day 49	Sum
Negative	2	3	5
Autoantibody only before MCAo	2	1	3
Autoantibody before and after MCAo	5	2	7
Autoantibody only after MCAo	2	0	2
Sum	11	6	17

6. DISCUSSION

By using 60 min middle cerebral artery occlusion and antibody-based depletion of circulating $CD4^+$ T cells in both MOG TCR transgenic 2D2 mice and WT mice, I postulated in the present thesis that the delayed infiltration of $CD4^+$ T cells is involved in tissue remodeling and the functional outcome after experimental stroke. I confirm that after transient priming and proliferation in the secondary lymphoid organs, activated $CD4^+$ T cells with autoreactive potential against MOG can selectively and massively infiltrate into the ischemic hemispheres of 2D2 mice during the delayed phase (day 14) of experimental stroke. In addition, the evidence that CD4 depletion did not influence deposition of fibrotic fibers within infarct core or release of TGFβ1 in the ischemic hemisphere indicates that $CD4^+$ T cells have no direct role in tissue fibrosis. However, CD4 depletion did impair proliferation of activated microglia/macrophages and periendothelial cells in the peri-infarct area, which suggests a modulatory role of $CD4^+$ T cells in vascular remodeling. Most importantly, CD4 depletion completely blocked infiltration of B cells into the ischemic hemisphere and their formation of follicle-like aggregates in 2D2 mice on day 14 after stroke. 2D2 mice with CD4 depletion also had significantly reduced impairment of their right hind limb on day 10 after stroke. Moreover, it is worth mentioning that B cells did infiltrate the ischemic hemispheres of WT mice but achieved peak infiltration with much delay (day 49) compared with 2D2 mice (day 14). The transient differentiation of plasmablasts/plasma cells as well as the expansion of marginal zone B cells in both ischemic brain and spleen, the production of autoreactive antibodies against CNS antigens in circulation jointly point to the possible relationship between the stroke-induced autoreactivity and memory impairment observed in WT mice on day 49 after stroke. Taken together, I conclude that delayed infiltration of $CD4^+$ T cells plays an important role in autoreactive responses and might affect functional long-term recovery after stroke.

6.1 Transient proliferation of lymphocytes in secondary lymphoid organs and their initial infiltration and proliferation in ischemic brain on day 7 after stroke

Brain injury following stroke releases multiple CNS antigens into the peripheral immune system (van Zwam, Huizinga et al. 2009, Planas, Gomez-Choco et al. 2012) where antigen-presenting cells (APCs) such as dendritic cells and macrophages can present CNS antigens to naïve lymphocytes and activate them toward either autoreactive or regulatory phenotype, depending on the route and mode of access of brain antigens to lymphoid tissue (Becker 2009, Urra, Miro et al. 2014). Stroke patients

are reported to have increased numbers of autoreactive T cells specific to various CNS antigens (Wang, Olsson et al. 1992) in their cerebrospinal fluid and peripheral blood.

In the present thesis, the increased proliferation of B cells was detected exclusively in spleen on day 1 (over 5%) after stroke compared with sham control. However, proliferation of B cells significantly reduced to less than 2% on day 3 after stroke. Similarly, $CD8^+$ T cells had their peak proliferation (over 5%) in superficial cervical lymph nodes, mesenteric lymph nodes and spleen on day 1 after stroke and later reduced to the level of sham control (around 2.5%). Even though overall proliferation of $CD4^+$ T cells after stroke was relatively less (1-2%) than that of B and $CD8^+$ T cells, the proportion of MOG TCR^+ cells in overall proliferating $CD4^+$ T cells transiently increased in CNS-draining lymph nodes, spleens and mesenteric lymph nodes on day 1 after stroke. This early and transient proliferation of both T and B lymphocytes upon CNS-antigen presentation in periphery after stroke is in line with a previous study reporting a significant increase in autoreactive $CD4^+$ and $CD8^+$ T cells, as well as autoreactive B cells upon ex vivo activation by multiple CNS antigens as early as 4 days after stroke onset (Ortega, Noorbhai et al. 2015). The evidence from labeling proliferating autoreactive MOG TCR^+ $CD4^+$ T cells in vivo provided further support to study reporting peak drainage of CNS antigens in cervical lymph nodes on day 1 after 60 min MCAo (van Zwam, Huizinga et al. 2009).

Not only peripheral lymphoid organs are actively involved with the induction of autoreactivity, ischemic brain is also the target and final destination for CNS-antigen reactive lymphocytes. Recruitment of lymphocytes from adaptive immunity is usually delayed compared with innate immune cells, such as monocytes, during ischemic injury (Gronberg, Johansen et al. 2013). Activated lymphocytes actually started to selectively infiltrate into the ischemic hemispheres on day 7 after stroke. On day 7, the number of CNS-infiltrating lymphocytes in the ipsilateral hemisphere was a bit higher than in the contralateral hemisphere. But the proliferation of lymphocytes in the ischemic hemispheres was much greater than in the contralateral hemisphere. The noticeable quantitative and proliferative differences between the two hemispheres suggest that either the cytokine environment or antigen-presentation was promoting the autoreactive proliferation of lymphocytes exclusively in the ischemic hemisphere. Nevertheless, day 7 was still during the early phase of lymphocyte infiltration into the ischemic brain. A significant difference between the two

hemispheres regarding lymphocyte infiltration should be anticipated at a later time point (day 14) after stroke (Stubbe, Ebner et al. 2013, Romer, Engel et al. 2015).

Although CNS-infiltrating MOG TCR^+ $CD4^+$ cells proliferated significantly more than the same cell types in spleen and mesenteric lymph nodes, the proportion of MOG TCR^+ $CD4^+$ cells was significantly lower in the ischemic brain compared with peripheral lymphoid organs. This indicates stroke can induce clonal expansion of autoreactive $CD4^+$ cells that have diverse TCR repertoires in 2D2 mice. Indeed, autoreactive T cells, which recognize myelin components such as myelin basic protein and proteolipid protein, were detected in the CSF of acute ischemic cerebrovascular disease (CVD) patients (Wang, Olsson et al. 1992). It is also notable that the percentage of MOG TCR^+ T cells in the $CD4^+$ population remained unchanged at different time points in the same secondary lymphoid organ and in different secondary lymphoid organs from the same time point, while the absolute count of $CD4^+$ T cells did decrease due to stroke-induced immunodepression (SIDS) (Prass, Meisel et al. 2003, Dirnagl, Klehmet et al. 2007). This result indicates that autoreactive T cells did not undergo more severe apoptosis than non-autoreactive T cells. Insufficient suppression of autoreactive T cells by SIDS in periphery allowed their infiltration into ischemic brain during the delayed phase of stroke. Altogether, the transient proliferation pattern of T cells in secondary lymphoid organs and subsequent targeted infiltration into ischemic hemispheres support the notion that adaptive immune cells might first get primed in periphery by CNS-antigen presentation, then infiltrate into ischemic brain during the delayed phase (7-14 days) and might contribute to chronic autoreactive responses.

6.2 Delayed infiltration of $CD4^+$ T cells temporally correlates with deposition of fibrotic fibers within ischemic tissue

Tissue fibrosis, or scar formation, is a common result of persistent inflammation as well as failed tissue regeneration and represents a repair mechanism which replaces the normal tissue with extracellular matrix (ECM) consisting predominantly of fibronectin and type I collagen (Ferguson and O'Kane 2004). The central nervous system (CNS) is special because fibrogenic cells such as fibroblasts are restricted to vascular and meningeal niches. However, disruption of the blood-brain barrier and inflammation can unleash stromal cells and trigger scar formation (Fernandez-Klett and Priller 2014). Accordingly, I observed deposition of collagen type I fibrotic fibers within the infarct

area on day 14 after stroke. Interestingly, CNS-infiltrating $CD4^+$ T cells distributed in close proximity to these fibrotic fibers and temporally matched with scar formation in ischemic tissue.

In inflamed tissues, both ECM turnover and protease secretion by tissue-resident cells are affected by cytokines, such as TGFβ1, TNF, IFNγ, and PDGF, which are released by the infiltrating cells (Sorokin 2010, Murray and Wynn 2011). On the other hand, upregulated ECM fragments can also activate immune cells, for example via signaling by the Toll-like receptor family that initiates innate immune responses and further influences the nature of the adaptive immune response. Therefore I considered there might be an interrelationship between $CD4^+$ T cells and the deposition of fibrotic fibers. However, delayed CD4 depletion in 2D2 mice with experimental stroke did not influence the process of tissue remodeling, including the deposition of fibrotic fibers (collagen type I) and the release of growth factors (BDNF, VEGF and NGF) at mRNA level. The expression of PDGFRβ was also not affected by CD4 depletion, indicating that $CD4^+$ T cells did not directly modulate stromal cells such as pericytes. Instead, significant correlation was detected between mRNA expressions of collagen type I and TGFβ1 in mice with either treatment. Additionally, mRNA expression of CCR2 (receptor for monocyte chemoattractant protein-1, MCP-1) increased parallel to TGFβ1. Since MCP-1/CCR-2 is crucial for the migration of hematogenous inflammatory cells following transient cerebral ischemia (Schuette-Nuetgen, Strecker et al. 2012), our findings suggest that resident cells and infiltrating macrophages might be the main producers of TGFβ1 (Iadecola and Anrather 2011) and therefore play a more direct role than $CD4^+$ T cells in tissue remodeling after stroke (He and Marneros 2013).

6.3 CD4 depletion significantly impairs proliferation of periendothelial cells in the peri-infarct area but has no influence on infarct maturation after stroke

Monocytes or macrophages are pioneers that invade the infarct core and actively take part in control of scar tissue resolution and production of growth factors (Raposo and Schwartz 2014, Jiang, Zhao et al. 2016). Moreover, myeloid linage antigen CD13, identical with aminopeptidase N (APN) and marker for pericytes and periendothelial cells of brain parenchyma vessels (Alliot, Rutin et al. can contribute to scar formation in inflamed tissue. Delayed CD4 depletion did not significantly reduce the number of $CD68^+$ activated microglia/macrophages in the ischemic hemispheres. But the proliferation of $CD68^+$ activated microglia/macrophages showed a trend of reduction by CD4 depletion. Moreover, the proliferation of $CD13^+$ periendothelial cells in the ischemic hemisphere of

2D2 mice were significantly reduced by CD4 depletion on day 14 post stroke. In situ proliferation of both myeloid cells and tissue-resident macrophages were reported to be a key feature of the inflammatory process (Davies, Rosas et al. 2013). The inflammation-induced activation and proliferation of endothelial and periendothelial cells might affect the stability and permeability of inflamed vasculature (Bergers and Song 2005). Thus, this finding highlights the potential anti-inflammatory and vessel-stabilizing roles of $CD4^+$ T cells during the chronic phase of stroke.

It has been reported that genetic deficiency of T and B cells results in reduction of infarct volume at 24 hours after experimental stroke (Hurn, Subramanian et al. 2007, Kleinschnitz, Schwab et al. 2010). $RAG1^{-/-}$ mice reconstituted with only B cells had still smaller infarct size compared to mice with combined deficiency (Kleinschnitz, Schwab et al. 2010). This result suggests that early infiltrating T cells play an important role in infarct formation. In contrast to previous studies, I targeted rather delayed infiltration of T cells by delayed CD4 depletion (starting on day 3 post stroke). Delayed CD4 depletion had no effect on infarct maturation on day 7 post stroke. During the late phase of stroke, while $CD4^+$ T cells mainly accumulated at the peri-infarct area (see 5.2.1), activated macrophages were the main cell population that infiltrated the ischemic hemisphere earlier than lymphocytes (Gelderblom, Leypoldt et al. 2009, Gronberg, Johansen et al. 2013) and heavily loaded the infarct core (Fernandez-Klett, Potas et al. 2013). Since CD4 depletion had almost no effect on the accumulation of macrophages, this might explain why there was no dramatic effect from CD4 depletion on infarct size on day 7 after stroke.

6.4 CD4 depletion exhibits a trend to improve mid-term motor recovery and Neuroscore in 2D2 mice after stroke

The promotion of post-ischemic motor recovery remains a major challenge in clinical neurology. Locomotor function was monitored with Catwalk on day 10 post stroke to reflect the mid-term outcome. In both control and anti-CD4-treated groups, 2D2 mice developed similarly typical stroke-induced alterations in gait, such as maximum contact area, especially of the right hind paw, normalized swing speed, phase dispersion and stride length (Hetze, Romer et al. 2012, Li, Shi et al. 2013). There were significantly different changes from baseline in run duration and normalized swing speed between the two treatments. In general, the control group had more parameters with stroke-induced deficits than the CD4 depletion group. Using a post hoc calculation of impairment

score of the right hind limb, I detected more obviously functional deficits in the control treatment compared with CD4 depletion.

However, a limitation of Catwalk to analyze mice with experimental stroke is its dependency on walking speed because they can hardly walk through the walkway without longer breaks (Hetze, Romer et al. 2012). Therefore, additional Neuroscore was evaluated before surgery and at 3, 7, 13 days after stroke. In both groups, neurological deficits developed immediately after surgery and continuously until day 7 after stroke. One week after stroke, functional impairment in 2D2 mice with control treatment went further until day 13, while WT mice or 2D2 mice with CD4 depletion all experienced recovery, possibly due to the absence or limited amount of autoreactive $CD4^+$ T cells.
Treg cells have been considered to be neuroprotective in ischemic stroke (Liesz, Suri-Payer et al. 2009, Li, Mao et al. 2013, Liesz, Zhou et al. 2013). However, delayed anti-CD25 depletion had no effect on functional recovery (Stubbe, Ebner et al. 2013). CD4 depletion eliminated all circulating $CD4^+$ T cells including autoreactive (pro-inflammatory) and regulatory (anti-inflammatory) T cells. Since I observed an overall benefit of CD4 depletion promoting neurological recovery in 2D2 mice on day 10 after stroke, this indicates that delayed infiltration of $CD4^+$ T cells mainly acts as a promotor of chronic inflammation and autoreactive responses which are detrimental to stroke outcome.

In contrast to a study reporting no reduction in infarct volume and no improvement in neurological score (up to 4 days) with blockage of infiltrating leukocytes by anti-CD49d treatment at 3 hours post stroke (Llovera, Hofmann et al. 2015), our findings suggest that delayed CD4 depletion has a high potential to promote functional recovery, compared to the control treatment, and the underlying mechanism could be independent of alterations in infarct size.

6.5 Delayed CD4 depletion robustly inhibits formation of follicle-like aggregates by B cells in the ischemic brains of 2D2 mice on day 14 after stroke

B cell aggregates are found in the meninges of patients with secondary progressive multiple sclerosis (MS) and are associated with early disease onset and severe cortical pathology. These aggregates show features reminiscent of B cell follicles in lymphoid tissue, such as B cell proliferation and differentiation into plasma cells, and the presence of a stromal network producing B lymphocyte chemoattractant (BLC) chemokine (C-X-C motif) ligand 13 (CXCL13) (Magliozzi,

Howell et al. 2007). Interestingly, condensed cellular clusters of B cells with close contact to $CD4^+$ T cells in inflamed CNS resemble peripheral follicles in secondary lymphoid organs, indicating possible B cell involvement in autoreactivity (Pitzalis, Jones et al. 2014). Not only autoimmune diseases, but also acute injury to the CNS can lead to chronic inflammation and subsequent formation of B cell aggregates. A previous study on ischemic spinal cord injury has found B cell aggregates which produce antibodies and impede recovery (Ankeny, Lucin et al. 2006). More recently, it was reported that C57BL/6L mice with DH stroke (60 min distal MCAo + hypoxia) have B cell aggregates in the ischemic hemisphere at 7 weeks after stroke (Doyle, Quach et al. 2015).

I found that infiltration of B cells into ischemic brain was significantly inhibited with delayed depletion of $CD4^+$ T cells in 2D2 mice on day 14 after stroke. For the first time, our data demonstrated sound evidence which linked autoreactive $CD4^+$ T cells to infiltration of B cells after ischemic stroke. Even though CD4 depletion did not robustly block infiltration of B cells into the ischemic hemisphere of WT mice on day 14 post stroke, similar follicle-like aggregates of B cells were formed in the peri-infarct areas of both 2D2 and WT mice. This indicates that the development of autoimmunity in the chronic phase of stroke includes B cell immunity and humoral autoreactive responses.

Compared with WT mice, 2D2 mice with their MOG-specific T cells with autoreactive potential had significantly more infiltration of $CD4^+$ T cells and quicker formation of follicle-like aggregates as early as 2 weeks after stroke. In WT mice, early infiltration with sparse B cells already started in the ischemic hemisphere at 2 weeks after stroke. B cell infiltration was significantly more severe on day 49 compared with day 14 after stroke. This delayed infiltration of B cells in WT mice might explain why significant blockage of B cell infiltration was not detectable on day 14 after stroke in WT mice with CD4 depletion. Even though I detected strongly increased protein and mRNA expressions of CXCL13 in the ischemic hemispheres of 2D2 mice, the concentration of CXCL13 in serum (periphery) was not significantly affected by CD4 depletion in either 2D2 or WT mice on day 14 after stroke. If peripheral concentration of CXCL13 remained stable with CD4 depletion, then the production of CXCL13 close to the site of B cell infiltration such as CNS parenchyma or other chemokines might contribute to the $CD4^+$ T cell-dependent migration of B cells towards ischemic brain.

There is developing interest in the role of B cells in autoimmune disorders with T cell dependency. Buckwalter's group has compared stroke outcomes in WT mice with either genetic deficiency of B cells or with delayed anti-CD20 treatment (beginning on day 5 after stroke). Unlike CD4 depletion, neither deficiency of B cells nor CD20 depletion affects recruitment of T cells, but they do prevent IgG accumulation. Comparing this finding with our own, it indicates that T cells might play a dominant role in facilitating the infiltration of other immune cells into ischemic brain, while B cells are mainly responsible for the production of pathogenic antibodies that could directly cause cognitive impairment (Kowal, DeGiorgio et al. 2004, Doyle, Quach et al. 2015).

6.6 Within B cell compartment, proportions of plasmablasts/plasma cells and marginal zone B cells in ischemic brain and spleen of WT mice increased transiently on day 14 after stroke

Germinal center-dependent humoral memory (serological memory) produces long-lived plasma cells, while germinal center-independent humoral memory induces extrafollicular foci of antibody production (Kurosaki, Kometani et al. 2015). Plasmablasts were reported to be migratory Ig-producing cells in the pathogenesis of neuromyelitis optica (Chihara, Aranami et al. 2013). In multiple sclerosis, the inflammatory CNS provides a unique B-cell-friendly environment in which B lineage cells (notably long-lived plasma cells) can survive for many years, perhaps even for a lifetime (Meinl, Krumbholz et al. 2006). B cells produce pathogenic antibodies and impair recovery after spinal cord injury in mice (Ankeny, Guan et al. 2009). Moreover, the notorious persistence and stability of cerebrospinal fluid oligoclonal bands as well as the accumulation of B cells were detected in stroke patients (Pruss, Iggena et al. 2012, Doyle, Quach et al. 2015). However, it is still elusive as to whether long-lived plasma cells are induced in the ischemic brain of human stroke patients.

After stroke, the number of B cells in the spleen was reduced compared to naïve controls, while B cells continuously infiltrated and accumulated in ischemic brain. The percentage of all B cells in total infiltrating leukocytes was significantly higher in ischemic brain on day 49 than on day 14 after stroke. Contrary to this trend, the percentages of plasmablasts/plasma cells and marginal zone B cells in both ischemic brain and spleen were higher on day 14 compared to day 49 after stroke. Since marginal zone B cells can contribute to T-cell-dependent (TD) immune responses (Zouali and Richard 2011) and even present autoantigen to diabetogenic T cells in nonobese diabetic mice (Marino, Batten et al. 2008), the presence of this cell type in ischemic brain suggests that marginal

zone B cells might contribute to the activation of autoreactive T cells. A previous study reported about 9.1% of CNS-infiltrating B cells at 7 weeks post stroke were plasma cells (Doyle, Quach et al. 2015). But in our experiment, the percentage of plasmablast/plasma cells was almost 25% on day 14 and then returned to around 10% on day 49 post stroke. This indicates that B cell autoreactive responses could take place as early as 2 weeks post stroke.

It was reported before that $RAG^{-/-}$ mice reconstituted with $CD3^{+}$ T cells had a similar infarct size as WT mice on day 1 post stroke (Kleinschnitz, Schwab et al. 2010). Recently, the same group concluded that B cells do not play a major pathophysiologic role in the acute phase (1-3 days) of ischemic stroke in mice (Schuhmann, Langhauser et al. 2017). However, our findings suggest infiltration and activation of B cells with expansion of potential autoantibody-producing plasma cells and marginal zone B cells during the delayed phase of stroke (14-49 days) are important processes for induction of chronic humoral autoimmunity and functional impairment.

6.7 Stroke induces autoantibody against hippocampal neurons and thus provides a possible mechanism for development of delayed cognitive impairment in WT mice

Circulating autoantibodies directed against CNS antigens have received much attention in recent years. Preexisting serum autoantibodies against the NMDAR subunit NR1 can modulate the evolution of lesion size in acute ischemic stroke (Zerche, Weissenborn et al. 2015). A high prevalence of NMDA receptor IgA/IgM antibodies exists in different dementia types (Doss, Wandinger et al. 2014). In animal stroke models, IgG/IgM is produced from week 1 and IgA appears with delay at week 7 in the ischemic hemisphere after stroke, and they correlate with delayed cognitive impairment (Doyle, Quach et al. 2015). A recent study even found that antibodies to myelin basic protein are associated with cognitive decline after stroke (Becker, Tanzi et al. 2016)

An important aspect of immunoglobulins in ischemic brain is that leakage of peripheral immunoglobulins into the ischemic hemisphere might occur at 24h and 72h after stroke due to acute breakdown and ensuing compromise of the blood-brain barrier (BBB) (Manwani, Friedler et al. 2014). I also detected preexisting IgG in over half of the WT mice before stroke. These autoantibodies mainly recognized the cytoplasm of cortical cells, neurons in dentate gyrus, neuronal nuclear antigen and, in rare cases, universal nuclear antigen beyond CNS. Only 2 out of 17 animals had production of autoantibody in the periphery, exclusively induced after stroke. The comparison

between autoantibody production and infarct size on day 1 after stroke revealed a tendency that animals with preexisting autoantibodies suffered from more severe infarction than animals without preexisting autoantibodies, which was consistent with findings from stroke patients (Zerche, Weissenborn et al. 2015). Our result reaffirmed that a preexisting autoantibody could modulate the evolution of lesion size in acute ischemic stroke and therefore be a risk factor for stroke outcome.

Over 50% of stroke survivors experience persisting long-term cognitive impairment, which can affect their daily functioning and quality of life (Jokinen, Melkas et al. 2015). Besides risk factors such as age, white matter lesions, vascular dementia and Alzheimer's disease for cognitive decline (Savva, Stephan et al. 2010, Iadecola 2013, Mahon, Parmar et al. 2017), B cells and autoantibody have been associated with cognitive decline in stroke (Doyle, Quach et al. 2015, Becker, Tanzi et al. 2016). Based on our own finding that ischemic stroke could induce autoantibodies against multiple self-antigens including hippocampal neurons, I performed a Y maze test to detect possible cognitive deficits in working memory after stroke. Compared to naïve controls, significantly reduced alternations towards a less recently visited arm were detected on day 48 rather than on day 13 after stroke. This data stressed again that the infiltration of lymphocytes and activation of adaptive immunity, especially humoral responses, are indispensable for the induction of delayed cognitive decline.

6.8 Modulation of lymphocytes can influence chronic autoreactivity and stroke outcome

So far, the most beneficial effects of immunomodulation in experimental stroke have not been successfully translated into a clinical trial. The only exception is Natalizumab, a humanized monoclonal antibody which binds with α4β1 integrin and prevents leukocytes from transmigrating through the BBB. This drug has been approved for clinical use in autoimmune diseases such as MS and Crohn's disease. Though three studies, including a preclinical randomized controlled multicenter trial, reported contradictory conclusions when blocking the very late antigen-4 (VLA-4)-vascular adhesion molecule-1 (VCAM-1) axis in ischemic stroke in mice (Liesz, Zhou et al. Langhauser, Kraft et al. 2014, Llovera, Hofmann et al. 2015), a randomized, double blinded, placebo controlled trial of Natalizumab (ACTION phase II trial) was carried out in acute ischemic stroke (AIS) (Mehta, Mitchell et al. 2016). Even though Natalizumab does not affect infarct volume growth on the National Institutes of Health Stroke Scale (NIHSS) score compared with placebo, it has a meaningful benefit over placebo treatment for global clinical and cognitive function at 30 and

90 days after AIS. Despite Natalizumab showing positive effects on functional outcomes similar to what was found in experimental models, further research is required to better understand how this happens without reducing the infarct volume (Simats, Garcia-Berrocoso et al. 2016).

Anti-CD20 antibody treatment was reported to successfully ablate B cells in the circulation, prevent the appearance of delayed cognitive deficits, and prevent the recruitment of B cells and IgG to the brain (Doyle, Quach et al. 2015). Rituximab (commercial monoclonal anti-CD20 antibody) has been approved to treat certain autoimmune diseases and types of cancer. However, insufficient disease inhibition by intrathecal rituximab was reported in progressive multiple sclerosis (Komori, Lin et al. 2016). Until now, no clinical trial has studied its potential benefits in stroke patients. Only the plasma-cell-depleting proteasome inhibitor Bortezomib was proved to reduce antibody titers and improve the clinical course of patients with severe anti-NMDAR encephalitis (Scheibe, Pruss et al. 2016). This might be relevant for stroke since autoantibodies were detected in experimental stroke and associated with cognitive impairment (Doyle, Quach et al. 2015, Doyle and Buckwalter 2016).

The delayed CD4 depletion I researched in this thesis has demonstrated benefits for controlling local inflammation, stabilizing vasculature from pathological angiogenesis and promoting motor recovery. Anti-CD4 treatment could simultaneously deplete circulating $CD4^+$ T cells and block infiltration of B cells into ischemic brain, while anti-CD20 treatment had no effect on T cells (Doyle, Quach et al. 2015). Therefore, it would be worthwhile to further explore whether delayed CD4 depletion has additional benefits such as neuroprotection and prevention of cognitive decline.

6.9 Considerations of methodology and limitations

In this thesis, experiments were mainly carried out on 2D2 mice. This strain has over 80% of peripheral $CD4^+$ T cells carrying transgenic T cell receptors specifically recognizing MOG fragment ($pMOG_{35-55}$) (Bettelli, Pagany et al. 2003). MOG, a membrane protein expressed on the oligodendrocyte cell surface, forms the outermost surface of myelin sheaths (Pham-Dinh, Della Gaspera et al. 1995). Due to this localization, MOG is easily accessible to activated immune cells and a primary target antigen in autoimmune-mediated demyelination such as multiple sclerosis. Synthetic MOG peptide ($pMOG_{35-55}$) has the highest encephalitogenic potential to induce neurological impairment in C57Bl/6J mice (Mendel, Kerlero de Rosbo et al. 1995) by activating innate immune cells via Toll-like receptors (TLRs) and promoting the pathogenic function of

autoreactive T cells (Mills 2011). However, the percentage of MOG TCR^+ $CD4^+$ T cells among all CNS-infiltrating $CD4^+$ T cells was only around 30% in the ischemic hemispheres (over 80% in the periphery). This indicates that activated T cells with TCRs recognizing multiple CNS antigens can accumulate in ischemic brain. Therefore, it is not warranted to attribute autoreactive responses seen in 2D2 mice only to autoreactive T cells or autoantibody against MOG. Moreover, compared with WT littermates, 2D2 mice have worse survival rate (only around 40%) until 14 days after stroke (see 5.1.1). The lower survival rate ultimately affected the sample size for statistical analysis.

The majority of thymocytes, most helper T cells, and a subset of NK-T cells (Bernstein, Plasterer et al. 2006) express CD4 on their surfaces, while dendritic cells and macrophages only express CD4 weakly (Vremec, Pooley et al. 2000). CD4 plays an important role in the development of T cells and is required for mature T cells to function optimally. Impairment of T cell function occurs in situations where mice were treated with relatively large doses of anti-CD4 antibody, while a low dose of anti-CD4 antibody with only 50% reduction of splenic $CD4^+$ T cells led to a significant augmentation of certain T-cell-dependent humoral responses (Cowdery, Tolaymat et al. 1991). We used the GK1.5 (IgG2b) rat anti-mouse CD4 antibody, which is known to deplete $CD4^+$ T cell in vivo and to be immunosuppressive (Rashid, Auchincloss et al. 1992). Splenic $CD4^+$ T cells were reduced by over 90% after two i.p. injections (200 ug per injection). The state of CD4 depletion was well maintained until day 14 after stroke. Since CD4 molecules can be weakly expressed on the surface of monocytes (Crowe, Mills et al. 1987), we also measured monocyte count in peripheral blood. No negative influences on mortality or reduction of monocytes were observed.

Proximal occlusion of the MCA via the intraluminal filament (or suture) method is most frequently used to model ischemic stroke (Macrae 2011). The 60 min filament MCA occlusion (MCAo) model offers the advantage of inducing reproductive pan-necrotic lesions in the cortex, and striatum was used in this thesis (Engel, Kolodziej et al. 2011). However, human strokes are mostly small in size, ranging from 4.5% to 14% of the ipsilateral hemisphere (Carmichael 2005). Malignant infarction can damage over 30% of one hemisphere. Accordingly, our model is classified as severe stroke and causes infarcts involving regions supplied by the MCA but also potentially deep regions such as the hippocampus, hypothalamus and/or thalamus (El Amki, Clavier et al. 2015). Therefore, mice with lesion in hippocampus were cautiously excluded from the final evaluation of cognitive impairment since I was interested only in the role of autoreactivity on cognitive decline after stroke.

Immunofluorescent stainings provided direct evidence of the anatomical distribution of $CD4^+$ T cells and their location with regard to deposition of fibrotic fibers. However, staining of cytokines and growth factors was quite challenging with immunohistochemistry. Therefore, a quantitative comparison of dynamic mRNA expression of fibrotic fibers and growth factors related to tissue remodeling was performed using qPCR. Contralateral hemispheres without infarction were used as internal control to compare stroke-induced changes of tissue-remodeling related genes in ipsilateral hemispheres. However, stroke-induced modulation of several genes such as nerve growth factor, vascular endothelial growth factor A and platelet-derived growth factor receptor β also affected the contralateral hemisphere. Thus, in addition I used hemispheres from the same side of naïve mice as a baseline control. However, a new experiment should include brain hemispheres from sham-operated mice to exclude possible influence from the surgical procedure on the evaluation of tissue fibrosis in ischemic brain.

The Catwalk system was used to detect locomotor deficits after stroke. Severe cerebral ischemia in mice disturbs the well-coordinated interplay among the four limbs. Swing subtask, intensity and maximal contact area in hind limbs, especially in the contralateral side, are impaired in the mid to long-term outcome after stroke (Hetze, Romer et al. 2012). In human stroke research, 3 months after stroke are accepted as the time point for assessing long-term outcome. In mice, the acute phase is completed within the first week after stroke (Dirnagl, Simon et al. 2003). Accordingly, measurement performed at 10 days after stroke reflects mid to long-term outcome (Hetze, Romer et al. 2012). Testing novel stroke treatments, there are only a few parameters which show an effect large enough to detect gait improvements. Due to high mortality caused by neurological reasons and medical complications like infections (Meisel and Meisel 2011) between day 3 and 6 post stroke, there were hardly enough animals (15-20 animals are recommended) from the same experiment to detect neuroprotective or regenerative effects at this late time point. Therefore stroke-induced mice that survived until day 10 were pooled together from 3 experiments. If the baseline parameters were significantly different among several experiments, it was not correct to directly compare gait parameters post stroke between control and CD4 depletion groups with pooled animals. Thus, I normalized the original result by calculating the change from baseline and calculated the post hoc impairment score of the right hind limb to detect focused lesion. In addition, an important limitation of the Catwalk system is the dependency on walking speed which influences many gait parameters. Catwalk can only be used as a measure if the stroke-induced mice are indeed able to walk at

minimum. Therefore, Neuroscore was introduced to evaluate not only the general status but also focal neurological dysfunction besides gait (Llovera, Hofmann et al. 2015).

After observing the formation of follicle-like aggregates by B cells in my own experiments and reading publications on B cell-mediated cognitive impairment (Doyle, Quach et al. 2015), I performed the Y maze test (Dudchenko 2004) to evaluate cognitive deficits in the spatial working memory of stroke-induced mice. However, there are limitations to modeling cognitive decline in humans by rodents because experimental stroke in young mice does not include typical risk factors such as age, white matter lesions, vascular dementia and Alzheimer's disease for cognitive decline (Savva, Stephan et al. 2010, Iadecola 2013, Mahon, Parmar et al. 2017). Since I only detected a significant difference between naïve mice and mice on day 48 post stroke, it is necessary to include sham-operated animals as a better control and also to evaluate delayed cognitive impairment over a longer period (3 months post stroke). It is also important to note that delayed cognitive impairment in experimental stroke was reported in distal MCAo plus hypoxia (DH) model (Doyle, Quach et al. 2015), while I used only distal MCAo. This might explain different courses of developing cognitive decline after stroke. Further experiments that include more time points should be planned to detect the worsening of cognition in the MCAo model.

The gold standard for testing patients with the presence of N-Methyl-D-aspartate (NMDAR) autoantibodies is the combined use of tissue immunohistochemistry and cell-based assays in which the protein of interest is transiently expressed in HEK cells (Pruss, Leubner et al. 2015). Here the less complex method with tissue immunohistochemistry was chosen to provide additional proof of functional formation of follicle-like aggregates by B cells in ischemic brain. CSF might contain more concentrated autoantibodies (Pruss, Leubner et al. 2015). However the negligible amount of cerebrospinal fluid collected from each mouse was not enough to complete one single staining. Consequently, serum samples were prepared before and after experimental stroke. Mice with either preexisting autoantibodies or stroke-induced autoantibodies against CNS antigens were quickly screened. However, the number of paired serum samples was too limited to detect any dominant epitopes of autoantibodies induced exclusively after stroke. Further experiments are needed to explore the complex patterns of autoreactivity after stroke. Moreover, a cell-based assay is still needed to finally confirm the observed autoreactivity against CNS nucleus and cerebellar purkinje cells.

In this thesis, I have not investigated all time points of interest, especially in WT mice. I observed strong inhibition of B cell infiltration into ischemic brain when circulating $CD4^+$ T cells were depleted in 2D2 mice on day 14 after stroke. However, this effect was not detected in WT mice at the same endpoint. Because peak accumulation of B cells in the ischemic brains of WT mice was actually detected on day 49 after stroke (5.3.2). 2D2 mice with MOG TCR had earlier and more severe infiltration of $CD4^+$ T cells and larger infarct volume compared with WT mice (5.1.1). Such differences in stroke-induced autoreactivity might lead to a remodeling/recovering differential in 2D2 mice and WT mice, but I have not validated all findings from 2D2 mice in WT mice, such as mRNA expression of growth factors and motor recovery. Moreover, a proper sham-operated control was also lacking to confirm whether the observed cognitive impairment on day 48 was indeed induced by stroke rather than the surgical procedure. Due to the small group size (N=3-5), I could not detect statistically significant differences between the control and CD4 depletion groups in accumulation of activated microglia/macrophages, motor recovery or neurological score. The limited amount of serum samples made it hard to summarize dominant epitopes of autoantibodies and their relevance to autoreactivity and functional recovery after stroke. All these limitations should be overcome in future experiments.

6.10 Future challenges

Previous research stressed that stroke does not systematically trigger autoimmunity. Only under certain circumstances, such as pronounced systemic inflammation or infection, can autoreactive T cells escape the tolerance controls (Urra, Miro et al. 2014). Delayed infiltration of $CD4^+$ T cells and differentiation of autoantibody-producing plasma cells in ischemic brain have opened a new avenue for the search of immunomodulatory agents to control autoimmune responses and protect neuronal function after stroke. The main findings demonstrate that delayed depletion of $CD4^+$ T cells inhibits infiltration of B cells and formation of follicle-like aggregates in the ischemic brain of 2D2 mice. CD4 depletion also controls local inflammation and instability of the BBB via inhibition of proliferation of activated microglia/macrophages and periendothelial cells. Functional recovery, especially impairment of the right hind limb, was reduced in 2D2 mice with CD4 depletion on day 10 after stroke. Further studies are needed to demonstrate whether these findings are causally involved in long-term outcome after stroke.

Even though CD4 depletion had strong effects in 2D2 mice post stroke, delayed CD4 depletion did not significantly reduce infiltration of B cells in WT mice on day 14 after stroke. B cells actually continued to accumulate in the ischemic hemispheres of WT mice between day 14 and day 49 after stroke. Thus, it cannot be excluded that in WT mice blockage of massive B cell infiltration by CD4 depletion might occur later than 14 days (end point defined for 2D2 mice). Further studies in WT mice should be planned with extended duration to detect the effects of CD4 depletion on autoreactive responses and functional recovery after stroke.

The detection of follicle-like aggregates in ischemic brain is consistent with previous findings in spinal cord injury (Ankeny, Lucin et al. 2006) and ischemic stroke (Doyle, Quach et al. 2015). Nevertheless, the cellular components of follicle-like aggregates, apart from B cells, were not investigated in depth. Follicular helper T cells (TFH cells) are present in B cell-rich regions of structurally organized lymphoid aggregates (Pitzalis, Jones et al. 2014). TFH cells can induce the differentiation of B cells into plasma cells (Ueno, Banchereau et al. 2015) and antibody production (Ding, Mountz et al. 2015). Whether TFH cells are detectable in such ectopic follicles in ischemic brain remains elusive. In addition, B cells and autoantibodies have been associated with the development of delayed cognitive impairment (Doyle, Quach et al. 2015, Becker, Tanzi et al. 2016).

B cell depletion with anti-CD20 antibody beginning 5 days after stroke ameliorates the development of delayed cognitive deficits (Doyle, Quach et al. 2015). Thus, it would be interesting to study further whether delayed CD4 depletion has equivalent protection against delayed cognitive decline during the chronic phase of stroke.

It was reported that B cells and IgG were positively stained in the brain after stroke in humans with concurrent dementia (Doyle, Quach et al. 2015). However, not all stroke patients develop delayed cognitive deficits and not all stroke-induced dementia have pathological immunoglobulins in the brain. In WT mice, I observed a transiently increased percentage of plasmablasts/plasma cells in overall infiltrating B cells in both ischemic brain and spleen on day 14 post stroke. With future experiments focusing on the effects of late CD4 depletion on composition of B cell subtypes in WT mice, it might be interesting to explore whether $CD4^+$ T cells can influence activation and differentiation of B cells into long-lived plasma cells during the chronic phase of stroke. In stroke patients it is also worth investigating whether plasma cells reside in ischemic brain and whether autoantibodies against CNS antigens are induced after stroke. By correlating autoantibodies and stroke outcomes, it might be helpful to distinguish between potentially protective and pathological autoantibodies (Becker, Tanzi et al. 2016) since only dementia-associated autoantibodies and long-lived plasma cells should be targeted for pharmacological elimination.

The findings here jointly demonstrate that modulating adaptive immune cells might be promising therapeutic targets in the chronic phase of ischemic stroke. To improve the quality and translational predictability of preclinical stroke research and obtain robust effects of immunomodulation on long-term outcome after stroke, preclinical randomized controlled multicenter trials with larger sample sizes and sufficient statistical power are warranted (Mergenthaler and Meisel 2012, Llovera, Hofmann et al. 2015).

7. CONCLUSION

The most important findings of my PhD thesis can be summarized as follows:

1. Delayed infiltration of $CD4^+$ T cells on day 14 after stroke was more severe in MOG TCR transgenic mice (2D2) than WT mice. Autoreactive potential against MOG also led to larger infarct size and worse survival post stroke in 2D2 mice. The transient priming and proliferation of naïve $CD4^+$ T cells in secondary lymphoid organs was crucial for targeted migration towards ischemic hemisphere on day 7 post stroke.

2. The mRNA expression of TGFβ1 rather than PDGFRβ correlated with deposition of collagen type I fibrotic fibers. This indicated that activated macrophages which occupied the infarct core rather than pericytes could be the main producer of fibrotic fibers in the ischemic hemisphere. Even though infiltration of $CD4^+$ T cells (7 to 14 days post stroke) temporally and spatially correlated with the deposition of fibrotic extracellular matrix, CD4 depletion did not directly influence the mRNA expression of either collagen type I or TGFβ on day 14 post stroke.

3. Delayed CD4 depletion had no effect on the infarct size on day 7 nor on the numbers of surviving neurons and activated microglia/macrophages on day 14 post stroke. Nevertheless, delayed CD4 depletion had a trend to impair the proliferation of activated microglia/macrophages and significantly inhibited the proliferation of $CD13^+$ periendothelial cells. Importantly, depletion of $CD4^+$ T cells in 2D2 mice reduced motor impairment in the right hind limb on day 10 and blocked the entry of B cells into the ischemic hemisphere and the subsequent formation of follicle-like aggregates on day 14 post stroke.

4. Depletion of $CD4^+$ T cells in WT mice did not significantly block the entry of B cells into the ischemic hemisphere on day 14 post stroke. This was due to delayed peak accumulation of B cells (49 days) in WT mice compared to 2D2 mice (14 days). Transiently increased differentiation of plasmablasts/plasma cells and expansion of marginal zone B cells on day 14 post stroke in ischemic brain and spleen of WT mice could contribute to the induction of B cell autoreactivity with production of autoantibodies. Indeed, autoreactivity induced by stroke led to the production of autoantibody against hippocampal neurons, which might be one potential mechanism for developing delayed memory impairment on day 49 rather than day 14 post stroke compared to naïve controls.

8. REFERENCES

Agrawal, S., P. Anderson, M. Durbeej, N. van Rooijen, F. Ivars, G. Opdenakker and L. M. Sorokin (2006). "Dystroglycan is selectively cleaved at the parenchymal basement membrane at sites of leukocyte extravasation in experimental autoimmune encephalomyelitis." J Exp Med **203**(4): 1007-1019.

Alliot, F., J. Rutin, P. J. Leenen and B. Pessac (1999). "Pericytes and periendothelial cells of brain parenchyma vessels co-express aminopeptidase N, aminopeptidase A, and nestin." J Neurosci Res **58**(3): 367-378.

Ankeny, D. P., Z. Guan and P. G. Popovich (2009). "B cells produce pathogenic antibodies and impair recovery after spinal cord injury in mice." J Clin Invest **119**(10): 2990-2999.

Ankeny, D. P., K. M. Lucin, V. M. Sanders, V. M. McGaughy and P. G. Popovich (2006). "Spinal cord injury triggers systemic autoimmunity: evidence for chronic B lymphocyte activation and lupus-like autoantibody synthesis." J Neurochem **99**(4): 1073-1087.

Arboix, A. and J. Alio (2010). "Cardioembolic stroke: clinical features, specific cardiac disorders and prognosis." Curr Cardiol Rev **6**(3): 150-161.

Armulik, A., G. Genove, M. Mae, M. H. Nisancioglu, E. Wallgard, C. Niaudet, L. He, J. Norlin, P. Lindblom, K. Strittmatter, B. R. Johansson and C. Betsholtz (2010). "Pericytes regulate the blood-brain barrier." Nature **468**(7323): 557-561.

Association, A. H. (2016). "Impact of Stroke (Stroke statistics)." from http://www.strokeassociation.org/STROKEORG/AboutStroke/Impact-of-Stroke-Stroke-statistics_UCM_310728_Article.jsp#.WaGbIygjFaR.

Becker, K. J. (2009). "Sensitization and tolerization to brain antigens in stroke." Neuroscience **158**(3): 1090-1097.

Becker, K. J. (2010). "Modulation of the postischemic immune response to improve stroke outcome." Stroke; a journal of cerebral circulation **41**(10 Suppl): S75-78.

Becker, K. J., A. J. Kalil, P. Tanzi, D. K. Zierath, A. V. Savos, J. M. Gee, J. Hadwin, K. T. Carter, D. Shibata and K. C. Cain (2011). "Autoimmune responses to the brain after stroke are associated with worse outcome." Stroke; a journal of cerebral circulation **42**(10): 2763-2769.

Becker, K. J., P. Tanzi, D. Zierath and M. S. Buckwalter (2016). "Antibodies to myelin basic protein are associated with cognitive decline after stroke." J Neuroimmunol **295-296**: 9-11.

Bederson, J. B., L. H. Pitts, M. Tsuji, M. C. Nishimura, R. L. Davis and H. Bartkowski (1986). "Rat middle cerebral artery occlusion: evaluation of the model and development of a neurologic examination." Stroke **17**(3): 472-476.

Benjamin, I. J., R. C. Griggs, E. J. Wing and J. G. Fitz (2016). Andreoli and Carpenter's Cecil essentials of medicine. Philadelphia, Elsevier Saunders.

Bergers, G. and S. Song (2005). "The role of pericytes in blood-vessel formation and maintenance." Neuro Oncol **7**(4): 452-464.

Bernstein, H. B., M. C. Plasterer, S. E. Schiff, C. M. Kitchen, S. Kitchen and J. A. Zack (2006). "CD4 expression on activated NK cells: ligation of CD4 induces cytokine expression and cell migration." J Immunol **177**(6): 3669-3676.

Bettelli, E., M. Pagany, H. L. Weiner, C. Linington, R. A. Sobel and V. K. Kuchroo (2003). "Myelin oligodendrocyte glycoprotein-specific T cell receptor transgenic mice develop spontaneous autoimmune optic neuritis." J Exp Med **197**(9): 1073-1081.

Bodhankar, S., Y. Chen, A. A. Vandenbark, S. J. Murphy and H. Offner (2014). "Treatment of experimental stroke with IL-10-producing B-cells reduces infarct size and peripheral and CNS inflammation in wild-type B-cell-sufficient mice." Metabolic brain disease **29**(1): 59-73.

Brait, V. H., T. V. Arumugam, G. R. Drummond and C. G. Sobey (2012). "Importance of T lymphocytes in brain injury, immunodeficiency, and recovery after cerebral ischemia." Journal of cerebral blood flow and metabolism : official journal of the International Society of Cerebral Blood Flow and Metabolism **32**(4): 598-611.

Carmichael, S. T. (2005). "Rodent models of focal stroke: size, mechanism, and purpose." NeuroRx **2**(3): 396-409.

Catanese, L., J. Tarsia and M. Fisher (2017). "Acute Ischemic Stroke Therapy Overview." Circ Res **120**(3): 541-558.

Chen, Y., S. Bodhankar, S. J. Murphy, A. A. Vandenbark, N. J. Alkayed and H. Offner (2012). "Intrastriatal B-cell administration limits infarct size after stroke in B-cell deficient mice." Metab Brain Dis **27**(4): 487-493.

Chihara, N., T. Aranami, S. Oki, T. Matsuoka, M. Nakamura, H. Kishida, K. Yokoyama, Y. Kuroiwa, N. Hattori, T. Okamoto, M. Murata, T. Toda, S. Miyake and T. Yamamura (2013). "Plasmablasts as migratory IgG-producing cells in the pathogenesis of neuromyelitis optica." PLoS One **8**(12): e83036.

Chu, H. X., H. A. Kim, S. Lee, J. P. Moore, C. T. Chan, A. Vinh, M. Gelderblom, T. V. Arumugam, B. R. Broughton, G. R. Drummond and C. G. Sobey (2014). "Immune cell infiltration in malignant middle cerebral artery infarction: comparison with transient cerebral ischemia." J Cereb Blood Flow Metab **34**(3): 450-459.

Cowdery, J. S., N. Tolaymat and S. P. Weber (1991). "The effect of partial in vivo depletion of CD4 T cells by monoclonal antibody. Evidence that incomplete depletion increases IgG production and augments in vitro thymic-dependent antibody responses." Transplantation **51**(5): 1072-1075.

Cregg, J. M., M. A. DePaul, A. R. Filous, B. T. Lang, A. Tran and J. Silver (2014). "Functional regeneration beyond the glial scar." Experimental Neurology **253**: 197-207.

Crowe, S., J. Mills and M. S. McGrath (1987). "Quantitative immunocytofluorographic analysis of CD4 surface antigen expression and HIV infection of human peripheral blood monocyte/macrophages." AIDS Res Hum Retroviruses **3**(2): 135-145.

Dambinova, S. A., G. A. Khounteev, G. A. Izykenova, I. G. Zavolokov, A. Y. Ilyukhina and A. A. Skoromets (2003). "Blood test detecting autoantibodies to N-methyl-D-aspartate neuroreceptors for evaluation of patients with transient ischemic attack and stroke." Clin Chem **49**(10): 1752-1762.

Davies, L. C., M. Rosas, S. J. Jenkins, C. T. Liao, M. J. Scurr, F. Brombacher, D. J. Fraser, J. E. Allen, S. A. Jones and P. R. Taylor (2013). "Distinct bone marrow-derived and tissue-resident macrophage lineages proliferate at key stages during inflammation." Nat Commun **4**: 1886.

Denes, A., R. Vidyasagar, J. Feng, J. Narvainen, B. W. McColl, R. A. Kauppinen and S. M. Allan (2007). "Proliferating resident microglia after focal cerebral ischaemia in mice." J Cereb Blood Flow Metab **27**(12): 1941-1953.

Ding, Y., J. D. Mountz and H. C. Hsu (2015). "Identification of follicular T helper cells in tissue sections." Methods Mol Biol **1291**: 13-25.

Dirnagl, U., J. Klehmet, J. S. Braun, H. Harms, C. Meisel, T. Ziemssen, K. Prass and A. Meisel (2007). "Stroke-induced immunodepression: experimental evidence and clinical relevance." Stroke **38**(2 Suppl): 770-773.

Dirnagl, U., R. P. Simon and J. M. Hallenbeck (2003). "Ischemic tolerance and endogenous neuroprotection." Trends Neurosci **26**(5): 248-254.

Dore-Duffy, P., C. Owen, R. Balabanov, S. Murphy, T. Beaumont and J. A. Rafols (2000). "Pericyte migration from the vascular wall in response to traumatic brain injury." Microvasc Res **60**(1): 55-69.

Doss, S., K. P. Wandinger, B. T. Hyman, J. A. Panzer, M. Synofzik, B. Dickerson, B. Mollenhauer, C. R. Scherzer, A. J. Ivinson, C. Finke, L. Schols, J. Muller Vom Hagen, C. Trenkwalder, H. Jahn, M. Holtje, B. B. Biswal, L. Harms, K. Ruprecht, R. Buchert, G. U. Hoglinger, W. H. Oertel, M. M. Unger, P. Kortvelyessy, D. Bittner, J. Priller, E. J. Spruth, F. Paul, A. Meisel, D. R. Lynch, U. Dirnagl, M. Endres, B. Teegen, C. Probst, L. Komorowski, W. Stocker, J. Dalmau and H. Pruss (2014). "High prevalence of NMDA receptor IgA/IgM antibodies in different dementia types." Annals of clinical and translational neurology **1**(10): 822-832.

Doyle, K. P. and M. S. Buckwalter (2016). "Does B lymphocyte-mediated autoimmunity contribute to post-stroke dementia?" Brain Behav Immun.

Doyle, K. P., L. N. Quach, M. Sole, R. C. Axtell, T. V. Nguyen, G. J. Soler-Llavina, S. Jurado, J. Han, L. Steinman, F. M. Longo, J. A. Schneider, R. C. Malenka and M. S. Buckwalter (2015). "B-lymphocyte-mediated delayed cognitive impairment following stroke." The Journal of neuroscience : the official journal of the Society for Neuroscience **35**(5): 2133-2145.

Dudchenko, P. A. (2004). "An overview of the tasks used to test working memory in rodents." Neurosci Biobehav Rev **28**(7): 699-709.

Duffield, J. S., M. Lupher, V. J. Thannickal and T. A. Wynn (2013). "Host responses in tissue repair and fibrosis." Annu Rev Pathol **8**: 241-276.

El Amki, M., T. Clavier, N. Perzo, R. Bernard, P. O. Guichet and H. Castel (2015). "Hypothalamic, thalamic and hippocampal lesions in the mouse MCAO model: Potential involvement of deep cerebral arteries?" Journal of neuroscience methods **254**: 80-85.

Engel, O., S. Kolodziej, U. Dirnagl and V. Prinz (2011). "Modeling stroke in mice - middle cerebral artery occlusion with the filament model." Journal of visualized experiments : JoVE(47).

Engel, O., S. Kolodziej, U. Dirnagl and V. Prinz (2011). "Modeling stroke in mice - middle cerebral artery occlusion with the filament model." J Vis Exp(47).

Engelhardt, B. (2006). "Molecular mechanisms involved in T cell migration across the blood-brain barrier." J Neural Transm (Vienna) **113**(4): 477-485.

Engelhardt, B. and L. Sorokin (2009). "The blood-brain and the blood-cerebrospinal fluid barriers: function and dysfunction." Seminars in immunopathology **31**(4): 497-511.

Engelhardt, B. and H. Wolburg (2004). "Mini-review: Transendothelial migration of leukocytes: through the front door or around the side of the house?" Eur J Immunol **34**(11): 2955-2963.

Enzmann, G., C. Mysiorek, R. Gorina, Y. J. Cheng, S. Ghavampour, M. J. Hannocks, V. Prinz, U. Dirnagl, M. Endres, M. Prinz, R. Beschorner, P. N. Harter, M. Mittelbronn, B. Engelhardt and L. Sorokin (2013). "The neurovascular unit as a selective barrier to polymorphonuclear granulocyte (PMN) infiltration into the brain after ischemic injury." Acta neuropathologica **125**(3): 395-412.

Faulkner, J. R., J. E. Herrmann, M. J. Woo, K. E. Tansey, N. B. Doan and M. V. Sofroniew (2004). "Reactive astrocytes protect tissue and preserve function after spinal cord injury." J Neurosci **24**(9): 2143-2155.

Felger, J. C., T. Abe, U. W. Kaunzner, A. Gottfried-Blackmore, J. Gal-Toth, B. S. McEwen, C. Iadecola and K. Bulloch (2010). "Brain dendritic cells in ischemic stroke: time course, activation state, and origin." Brain Behav Immun **24**(5): 724-737.

Felten, D. L., S. Y. Felten, D. L. Bellinger, S. L. Carlson, K. D. Ackerman, K. S. Madden, J. A. Olschowki and S. Livnat (1987). "Noradrenergic sympathetic neural interactions with the immune system: structure and function." Immunol Rev **100**: 225-260.

Ferguson, M. W. and S. O'Kane (2004). "Scar-free healing: from embryonic mechanisms to adult therapeutic intervention." Philos Trans R Soc Lond B Biol Sci **359**(1445): 839-850.

Fernandez-Klett, F., J. R. Potas, D. Hilpert, K. Blazej, J. Radke, J. Huck, O. Engel, W. Stenzel, G. Genove and J. Priller (2013). "Early loss of pericytes and perivascular stromal cell-induced scar formation after stroke." J Cereb Blood Flow Metab **33**(3): 428-439.

Fernandez-Klett, F. and J. Priller (2014). "The fibrotic scar in neurological disorders." Brain pathology **24**(4): 404-413.

Fernandez-Klett, F. and J. Priller (2015). "Diverse functions of pericytes in cerebral blood flow regulation and ischemia." J Cereb Blood Flow Metab **35**(6): 883-887.

Fisher, C. M. (1965). "Lacunes: Small, Deep Cerebral Infarcts." Neurology **15**: 774-784.

Fluri, F., M. K. Schuhmann and C. Kleinschnitz (2015). "Animal models of ischemic stroke and their application in clinical research." Drug Des Devel Ther **9**: 3445-3454.

Font, M. A., A. Arboix and J. Krupinski (2010). "Angiogenesis, neurogenesis and neuroplasticity in ischemic stroke." Curr Cardiol Rev **6**(3): 238-244.

Frenkel, D., Z. Huang, R. Maron, D. N. Koldzic, W. W. Hancock, M. A. Moskowitz and H. L. Weiner (2003). "Nasal vaccination with myelin oligodendrocyte glycoprotein reduces stroke size by inducing IL-10-producing CD4+ T cells." Journal of immunology **171**(12): 6549-6555.

Frenkel, D., Z. Huang, R. Maron, D. N. Koldzic, M. A. Moskowitz and H. L. Weiner (2005). "Neuroprotection by IL-10-producing MOG CD4+ T cells following ischemic stroke." Journal of the neurological sciences **233**(1-2): 125-132.

Gee, J. M., D. Zierath, J. Hadwin, A. Savos, A. Kalil, M. Thullbery and K. J. Becker (2009). "Long term immunologic consequences of experimental stroke and mucosal tolerance." Experimental & translational stroke medicine **1**: 3.

Gelderblom, M., F. Leypoldt, K. Steinbach, D. Behrens, C. U. Choe, D. A. Siler, T. V. Arumugam, E. Orthey, C. Gerloff, E. Tolosa and T. Magnus (2009). "Temporal and spatial dynamics of cerebral immune cell accumulation in stroke." Stroke; a journal of cerebral circulation **40**(5): 1849-1857.

Golde, W. T., P. Gollobin and L. L. Rodriguez (2005). "A rapid, simple, and humane method for submandibular bleeding of mice using a lancet." Lab Anim (NY) **34**(9): 39-43.

Goritz, C., D. O. Dias, N. Tomilin, M. Barbacid, O. Shupliakov and J. Frisen (2011). "A pericyte origin of spinal cord scar tissue." Science **333**(6039): 238-242.

Gronberg, N. V., F. F. Johansen, U. Kristiansen and H. Hasseldam (2013). "Leukocyte infiltration in experimental stroke." Journal of neuroinflammation **10**(1): 115.

Hamann, G. F., Y. Okada, R. Fitridge and G. J. del Zoppo (1995). "Microvascular basal lamina antigens disappear during cerebral ischemia and reperfusion." Stroke **26**(11): 2120-2126.

Hamers, F. P., G. C. Koopmans and E. A. Joosten (2006). "CatWalk-assisted gait analysis in the assessment of spinal cord injury." J Neurotrauma **23**(3-4): 537-548.

He, L. and A. G. Marneros (2013). "Macrophages are essential for the early wound healing response and the formation of a fibrovascular scar." The American journal of pathology **182**(6): 2407-2417.

Heiss, W. D. (2016). "Malignant MCA Infarction: Pathophysiology and Imaging for Early Diagnosis and Management Decisions." Cerebrovasc Dis **41**(1-2): 1-7.

Hetze, S., O. Engel, C. Romer, S. Mueller, U. Dirnagl, C. Meisel and A. Meisel (2013). "Superiority of preventive antibiotic treatment compared with standard treatment of poststroke pneumonia in experimental stroke: a bed to bench approach." Journal of cerebral blood flow and metabolism : official journal of the International Society of Cerebral Blood Flow and Metabolism **33**(6): 846-854.

Hetze, S., C. Romer, C. Teufelhart, A. Meisel and O. Engel (2012). "Gait analysis as a method for assessing neurological outcome in a mouse model of stroke." Journal of neuroscience methods **206**(1): 7-14.

Hetze, S., C. Romer, C. Teufelhart, A. Meisel and O. Engel (2012). "Gait analysis as a method for assessing neurological outcome in a mouse model of stroke." J Neurosci Methods **206**(1): 7-14.

Howard, R. J. and R. L. Simmons (1974). "Acquired immunologic deficiencies after trauma and surgical procedures." Surg Gynecol Obstet **139**(5): 771-782.

Huber, A. K. and D. N. Irani (2015). "Targeting CXCL13 During Neuroinflammation." Adv Neuroimmune Biol **6**(1): 1-8.

Hurn, P. D., S. Subramanian, S. M. Parker, M. E. Afentoulis, L. J. Kaler, A. A. Vandenbark and H. Offner (2007). "T- and B-cell-deficient mice with experimental stroke have reduced lesion size and inflammation." J Cereb Blood Flow Metab **27**(11): 1798-1805.

Iadecola, C. (2013). "The pathobiology of vascular dementia." Neuron **80**(4): 844-866.

Iadecola, C. and J. Anrather (2011). "The immunology of stroke: from mechanisms to translation." Nature medicine **17**(7): 796-808.

Iadecola, C. and J. Anrather (2011). "Stroke research at a crossroad: asking the brain for directions." Nat Neurosci **14**(11): 1363-1368.

Jauch, E. C., C. Lindsell, J. Broderick, S. C. Fagan, B. C. Tilley, S. R. Levine and N. r.-P. S. S. Group (2006). "Association of serial biochemical markers with acute ischemic stroke: the National Institute of Neurological Disorders and Stroke recombinant tissue plasminogen activator Stroke Study." Stroke **37**(10): 2508-2513.

Jiang, M. Q., Y. Y. Zhao, W. Cao, Z. Z. Wei, X. Gu, L. Wei and S. P. Yu (2016). "Long-term survival and regeneration of neuronal and vasculature cells inside the core region after ischemic stroke in adult mice." Brain Pathol.

Jokinen, H., S. Melkas, R. Ylikoski, T. Pohjasvaara, M. Kaste, T. Erkinjuntti and M. Hietanen (2015). "Post-stroke cognitive impairment is common even after successful clinical recovery." Eur J Neurol **22**(9): 1288-1294.

Juenemann, M., T. Braun, S. Doenges, M. Nedelmann, C. Mueller, G. Bachmann, P. Singh, F. Blaes, T. Gerriets and M. Tschernatsch (2015). "Aquaporin-4 autoantibodies increase vasogenic edema formation and infarct size in a rat stroke model." BMC Immunol **16**: 30.

Kalra, L., S. Irshad, J. Hodsoll, M. Simpson, M. Gulliford, D. Smithard, A. Patel, I. Rebollo-Mesa and S.-I. Investigators (2015). "Prophylactic antibiotics after acute stroke for reducing pneumonia in patients with dysphagia (STROKE-INF): a prospective, cluster-randomised, open-label, masked endpoint, controlled clinical trial." Lancet **386**(10006): 1835-1844.

Kimmelman, J., J. S. Mogil and U. Dirnagl (2014). "Distinguishing between exploratory and confirmatory preclinical research will improve translation." PLoS Biol **12**(5): e1001863.

Kipnis, J., S. Gadani and N. C. Derecki (2012). "Pro-cognitive properties of T cells." Nat Rev Immunol **12**(9): 663-669.

Kleinschnitz, C., P. Kraft, A. Dreykluft, I. Hagedorn, K. Gobel, M. K. Schuhmann, F. Langhauser, X. Helluy, T. Schwarz, S. Bittner, C. T. Mayer, M. Brede, C. Varallyay, M. Pham, M. Bendszus, P. Jakob, T. Magnus, S. G. Meuth, Y. Iwakura, A. Zernecke, T. Sparwasser, B. Nieswandt, G. Stoll and H. Wiendl (2013). "Regulatory T cells are strong promoters of acute ischemic stroke in mice by inducing dysfunction of the cerebral microvasculature." Blood **121**(4): 679-691.

Kleinschnitz, C., N. Schwab, P. Kraft, I. Hagedorn, A. Dreykluft, T. Schwarz, M. Austinat, B. Nieswandt, H. Wiendl and G. Stoll (2010). "Early detrimental T-cell effects in experimental cerebral ischemia are neither related to adaptive immunity nor thrombus formation." Blood **115**(18): 3835-3842.

Komori, M., Y. C. Lin, I. Cortese, A. Blake, J. Ohayon, J. Cherup, D. Maric, P. Kosa, T. Wu and B. Bielekova (2016). "Insufficient disease inhibition by intrathecal rituximab in progressive multiple sclerosis." Ann Clin Transl Neurol **3**(3): 166-179.

Kowal, C., L. A. DeGiorgio, T. Nakaoka, H. Hetherington, P. T. Huerta, B. Diamond and B. T. Volpe (2004). "Cognition and immunity; antibody impairs memory." Immunity **21**(2): 179-188.

Kurosaki, T., K. Kometani and W. Ise (2015). "Memory B cells." Nat Rev Immunol **15**(3): 149-159.

Langhauser, F., P. Kraft, E. Gob, J. Leinweber, M. K. Schuhmann, K. Lorenz, M. Gelderblom, S. Bittner, S. G. Meuth, H. Wiendl, T. Magnus and C. Kleinschnitz (2014). "Blocking of alpha4 integrin does not protect from acute ischemic stroke in mice." Stroke **45**(6): 1799-1806.

Li, G., X. Wang, L. H. Huang, Y. Wang, J. J. Hao, X. Ge and X. Y. Xu (2013). "Cytotoxic function of CD8+ T lymphocytes isolated from patients with acute severe cerebral infarction: an assessment of stroke-induced immunosuppression." BMC Immunol **14**: 1.

Li, P., L. Mao, G. Zhou, R. K. Leak, B. L. Sun, J. Chen and X. Hu (2013). "Adoptive Regulatory T-Cell Therapy Preserves Systemic Immune Homeostasis After Cerebral Ischemia." Stroke; a journal of cerebral circulation.

Li, S., Z. Shi, H. Zhang, X. Liu, S. Chen, J. Jin, Y. Wang, W. Jia and H. Li (2013). "Assessing gait impairment after permanent middle cerebral artery occlusion in rats using an automated computer-aided control system." Behav Brain Res **250**: 174-191.

Liesz, A., E. Suri-Payer, C. Veltkamp, H. Doerr, C. Sommer, S. Rivest, T. Giese and R. Veltkamp (2009). "Regulatory T cells are key cerebroprotective immunomodulators in acute experimental stroke." Nature medicine **15**(2): 192-199.

Liesz, A., W. Zhou, E. Mracsko, S. Karcher, H. Bauer, S. Schwarting, L. Sun, D. Bruder, S. Stegemann, A. Cerwenka, C. Sommer, A. H. Dalpke and R. Veltkamp (2011). "Inhibition of

lymphocyte trafficking shields the brain against deleterious neuroinflammation after stroke." Brain **134**(Pt 3): 704-720.

Liesz, A., W. Zhou, S. Y. Na, G. J. Hammerling, N. Garbi, S. Karcher, E. Mracsko, J. Backs, S. Rivest and R. Veltkamp (2013). "Boosting regulatory T cells limits neuroinflammation in permanent cortical stroke." The Journal of neuroscience : the official journal of the Society for Neuroscience **33**(44): 17350-17362.

Llovera, G., K. Hofmann, S. Roth, A. Salas-Perdomo, M. Ferrer-Ferrer, C. Perego, E. R. Zanier, U. Mamrak, A. Rex, H. Party, V. Agin, C. Fauchon, C. Orset, B. Haelewyn, M. G. De Simoni, U. Dirnagl, U. Grittner, A. M. Planas, N. Plesnila, D. Vivien and A. Liesz (2015). "Results of a preclinical randomized controlled multicenter trial (pRCT): Anti-CD49d treatment for acute brain ischemia." Sci Transl Med **7**(299): 299ra121.

Llovera, G., S. Roth, N. Plesnila, R. Veltkamp and A. Liesz (2014). "Modeling stroke in mice: permanent coagulation of the distal middle cerebral artery." J Vis Exp(89): e51729.

Louveau, A., I. Smirnov, T. J. Keyes, J. D. Eccles, S. J. Rouhani, J. D. Peske, N. C. Derecki, D. Castle, J. W. Mandell, K. S. Lee, T. H. Harris and J. Kipnis (2015). "Structural and functional features of central nervous system lymphatic vessels." Nature **523**(7560): 337-341.

Macrae, I. M. (2011). "Preclinical stroke research--advantages and disadvantages of the most common rodent models of focal ischaemia." British journal of pharmacology **164**(4): 1062-1078.

Magliozzi, R., O. Howell, A. Vora, B. Serafini, R. Nicholas, M. Puopolo, R. Reynolds and F. Aloisi (2007). "Meningeal B-cell follicles in secondary progressive multiple sclerosis associate with early onset of disease and severe cortical pathology." Brain **130**(Pt 4): 1089-1104.

Mahon, S., P. Parmar, S. Barker-Collo, R. Krishnamurthi, K. Jones, A. Theadom and V. Feigin (2017). "Determinants, Prevalence, and Trajectory of Long-Term Post-Stroke Cognitive Impairment: Results from a 4-Year Follow-Up of the ARCOS-IV Study." Neuroepidemiology **49**(3-4): 129-134.

Makin, S. D., S. Turpin, M. S. Dennis and J. M. Wardlaw (2013). "Cognitive impairment after lacunar stroke: systematic review and meta-analysis of incidence, prevalence and comparison with other stroke subtypes." J Neurol Neurosurg Psychiatry **84**(8): 893-900.

Mantovani, A., S. K. Biswas, M. R. Galdiero, A. Sica and M. Locati (2013). "Macrophage plasticity and polarization in tissue repair and remodelling." The Journal of pathology **229**(2): 176-185.

Manwani, B., B. Friedler, R. Verma, V. R. Venna, L. D. McCullough and F. Liu (2014). "Perfusion of ischemic brain in young and aged animals: a laser speckle flowmetry study." Stroke **45**(2): 571-578.

Marino, E., M. Batten, J. Groom, S. Walters, D. Liuwantara, F. Mackay and S. T. Grey (2008). "Marginal-zone B-cells of nonobese diabetic mice expand with diabetes onset, invade the pancreatic lymph nodes, and present autoantigen to diabetogenic T-cells." Diabetes **57**(2): 395-404.

Marsh, B. J., R. L. Williams-Karnesky and M. P. Stenzel-Poore (2009). "Toll-like receptor signaling in endogenous neuroprotection and stroke." Neuroscience **158**(3): 1007-1020.

Maurice, T., M. Hiramatsu, J. Itoh, T. Kameyama, T. Hasegawa and T. Nabeshima (1994). "Low dose of 1,3-di(2-tolyl)guanidine (DTG) attenuates MK-801-induced spatial working memory impairment in mice." Psychopharmacology (Berl) **114**(3): 520-522.

Mehta, J. E., E. Mitchell, V. Roland, M. Joan, S. Johnston, S. Aneesh, B. Kyra, L. Maarten, C. Ih, T. Weihua, G. Sarah and Lahar (2016). "Natalizumab Versus Placebo in Patients with Acute

Ischemic Stroke (AIS): Results from ACTION, a Multicenter, Double-Blind, Placebo-Controlled, Randomized Phase 2 Clinical Trial (S7.005)."

Meinl, E., M. Krumbholz and R. Hohlfeld (2006). "B lineage cells in the inflammatory central nervous system environment: migration, maintenance, local antibody production, and therapeutic modulation." Ann Neurol **59**(6): 880-892.

Meisel, A. (2015). "Preventive antibiotic therapy in stroke: PASSed away?" Lancet **385**(9977): 1486-1487.

Meisel, C. and A. Meisel (2011). "Suppressing immunosuppression after stroke." The New England journal of medicine **365**(22): 2134-2136.

Meisel, C., J. M. Schwab, K. Prass, A. Meisel and U. Dirnagl (2005). "Central nervous system injury-induced immune deficiency syndrome." Nat Rev Neurosci **6**(10): 775-786.

Mendel, I., N. Kerlero de Rosbo and A. Ben-Nun (1995). "A myelin oligodendrocyte glycoprotein peptide induces typical chronic experimental autoimmune encephalomyelitis in H-2b mice: fine specificity and T cell receptor V beta expression of encephalitogenic T cells." Eur J Immunol **25**(7): 1951-1959.

Mergenthaler, P., U. Dirnagl and A. Meisel (2004). "Pathophysiology of stroke: lessons from animal models." Metab Brain Dis **19**(3-4): 151-167.

Mergenthaler, P. and A. Meisel (2012). "Do stroke models model stroke?" Dis Model Mech **5**(6): 718-725.

Mills, K. H. (2011). "TLR-dependent T cell activation in autoimmunity." Nat Rev Immunol **11**(12): 807-822.

Murray, P. J. and T. A. Wynn (2011). "Protective and pathogenic functions of macrophage subsets." Nat Rev Immunol **11**(11): 723-737.

Orsini, F., P. Villa, S. Parrella, R. Zangari, E. R. Zanier, R. Gesuete, M. Stravalaci, S. Fumagalli, R. Ottria, J. J. Reina, A. Paladini, E. Micotti, R. Ribeiro-Viana, J. Rojo, V. I. Pavlov, G. L. Stahl, A. Bernardi, M. Gobbi and M. G. De Simoni (2012). "Targeting mannose-binding lectin confers long-lasting protection with a surprisingly wide therapeutic window in cerebral ischemia." Circulation **126**(12): 1484-1494.

Ortega, S. B., I. Noorbhai, K. Poinsatte, X. Kong, A. Anderson, N. L. Monson and A. M. Stowe (2015). "Stroke induces a rapid adaptive autoimmune response to novel neuronal antigens." Discov Med **19**(106): 381-392.

Perez-de-Puig, I., F. Miro-Mur, M. Ferrer-Ferrer, E. Gelpi, J. Pedragosa, C. Justicia, X. Urra, A. Chamorro and A. M. Planas (2015). "Neutrophil recruitment to the brain in mouse and human ischemic stroke." Acta Neuropathol **129**(2): 239-257.

Pfaffl, M. W., G. W. Horgan and L. Dempfle (2002). "Relative expression software tool (REST) for group-wise comparison and statistical analysis of relative expression results in real-time PCR." Nucleic Acids Res **30**(9): e36.

Pham-Dinh, D., B. Della Gaspera, N. Kerlero de Rosbo and A. Dautigny (1995). "Structure of the human myelin/oligodendrocyte glycoprotein gene and multiple alternative spliced isoforms." Genomics **29**(2): 345-352.

Pitzalis, C., G. W. Jones, M. Bombardieri and S. A. Jones (2014). "Ectopic lymphoid-like structures in infection, cancer and autoimmunity." Nature reviews. Immunology **14**(7): 447-462.

Planas, A. M., M. Gomez-Choco, X. Urra, R. Gorina, M. Caballero and A. Chamorro (2012). "Brain-derived antigens in lymphoid tissue of patients with acute stroke." J Immunol **188**(5): 2156-2163.

Prass, K., C. Meisel, C. Hoflich, J. Braun, E. Halle, T. Wolf, K. Ruscher, I. V. Victorov, J. Priller, U. Dirnagl, H. D. Volk and A. Meisel (2003). "Stroke-induced immunodeficiency promotes spontaneous bacterial infections and is mediated by sympathetic activation reversal by poststroke T helper cell type 1-like immunostimulation." J Exp Med **198**(5): 725-736.

Pruss, H., D. Iggena, T. Baldinger, V. Prinz, A. Meisel, M. Endres, U. Dirnagl and J. M. Schwab (2012). "Evidence of intrathecal immunoglobulin synthesis in stroke: a cohort study." Arch Neurol **69**(6): 714-717.

Pruss, H., J. Leubner, N. K. Wenke, G. A. Czirjak, C. A. Szentiks and A. D. Greenwood (2015). "Anti-NMDA Receptor Encephalitis in the Polar Bear (Ursus maritimus) Knut." Sci Rep **5**: 12805.

Ransohoff, R. M. and B. Engelhardt (2012). "The anatomical and cellular basis of immune surveillance in the central nervous system." Nat Rev Immunol **12**(9): 623-635.

Raposo, C. and M. Schwartz (2014). "Glial scar and immune cell involvement in tissue remodeling and repair following acute CNS injuries." Glia **62**(11): 1895-1904.

Rashid, A., H. Auchincloss, Jr. and J. Sharon (1992). "Comparison of GK1.5 and chimeric rat/mouse GK1.5 anti-CD4 antibodies for prolongation of skin allograft survival and suppression of alloantibody production in mice." J Immunol **148**(5): 1382-1388.

Ren, X., K. Akiyoshi, S. Dziennis, A. A. Vandenbark, P. S. Herson, P. D. Hurn and H. Offner (2011). "Regulatory B cells limit CNS inflammation and neurologic deficits in murine experimental stroke." J Neurosci **31**(23): 8556-8563.

Ren, X., K. Akiyoshi, M. R. Grafe, A. A. Vandenbark, P. D. Hurn, P. S. Herson and H. Offner (2012). "Myelin specific cells infiltrate MCAO lesions and exacerbate stroke severity." Metab Brain Dis **27**(1): 7-15.

Robinson, R. G. and R. E. Jorge (2016). "Post-Stroke Depression: A Review." Am J Psychiatry **173**(3): 221-231.

Romer, C., O. Engel, K. Winek, S. Hochmeister, T. Zhang, G. Royl, J. Klehmet, U. Dirnagl, C. Meisel and A. Meisel (2015). "Blocking stroke-induced immunodeficiency increases CNS antigen-specific autoreactivity but does not worsen functional outcome after experimental stroke." J Neurosci **35**(20): 7777-7794.

Romer, C., O. Engel, K. Winek, S. Hochmeister, T. Zhang, G. Royl, J. Klehmet, U. Dirnagl, C. Meisel and A. Meisel (2015). "Blocking stroke-induced immunodeficiency increases CNS antigen-specific autoreactivity but does not worsen functional outcome after experimental stroke." The Journal of neuroscience : the official journal of the Society for Neuroscience **35**(20): 7777-7794.

Savva, G. M., B. C. Stephan and G. Alzheimer's Society Vascular Dementia Systematic Review (2010). "Epidemiological studies of the effect of stroke on incident dementia: a systematic review." Stroke **41**(1): e41-46.

Scheibe, F., H. Pruss, A. M. Mengel, S. Kohler, A. Numann, M. Kohnlein, K. Ruprecht, T. Alexander, F. Hiepe and A. Meisel (2016). "Bortezomib for treatment of therapy-refractory anti-NMDA receptor encephalitis." Neurology.

Schilling, M., M. Besselmann, M. Muller, J. K. Strecker, E. B. Ringelstein and R. Kiefer (2005). "Predominant phagocytic activity of resident microglia over hematogenous macrophages

following transient focal cerebral ischemia: an investigation using green fluorescent protein transgenic bone marrow chimeric mice." Exp Neurol **196**(2): 290-297.

Schuette-Nuetgen, K., J. K. Strecker, J. Minnerup, E. B. Ringelstein and M. Schilling (2012). "MCP-1/CCR-2-double-deficiency severely impairs the migration of hematogenous inflammatory cells following transient cerebral ischemia in mice." Exp Neurol **233**(2): 849-858.

Schuhmann, M. K., F. Langhauser, P. Kraft and C. Kleinschnitz (2017). "B cells do not have a major pathophysiologic role in acute ischemic stroke in mice." J Neuroinflammation **14**(1): 112.

Shichita, T., Y. Sugiyama, H. Ooboshi, H. Sugimori, R. Nakagawa, I. Takada, T. Iwaki, Y. Okada, M. Iida, D. J. Cua, Y. Iwakura and A. Yoshimura (2009). "Pivotal role of cerebral interleukin-17-producing gammadeltaT cells in the delayed phase of ischemic brain injury." Nat Med **15**(8): 946-950.

Simats, A., T. Garcia-Berrocoso and J. Montaner (2016). "Natalizumab: a new therapy for acute ischemic stroke?" Expert Rev Neurother **16**(9): 1013-1021.

Smith, E. E., G. Saposnik, G. J. Biessels, F. N. Doubal, M. Fornage, P. B. Gorelick, S. M. Greenberg, R. T. Higashida, S. E. Kasner, S. Seshadri, C. American Heart Association Stroke, R. Council on Cardiovascular, Intervention, G. Council on Functional, B. Translational and H. Council on (2017). "Prevention of Stroke in Patients With Silent Cerebrovascular Disease: A Scientific Statement for Healthcare Professionals From the American Heart Association/American Stroke Association." Stroke **48**(2): e44-e71.

Sommer, C. J. (2017). "Ischemic stroke: experimental models and reality." Acta Neuropathol **133**(2): 245-261.

Sorokin, L. (2010). "The impact of the extracellular matrix on inflammation." Nat Rev Immunol **10**(10): 712-723.

Steinman, R. M. and M. C. Nussenzweig (2002). "Avoiding horror autotoxicus: the importance of dendritic cells in peripheral T cell tolerance." Proc Natl Acad Sci U S A **99**(1): 351-358.

Stubbe, T., F. Ebner, D. Richter, O. Engel, J. Klehmet, G. Royl, A. Meisel, R. Nitsch, C. Meisel and C. Brandt (2013). "Regulatory T cells accumulate and proliferate in the ischemic hemisphere for up to 30 days after MCAO." Journal of cerebral blood flow and metabolism : official journal of the International Society of Cerebral Blood Flow and Metabolism **33**(1): 37-47.

Ueno, H., J. Banchereau and C. G. Vinuesa (2015). "Pathophysiology of T follicular helper cells in humans and mice." Nature immunology **16**(2): 142-152.

Urra, X., F. Miro, A. Chamorro and A. M. Planas (2014). "Antigen-specific immune reactions to ischemic stroke." Front Cell Neurosci **8**: 278.

van Rooij, F. G., P. Schaapsmeerders, N. A. Maaijwee, D. A. van Duijnhoven, F. E. de Leeuw, R. P. Kessels and E. J. van Dijk (2014). "Persistent cognitive impairment after transient ischemic attack." Stroke **45**(8): 2270-2274.

van Zwam, M., R. Huizinga, M. J. Melief, A. F. Wierenga-Wolf, M. van Meurs, J. S. Voerman, K. P. Biber, H. W. Boddeke, U. E. Hopken, C. Meisel, A. Meisel, I. Bechmann, R. Q. Hintzen, B. A. t Hart, S. Amor, J. D. Laman and L. A. Boven (2009). "Brain antigens in functionally distinct antigen-presenting cell populations in cervical lymph nodes in MS and EAE." J Mol Med (Berl) **87**(3): 273-286.

Vermeer, S. E., W. T. Longstreth, Jr. and P. J. Koudstaal (2007). "Silent brain infarcts: a systematic review." Lancet Neurol **6**(7): 611-619.

Vremec, D., J. Pooley, H. Hochrein, L. Wu and K. Shortman (2000). "CD4 and CD8 expression by dendritic cell subtypes in mouse thymus and spleen." J Immunol **164**(6): 2978-2986.

Wang, W. Z., T. Olsson, V. Kostulas, B. Hojeberg, H. P. Ekre and H. Link (1992). "Myelin antigen reactive T cells in cerebrovascular diseases." Clin Exp Immunol **88**(1): 157-162.

Westendorp, W. F., J. D. Vermeij, E. Zock, I. J. Hooijenga, N. D. Kruyt, H. J. Bosboom, V. I. Kwa, M. Weisfelt, M. J. Remmers, R. ten Houten, A. H. Schreuder, S. E. Vermeer, E. J. van Dijk, D. W. Dippel, M. G. Dijkgraaf, L. Spanjaard, M. Vermeulen, T. van der Poll, J. M. Prins, F. H. Vermeij, Y. B. Roos, R. P. Kleyweg, H. Kerkhoff, M. C. Brouwer, A. H. Zwinderman, D. van de Beek, P. J. Nederkoorn and P. investigators (2015). "The Preventive Antibiotics in Stroke Study (PASS): a pragmatic randomised open-label masked endpoint clinical trial." Lancet **385**(9977): 1519-1526.

Wilson, E. H., W. Weninger and C. A. Hunter (2010). "Trafficking of immune cells in the central nervous system." J Clin Invest **120**(5): 1368-1379.

Wong, C. H., C. N. Jenne, W. Y. Lee, C. Leger and P. Kubes (2011). "Functional innervation of hepatic iNKT cells is immunosuppressive following stroke." Science **334**(6052): 101-105.

Wu, C., F. Ivars, P. Anderson, R. Hallmann, D. Vestweber, P. Nilsson, H. Robenek, K. Tryggvason, J. Song, E. Korpos, K. Loser, S. Beissert, E. Georges-Labouesse and L. M. Sorokin (2009). "Endothelial basement membrane laminin alpha5 selectively inhibits T lymphocyte extravasation into the brain." Nat Med **15**(5): 519-527.

Yilmaz, G., T. V. Arumugam, K. Y. Stokes and D. N. Granger (2006). "Role of T lymphocytes and interferon-gamma in ischemic stroke." Circulation **113**(17): 2105-2112.

Yousif, L. F., J. Di Russo and L. Sorokin (2013). "Laminin isoforms in endothelial and perivascular basement membranes." Cell Adh Migr **7**(1): 101-110.

Zerche, M., K. Weissenborn, C. Ott, E. Dere, A. R. Asif, H. Worthmann, I. Hassouna, K. Rentzsch, A. B. Tryc, L. Dahm, J. Steiner, L. Binder, J. Wiltfang, A. L. Siren, W. Stocker and H. Ehrenreich (2015). "Preexisting Serum Autoantibodies Against the NMDAR Subunit NR1 Modulate Evolution of Lesion Size in Acute Ischemic Stroke." Stroke; a journal of cerebral circulation **46**(5): 1180-1186.

Zierath, D., A. Kunze, L. Fecteau and K. Becker (2015). "Promiscuity of autoimmune responses to MBP after stroke." J Neuroimmunol **285**: 101-105.

Zouali, M. and Y. Richard (2011). "Marginal zone B-cells, a gatekeeper of innate immunity." Front Immunol **2**: 63.

9. ABBREVIATIONS

AIS	acute ischemic stroke
ANOVA	one-way analysis of variance
APC	antigen-presenting cell
APN	aminopeptidase N
AQP4	aquaporin-4
AU	arbitrary unit
BBB	blood-brain barrier
BDNF	brain derived neurotrophic factor
BLC	B lymphocyte chemoattractant
BM	basement membrane
BrdU	bromdesoxyuridin
BSA	bovine serum albumin
CCR2	C-C chemokine receptor type 2
CD	cluster of differentiation
cDNA	complementary DNA
CIA	collagen induced arthritis
CIDS	CNS injury-induced immunodepression
CLN	cervical lymph node
CNS	central nervous system
ColI	collagen type I
contra.	contralateral
CSF	cerebrospinal fluid
CSPG	chondroitin sulfate proteoglycan
CVD	cerebrovascular disease
CXCL13	C-X-C Motif Chemokine Ligand 13
DAMP	danger-associated molecular pattern molecule
DCLN	deep cervical lymph node
DC	dendritic cell
DEPC	diethyl pyrocarbonate
depl.	depletion
DNA	deoxyribonucleic acid
EAE	experimental autoimmune encephalitis
EC	endothelial cell
ECM	extracellular matrix
EDTA	ethylenediaminetetraacetic acid
ELISA	enzyme-linked immunosorbent assay
FACS	fluorescence-activated cell sorting
FCS	fetal calf serum
FDA	Food and Drug Administration
FITC	fluorescein isothiocyanate
fpmCTX	frontal premotor cortex
FSC	forward scatter
GAG	glycosaminoglycan
GC	germinal center
GOI	gene of interest
HEV	high endothelial venule
HPA	hypothalamic-pituitary-adrenal
IFN	interferon
Ig	immunoglobulin
IL	interleukin
iNKT	invariant nature killer
ipsi.	ipsilateral

ISF	interstitial fluid
LF	left front paw
LH	left hind paw
LLN	lumbar lymph node
LN	lymph node
MCA	middle cerebral artery
MCAo	middle cerebral artery occlusion
MCP-1	monocyte chemotactic protein-1
MHC	major histocompatibility complex
MLN	mesenteric lymph node
MMP	matrix metalloproteinase
MNC	mononuclear cell
MOG	myelin oligodendrocyte glycoprotein
MRI	magnetic resonance imaging
MS	multiple sclerosis
MZ	marginal zone
NF-L	neurofilament light
NG2+	chondroitin sulfate proteoglycan 4
NGF	nerve growth factor
NIHSS	national institute of health stroke scale
NK	nature killer
NMDAR1	N-methyl-D-aspartate-receptor NMDAR subunit NR1
NMO	neuromyelitis optica
NVU	neurovascular unit
PASS	Preventative Antibiotics Stroke Study
PBS	phosphate buffered saline
PC	pericyte
PCR	polymerase chain reaction
PDGFRβ	platelet-derived growth factor receptor beta
PD-L	programmed cell death ligand
PE	phycoerythrin
PE-Cy7	tandem conjugate (PE and a cyanine dye 7)
PerCP	peridinin chlorophyll protein
PFA	paraformaldehyde
PLP	proteolipid protein
PO	pacific orange
qRT-PCR	quantitative real time polymerase chain reaction
RBC	red blood cell
RF	right front paw
RH	right hind paw
ROS	reactive oxygen species
RPMI 1640	Roswell Park Memorial Institute 1640
rt-PA	recombinant tissue-type plasminogen activator
RT	room temperature
SAH	subarachnoid hemorrhage
SAM	sympathetic-adrenal-medullary

SCI	spinal cord injury
SCID	severe combined immunodeficiency
SCLN	superficial lymph node
SD	standard deviation
SIDS	stroke injury-induced immunodepression
SSC	side scatter
TBI	traumatic brain injury
TCR	T cell receptor
Tfh	follicular helper T
TGF	tissue growth factor
Th	helper T
TJ	tight junction
TLR	toll-like receptor
TNF	tumor necrosis factor
Treg	regulatory T
VEGFa	vascular endothelial growth factor a
UTI	urinary tract infection
WT	wild type

10. EIDESSTATTLICHE VERSICHERUNG

„Ich, Tian Zhang, versichere an Eides statt durch meine eigenhändige Unterschrift, dass ich die vorgelegte Dissertation mit dem Thema , Effects of $CD4^+$ T cells on tissue remodeling and autoreactive responses after experimental stroke‘ selbstständig und ohne nicht offengelegte Hilfe Dritter verfasst und keine anderen als die angegebenen Quellen und Hilfsmittel genutzt habe.

Alle Stellen, die wörtlich oder dem Sinne nach auf Publikationen oder Vorträgen anderer Autoren beruhen, sind als solche in korrekter Zitierung (siehe „Uniform Requirements for Manuscripts (URM)“ des ICMJE www.icmje.org) kenntlich gemacht. Die Abschnitte zu Methodik (insbesondere praktische Arbeiten, Laborbestimmungen, statistische Aufarbeitung) und Resultaten (insbesondere Abbildungen, Graphiken und Tabellen) entsprechen den URM (s. o.) und werden von mir verantwortet.

Meine Anteile an etwaigen Publikationen zu dieser Dissertation entsprechen denen, die in der untenstehenden gemeinsamen Erklärung mit dem/der Betreuer/in, angegeben sind. Sämtliche Publikationen, die aus dieser Dissertation hervorgegangen sind und bei denen ich Autor bin, entsprechen den URM (s. o.) und werden von mir verantwortet.

Die Bedeutung dieser eidesstattlichen Versicherung und die strafrechtlichen Folgen einer unwahren eidesstattlichen Versicherung (§156,161 des Strafgesetzbuches) sind mir bekannt und bewusst.“

_____ _____

Datum Unterschrift der Doktorandin Tian Zhang

Anteilserklärung an etwaigen erfolgten Publikationen

Tian Zhang hatte folgenden Anteil an den folgenden Publikationen (siehe auch 12.):

Publikation 1:

Römer C, Engel O, Winek K, Hochmeister S, **Zhang T**, Royl G, Klehmet J, Dirnagl U, Meisel C, Meisel A.
Blocking stroke-induced immunodeficiency increases cns antigen-specific autoreactivity but does not worsen functional outcome after experimental stroke. J Neurosci. 2015; 35:7777-7794

Beitrag im Einzelnen: Durchführung einzelner Experimente sowie Datenauswertung für Immunofluoreszenz Färbungen von Maus-Gehirnschnitten und Multiplex Analysen; Verfassen des Methodenteils und der entsprechenden Ergebnisse des Manuskriptes.

Publikation 2:

Watzlawick R, Rind J, Sena ES, Brommer B, **Zhang T**, Kopp MA, Dirnagl U, Macleod MR, Howells DW, Schwab JM.
Olfactory ensheathing cell transplantation in experimental spinal cord injury: Effect size and reporting bias of 62 experimental treatments: A systematic review and meta-analysis.
PLoS biology. 2016; 14:e1002468

Beitrag im Einzelnen: Zusammenfassung und Übersetzung von chinesischen Literaturquellen.

_____
Unterschrift, Datum und Stempel Prof. Dr. med. Andreas Meisel

_____
Unterschrift der Doktorandin Tian Zhang

11. CURRICULUM VITAE

My curriculum vitae does not appear in the electronic version of my paper for reasons of data protection.

12. PUBLICATION LIST

1) Römer C, Odilo E., Winek K, Hochmeister S, **Zhang T**, Royl G, Klehmet J, Dirnagl U, Meisel C, Meisel A.

Blocking stroke-induced immunodeficiency increases cns antigen-specific autoreactivity but does not worsen functional outcome after experimental stroke.
The Journal of Neuroscience. 2015; 35:7777-7794

2) Watzlawick R, Rind J, Sena ES, Brommer B, **Zhang T**, Kopp MA, Dirnagl U, Macleod MR, Howells DW, Schwab JM.

Olfactory ensheathing cell transplantation in experimental spinal cord injury: Effect size and reporting bias of 62 experimental treatments: A systematic review and meta-analysis.
PLoS biology. 2016; 14:e1002468

13. ACKNOWLEDGEMENTS

First of all, I would like to thank Prof. Andreas Meisel for providing me with the interesting topic and supervising my doctoral thesis and for his endless encouragement and belief in this project. I would like to acknowledge Prof. Ulrich Dirnagl for his valuable advice and inspiration for both my research and career development. I am grateful to Dr. Christian Meisel for his continuous scientific support.

Many thanks go to the International Max Planck Research School for Infectious Diseases and Immunology (IMPRS-IDI) and the International Graduate Program Medical Neurosciences for providing excellent opportunities to develop my personal skills and enhance my scientific communication.

I am thankful to all former and current colleagues of the AG Meisel: Katarzyna Winek, Odilo Engel, Christine Römer, Juliane Klehment, Ewa Andrzejak, Andreas Pelz, Priscilla Koduah, Kristin Wendland, Claudia Dames, Levent Akyüz, Naoki Oyama, Mareike Thielke, Heike Lerch, Yvonne Amoneit, Sabine Kolodziej, Claudia Muselmann-Genschow and Susanne Metzkow for their continuous support and collaboration. It has been a truly fruitful and joyful experience to work together with you. I also thank Christa, Ingo and Larissa for their technical advice.

I thank Prof. Birgit Sawitzki, Prof. Sorokin Lydia (University of Münster), Prof. Jon Laman (University of Groningen), PD Dr. Harald Prüß, Dr. Ana-Luisa Pina, Dr. Francisco Fernandez Klett, Dr. Jason Millward and Dr. Rene Bernard for kindly sharing their scientific knowledge and experimental skills. I also thank Mrs. Suzanne von Engelhardt for editing this thesis and Dr. Sophie Piper for her advice on statistics.

I am most grateful to my family in Germany and China. I deeply thank my parents for their love and confidence in me. I owe many thanks to my husband Qingzhou who took care of me with love, provided invaluable advice and encouraged me through all difficulties. I owe thanks to my friends, particularly Priscilla and Jia for their company, prayer and encouragement.

Last but not least, I am very grateful to the Almighty God for seeing me through this project and my life in Berlin.